Performance of Geogrid Reinforced Ballast under Dynamic Loading

By

Milad Jowkar

B.S., University of Kansas, Lawrence, Spring 2010

Submitted to the Department of Civil, Environmental, and Architectural Engineering and the Graduate Faculty of the University of Kansas in partial fulfillment of the requirements for the degree of Master of Science

_____

Chairperson Dr. Robert L. Parsons

Committee members

_____

Dr. Jie Han

_____

Dr. Steven D. Schrock

The Thesis Committee for Milad Jowkar certifies that

this is the approved version of the following thesis:

Experimental Study on Geogrid Reinforced Ballast under Dynamic Loading

_____

Dr. Robert L. Parsons Chairperson

Date approved: December 20, 2011

ABSTRACT

Railroad ballast consists of open graded crushed stone used as a bed for railroad track to provide stability. It plays a significant role in providing support for the track base and distributing the load to the weaker subgrade below. Ballast also helps with drainage, which is an important factor for any type of transportation structure, including railroads. This issue has become more acute as heavier car loads place more demand on track structure than before.

Over time ballast degrades and loses its strength. Fouling of ballast with fines has been a major issue of railway engineering. Fouling could be caused by break down of ballast itself or intrusion of fines from below or from the environment.

In this experimental study a full-scale railroad section five feet in length was constructed with and without geogrid reinforcement. A full-scale trapezoidal cross section of a railroad was built. The subgrade was covered with 2 feet of ballast 9 feet wide at the top and sloped down on both sides on a 2:1 slope. The track panel ties were embedded in the ballast to a depth of 7 inches.

The reinforced section with geogrid placed 7 inches below the tie performed better than the unreinforced test in terms of settlement and fouling of ballast. Overall settlement was less up to 1 inch less in some places under the ties. Fouling of ballast was reduced under the tie by 30% and at the subgrade level by 20% in reinforced case.

Dedicated to my parents,

Mr. Ali Jowkar And Mrs. Keyhan Mokayyef

ACKNOWLEDGMENT

I would like to express my appreciation to Professor Robert Parsons for giving me this opportunity to work on this exciting project. I would not be able to complete this work without his remarkable guidance, encouragement and support.

I would like to thank Professors Jie Han, Steven Schrock, to be the members of my committee and their helpful suggestions.

I am grateful to the Mid-America Transportation Center (MATC), BNSF and Tensar International Corporation for supporting this research project.

I also would like to thank my friends Mr. Danny Syml, Mr. Aj Rahman, Mr. Jitendra Thakur, Mr. Kahle Lovless, Mr. Baghaban Acharya, Mr. Deep Khatri, Mr. Cheng Lin, Mr. Raju Acharya for their help in this experimental work.

This acknowledgment will not be complete without thanking Mr. Jim Weaver and Matthew Maksimowicz for their excellent technical support.

My endless thank to my parents, Mr. Ali Jowkar and Mrs. Keyhan Mokayyef, who supported me throughout my life in the past 28 years. They were my source of strength.

ABSTRACT iii
Chapter One Introduction 1
Chapter Two Literature Review 4
2.1 Fouling ballast 4
2.2 Stiffness of geocell material 5
2.3 Load carrying capacity 6
2.4 Improving poor track formations using geosynthetics 7
2.4.1 Geosynthetics for improving poor track formation. 8
2.5 Stabilizations of ballasted rail tracks 9
2.6 Use of geosynthetics in railways including geocomposites and vertical drains 10
Chapter Three Research Scope 11
3.1 Test section design 11
3.1.1 Loading frame 13
3.1.2 Wooden frames 15
3.2 Subgrade 16
3.6 Direct shear 28
3.3 Instrumentation 21
3.3.1 Tell-tales 21
3.3.2 Pressure cells 21
3.3.4 Displacement transducers 23
3.3.5 String pots 24
3.4 Ballast 25
3.4.1 Sieve analysis of ballast: 26
3.5 Track 29
3.8 Geogrid 30
3.9 Quality control tests 31
3.9.1 Light weight deflectometer test (LWD) 31
3.9.2 Density testing by drive tube 32
3.9.3 DCP (Dynamic Cone Penetrometer) 33
Chapter Four Test Results 34
4.1 Loading sequence for the unreinforced test 36

4.1.1 East string pot 37
4.1.2 East string pot versus dynamic loading at 1100 psi (9 psi tie bearing pressure) 37
4.1.3 East string pot versus dynamic loading at 2500 psi (21 psi tie bearing pressure) 38
4.1.4 East string pot versus dynamic loading at 3500 psi (31 psi tie bearing pressure) 39
4.1.5 East string pot versus dynamic loading at 4500 psi (38 psi tie bearing pressure) 41
4.1.6 East string pot versus dynamic loading at 4500 psi (soaked) (40 psi tie bearing pressure) 43
4.2 Unreinforced test 45
4.2.1 West string pot 45
4.3 Unreinforced test (Displacement Transducers) 51
4.3.1 Displacement Transducers at 1100 psi (South-East) (9 psi tie bearing pressure) 52
4.3.5 Displacement transducers at 4500 psi dry (South-East) 56
4.3.9 Displacement transducers at 4500 psi soaked (40 psi tie bearing pressure) 60
4.4.1 Pressure cell results for unreinforced test 65
4.4.2 Pressure cells results under ties 67
4.5 Loading sequence for the reinforced section 69
4.5.1 East string pot (reinforced test) 70
4.5.2 East string pot versus dynamic loading at 1100 psi – reinforced (9 psi tie bearing pressure) 71
4.5.3 East string pot versus dynamic loading at 2500 psi – reinforced (21 psi tie bearing pressure) 72
4.5.4 East string pot versus dynamic loading at 3500 psi – reinforced (29 psi tie bearing pressure) 73
4.5.5 East string pot versus dynamic loading at 4500 psi – reinforced (not soaked, 39 psi tie bearing pressure) 74
4.5.6 East string pot versus dynamic loading at 4500 psi – reinforced (soaked, 39 psi tie bearing pressure) 76
4.6 Reinforced test 78
4.6.1 West string pot (reinforced test) 78
4.7 Reinforced test (Displacement Transducers) 84
4.7.1 Displacement transducers (DT) at 1100 psi (South-East, 9psi bearing pressure) 85
4.8.1 Pressure cells results for reinforced Test 89
4.8.2 Pressure cells results at subgrade level 90
4.8.3 Pressure cells results under ties 92
4.9 Unreinforced vs. reinforced: settlement comparison 94
4.9.1 Reinforced vs. unreinforced (East String Pot) 98
4.9.2 Number of cycles versus settlement (West string pot) 101
4.9.3 Number of cycles versus settlement (East string pot) 102
4.9.4 Actual pressure vs. settlement 102
4.10 Additional testing such as LWD, CBR, Sieve Analysis and Tell-Tale readings 106
4.10.1 LWD 106

4.10.2 CBR 107
4.10.3 Tell-Tale 109
4.10.4 Sieve Analysis 110
4.11 General observations 112
Chapter Five Conclusions and Recommendations 113
5.1 Conclusions 113
5.2 Recommendations for Future Study 113
5.3 References 126-127

List of Figures

Figure	Caption	Page Number
1.1	Placing geocell in the field	3
1.2	Placing geocell in the field	3
1.3	Placement geogrid under railroad track	9
2.1	Critical ballast fouling and illustration of loss of aggregate to aggregate contact (Tutumlur, Dombrow and Huang 2008)	5
2.2	Performance of the geoweb system under track	5
2.3	Measured vertical stresses on subgrade, unreinforced sand (1) and geocell “typ1” reinforced sand (r).	7
2.4	Placing geotextiles sheet	7
2.5	Placing geocell	7
2.6	Placement of soil in geocell	8
2.7	Placement of soil in geocell	8
2.8	Stress reduction	8
2.9	Effect of geosynthetics on the settlement of ballast (Indraratna et al.,2004)	9
2.10	Vertical deformation of the ballast layer (modified after Indraratna et al., 2010 a)	10
2.11	Section of ballasted track bed with geocomposite layer (modified Indraratna et al. 2010b)	10

Figure	Caption	Page Number
3.1	Schematic of the rail road cross section unreinforced (not to scale)	11
3.2	3-D view of the test section (not to scale)	12
3.3	Schematic of the rail road cross section reinforced (not to scale)	12
3.4	Loading frame	13
3.5	Loading cylinder	14
3.6	Wooden frames	15
3.7	Grain size distributions for subgrade	16
3.8	Standard proctor compaction curve of the subgrade	17
3.9	Standard atterberg limit test curve of the subgrade	18
3.10	Unconfined compression test curves	19
3.11	Placing subgrade and compaction	20
3.12	Direct shear box	21
3.13	Tell-tale	21
3.14	Location of tell-tales	22
3.15	Model 3515 circular earth pressure cells during placement	23

3.16	Pressure cell locations (not to scale)	23
3.17	Displacement transducer placement	24
3.18	String pot	25
3.19	Recycled ballast after sieve	26
3.20	Washed rock	27
3.21	3.21 Sieve Analysis for ballast.	28
3.22	Sieve shaker for ballast	29
3.23	A Wooden tie track panel	30
3.24	Triaxial Geogrid used in reinforced test	31
3.25	Light weight deflectometer	33
3.26	Drive tube and sampler driver.	34
4.1	Unreinforced Test section	35
4.2	Geogrid after replacement in the reinforced test	36
4.3	Test during dynamic loading	36
4.1.1	Dynamic loading vs. deformation. (East String Pot)	38
4.1.2	East string pot deformations versus dynamic loading at 1100 psi	39
4.1.3	East string pot versus dynamic loading at 2500 psi	40
4.1.4	East string pot versus dynamic loading at 3500 psi	41

4.1.5	East string pot versus dynamic loading at 4500 psi (not soaked)	43
4.1.6	Figure 4.1.6 East string pot reading versus dynamic loading at 4500 psi soaked.	45
4.2.1	Dynamic loading vs. Deformation. (West String Pot)	46
4.2.2	West string pot versus dynamic loading at 1100 psi	47
4.2.3	West string pot versus dynamic loading at 2500 psi	48
4.2.4	West string pot versus dynamic loading at 3500 psi	49
4.2.5	West string pot versus dynamic loading at 4500 psi (not soaked)	50
4.2.6	West string pot versus dynamic loading at 4500 psi (soaked)	51
4.3	Displacement Transducers	52
4.3.1	Displacement transducer reading at 1100 psi (South-East)	53
4.3.2	Displacement transducer reading at 1100 psi (North-East)	54
4.3.3	Displacement transducer reading at 1100 psi (North-West)	55
4.3.4	Displacement transducer reading at 1100 psi (South-West)	56
4.3.5	Displacement transducer reading at 4500 psi not soaked (South-East)	57
4.3.6	Displacement transducer reading at 4500 psi not soaked (North-East)	58
4.3.7	Displacement transducer reading at 4500 psi not soaked (North-West)	59
4.3.8	Displacement transducer reading at 4500 psi not soaked (South-West)	60
4.3.9	Displacement transducer reading at 4500 psi soaked (South-East)	62

4.3.10	Displacement transducer reading at 4500 psi soaked (North-East)	63
4.3.11	Displacement transducer reading at 4500 psi soaked (North-West)	64
4.3.12	Displacement transducer reading at 4500 psi soaked (South-West)	65
4.4.1	Pressure Cells	66
4.4.2	Pressure cells vs. pump pressure at subgrade level	67
4.4.3	Pressure cells vs. tie bearing pressure on ballast	68
4.5.1	Dynamic loading vs. deformation. (reinforced test)	71
4.5.2	East string pot deformations versus dynamic loading at 1100 psi	72
4.5.3	East string pot deformations versus dynamic loading at 2500 psi	73
4.5.4	East string pot deformations versus dynamic loading at 3500 psi	74
4.5.5	East String Pot versus dynamic loading at 4500 psi (not soaked)	76
4.5.6	East String Pot versus dynamic loading at 4500 psi (soaked)	78
4.6.1	Dynamic loading vs. deformation. (reinforced test)	79
4.6.2	West string pot versus dynamic loading at 1100 psi	80
4.6.3	West string pot versus dynamic loading at 2500 psi	81
4.6.4	West string pot versus dynamic loading at 3500 psi	82
4.6.5	West string pot versus dynamic loading at 4500 psi (not soaked)	83
4.6.6	West string pot versus dynamic loading at 4500 psi (soaked)	84

4.7	Displacement transducers	85
4.7.1	Displacement transducer readings at 1100 psi (South-East)	87
4.7.2	Displacement transducer readings at 1100 psi (North-West)	88
4.7.3	Displacement transducer readings at 1100 psi (South-West)	89
4.8.1	Pressure Cells	90
4.8.2	Pressure cells vs. pump pressure at subgrade level	91
4.8.3	Pressure cells vs. tie bearing pressure	93
4.9.1	West string pot result comparison	
4.9.2	West string pot result comparison (after adjusting loads)	98
4.9.3	East string pot result comparison	99
4.9.4	East string pot result comparison (after adjusting loads)	101
4.9.5	Number of cycles vs. settlement (west string pot)	102
4.9.6	Number of cycles vs. settlement (east string pot)	103
4.9.7	Deformation vs. actual tie bearing pressure at early cycles (west)	104
4.9.8	Deformation vs. actual tie bearing pressure at middle cycles (west)	104
4.9.9	Deformation vs. actual tie bearing pressure at later cycles (west)	105
4.9.10	Deformation vs. actual tie bearing pressure at early cycles (east)	105
4.9.11	Deformation vs. actual tie bearing pressure at middle cycles (east)	106

4.9.12	Deformation vs. actual tie bearing pressure at later cycles (east)	106
4.10.1	LWD reading locations	108
4.10.2	CBR vs. depth	109
4.10.3	Tell-Tales locations (not to scale)	110
4.10.4	Grain size distribution of ballast	111
4.10.5	Grain size distribution of ballast under the tie	112

List of Tables

Table	Caption	Page Number
3.1	ASTM Standards	16
3.2	Atterberg Limit	18
3.3	Unconfined compression tests on subgrade	19
3.4.1	BNSF Specification Limits (class 1)	27
3.5	Sieve Analysis for Ballast	29
4.1.1	Loading information for unreinforced test	37
4.4.2	Pressure cells vs. pump pressure at subgrade level (unreinforced test)	68
4.4.3	Pressure cells vs. tie bearing pressure	69
4.5.1	Loading information for reinforced test	70
4.8.1	Pressure cells vs. pump at subgrade level	92
4.8.2	Pressure cells vs. tie bearing pressure (reinforced)	94
4.9.1	Comparison between unreinforced and reinforced test for unit weight and number of cycles.	95
4.9.2	Comparison of settlement between the reinforced test and unreinforced test (west string pot)	97
4.9.3	Reinforced loading vs. unreinforced loading	98
4.9.4	Comparison of settlement between reinforced test and unreinforced test (East string pot).	100
4.10.1	LWD results	106
4.10.2	Tell-Tales reading	109
4.10.3	Compression of ballast after the test	111

Chapter One

Introduction

Railroad ballast consists of open graded crushed stone used as a bed for railroad track to provide stability. It plays a significant role in providing vertical and lateral support for the track base and distributing the load to the weaker subgrade below. Ballast also helps with drainage, which is an important factor for any type of transportation structure, including railroads. This issue has become more acute as heavier car loads place more demand on track structure than in the past.

Over time ballast degrades and loses its strength. Fouling of ballast with fines has been a major issue of railway engineering. Fouling can be caused by breaking down or by contamination or upwards migration from the subgrade.

Five sources of fouling have been identified as follows: ballast breakdown; infiltration from the ballast surface; sleeper (tie) wear; infiltration from underlying granular layers; and subgrade infiltration (Selig and Waters 1994). Major causes of ballast fouling include tamping and undercutting procedures, repetitive loading and vibration from trains, and contamination from both above and below the ballast level (Collingwood et al 1988).

The specific area of research addressed in this thesis is extension of the life of ballast by limiting fouling of the ballast and improving performance. Development of an effective method for extending the ballast life cycle would have significant value. The research in this thesis focused on how to reinforce ballast using geogrids to reduce fouling. Having a stable reinforced

section would help reduce the number of maintenance actions required to keep the railroad in good repair.

Track maintenance operations are very time consuming and costly. Track maintenance can cost between 26 and 80 thousand dollars per mile of track (Zarembski and Cikota 2008). In addition, trains have become much heavier and faster than in the past, while the majority of the track condition has not been substantially improved.

An increase of high-speed rail (HSR) in United States would most likely increase track maintenance cost. Therefore research that would help in reducing this cost would be beneficial. As mentioned before the amount of maintenance required would decrease if fouling in the ballast were reduced (HAL Revenue Service Testing Update: Eastern Mega Site 2006).

Geosynthetics are very durable polymeric products being used in different civil engineering applications in order to provide strength, stability, and durability. Use of geosynthetic materials has become more and more common in the past 40 years for a number of applications and they have the potential to reduce the cost of maintenance by increasing the design life. Geosynthetics could be categorized into eight different products as follows: geotextiles, geogrids, geonets, geomembranes, geosynthetic clay liners, geofoam, and geocells.

Geocells are three-dimensional honeycomb shape product made of high-density polyethylene (HDPE). The United States Army Corps of Engineers used geocells for providing lateral confinement to the granular material during the 1970s (Webster, 1979). Examples of geocells are shown Figure 1.1 and 1.2.

Figure 1.1 Placing geocell in the field Figure 1.2 Filling geocell

Geogrids are a flexible polymeric product, consisting of sets of parallel tensile ribs used in civil engineering for their major five functions: separation, reinforcement, filtration, drainage, and containment (Koerner 1998).

The primary potential advantage of geogrids is to extend the maintenance cycle through reinforcement of the ballast. It could also reinforce the sub-ballast which increases the bearing capacity of soft subgrade.

Figure 1.3 Placement geogrid under railroad track

Chapter Two

Literature Review

Degradation of ballast in railway engineering has long been an issue because it can lead to misalignment of the rails. Several factors, such as number of load cycles, gradation of aggregates, track confining pressure, and angularity and fracture of individual grains of ballast can cause ballast degradation and deformation.

Some studies have been published regarding reinforcement of ballast with geogrid, which is a geosynthetic. A summary of selected previous research is provided in this chapter.

2.1 Fouling ballast

Tumkur et al (2008) Fouling of ballast in the railroad industry occurs as the voids within the ballast are filled with finer particles. Accumulation of coal dust in ballast is a primary concern for railroad engineers. In this paper several tests such as Atterberg limits, specific gravity, moisture-density relationships (Proctor), and shear strength were conducted to determine coal dust mechanical and physical properties. After mixing ballast with coal dust at a series of different moisture contents, and coal dust weight percentages, it was found that it takes about 25% coal dust by weight to fill up all the voids in ballast, given a void ratio for the ballast of 43%. Also when the ballast was fully fouled with coal dust with a 35% moisture content, it was determined that the friction angle of ballast was approximately the same as friction angle of coal dust. The study found that under this condition the ballast particles will be separated by coal fines as shown in Figure 2.1 which can result in the track misalignment.

(a) Clean Ballast (b) dirty ballast with fine particles filling voids (c) fouled ballast with aggregate to aggregate contact lost

Figure 2.1 Critical ballast fouling and illustration of loss of aggregate to aggregate contact (Tumkur et al 2008).

2.2 Stiffness of geocell material

Mengelt et al (2000) and Mengelt et al (2006) This paper focused on the resilient modulus of coarse-grained soil (gravel & sand) and fine-grained soil (silty & clay). An increase in resilient modulus was found using single geocell reinforcement for both soil types; however only the improvement of resilient modulus for the case of fine grained soil was significant. Resilient modulus increased by only 1.4–3.2% when the infill was coarse-grained, but increased by 16.5–17.9% when the infill was fine-grained

As the subgrade stiffness increased, the ultimate bearing capacity of reinforced sand was observed to increase. Reinforcement provided very good improvement of resistance to repeated loads**.**

2.3 Load carrying capacity

Emersleben & Meyer (2005). Investigated the vertical stress distribution on an artificial mixed soil called " Glyben" used to simulate soft subgrade material. Three different vertical loads (200 kN/m^3, 300 kN/m^3 and 400 kN/m^3) were applied on the base. The vertical stress on glyben subgrade, unreinforced sand and geocell reinforced sand were measured. The reinforced soil had higher stiffness and also the stress on subgrade was reduced between 30% and 36% depending on the applied load. The test results also showed that for the unreinforced case, stresses were concentrated more directly beneath the load plate while for the reinforced case stresses were distributed over a larger area as shown in figure 2.3. This result indicates that geocell layer acts like a stiff mat and distributes the footing load over a larger area, thus reducing the vertical stresses directly beneath the load plate (Emersleben & Meyer 2005).

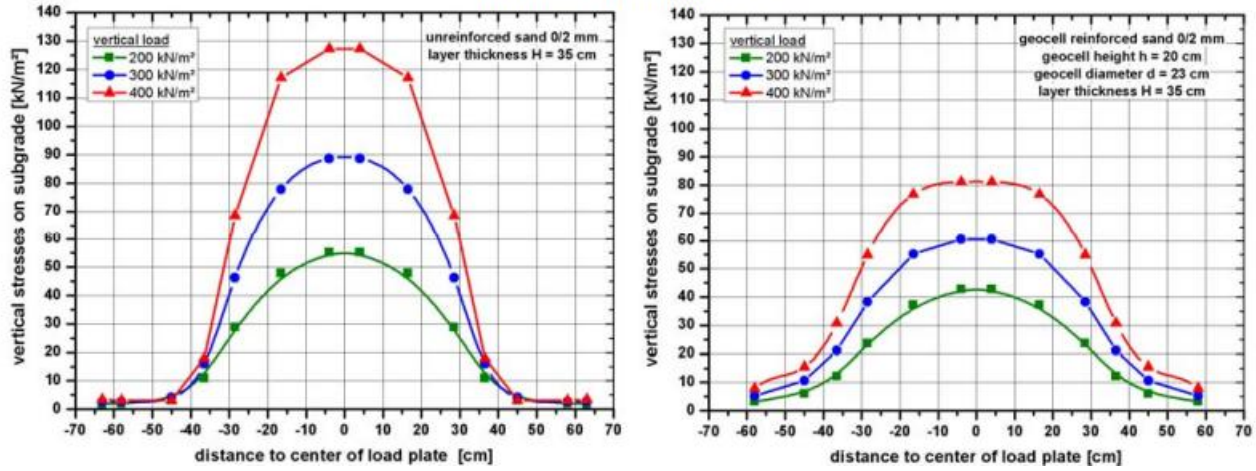

Figure 2.3 Measured vertical stresses on subgrade, unreinforced sand (l) and geocell "typ1" reinforced sand (r).

2.4 Improving poor track formations using geosynthetics

Kea et al (2007). Showed that shrinkage and swelling of a clay subgrade would result in both upward and downward movement of the rail profile. Geocell reinforcement provides tensile strength as well as shear strength. It also has a major effect on increasing the bearing capacity of the subgrade. Geotextiles were also used to prevent migration of fine particles in to ballast. Figures 2.4 through 2.7 show the construction process.

Figure 2.4 Placing geotextile sheet

Figure 2.5 Placing geocell

Figure 2.6 Placement of soil in geocell

Figure 2.7 Placement of soil in geocell

2.4.1 Geosynthetics for improving poor track formations

Hannes Grabe (2010). Laboratory work shows a significant stress reduction on the subgrade for different depths to the top of treatment. Stress reductions observed for series of products are shown in Figure 2.8.

Products	Depth mm		
	200	400	600
Geotextiles			
GT1	51%	61%	87%
GT2	22%	52%	83%
Geogrids			
GG1	54%	34%	66%
Geocells			
GC1	24%	5%	24%
Gc2	25%	5%	85%
GC3	1%	16%	96%
GC4	34%	53%	93%

Figure 2.8 Stress reduction (reproduced from Grabe, 2010)

2.5 Stabilizations of ballasted rail tracks

Indraratna et al (2006) conducted a series of tests to measure the settlement, vertical strain, and lateral strain of reinforced (geogrid-geotextile) recycled ballast in wet and dry conditions. The usage of geogrid-geotextile showed an increase in the bearing capacity and resilient modulus of recycled ballast. The results also indicated a decrease in degradation and lateral movement of ballast. A finite element analysis was conducted to determine the optimum depth at which the geosynthetics is the most effective. It was found that optimum depth for geosynthetics is in the range of 150 to 200mm beneath the ties.

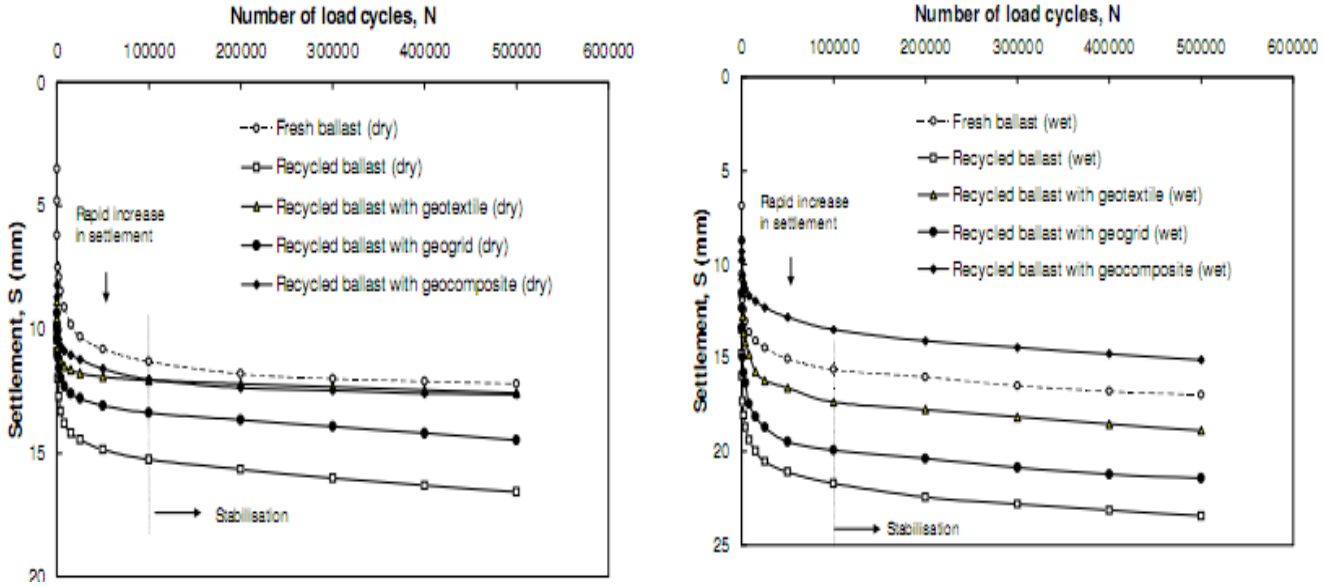

(a) Dry Samples (b) Wet Samples

Figure 2.9 Effect of geosynthetics on the settlement of ballast (Indraratna et al.,2004)

2.6 Use of geosynthetics in railways including geocomposites and vertical drains

Buddhima Indraratna et al (2011) conducted series of tests using fresh ballast , recycled ballast, fresh ballast with geocomposite, and recycled ballast with geocomposite. The geocomposite was used between the sub-ballast and ballast interface. Figure 2.10 shows a reduction in average vertical deformations of recycled ballast at a large number of cycles when reinforcement is used.

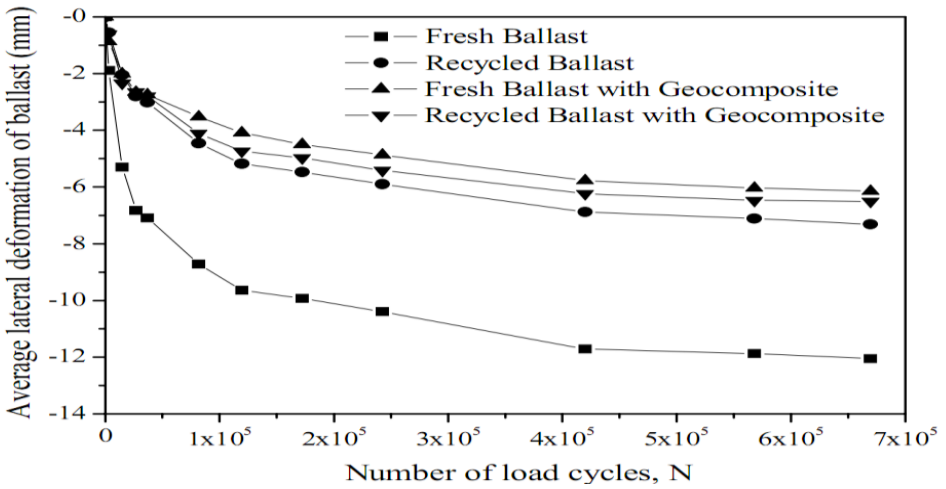

Figure 2.10 Vertical deformation of the ballast layer (modified after Indraratna et al., 2010 a)

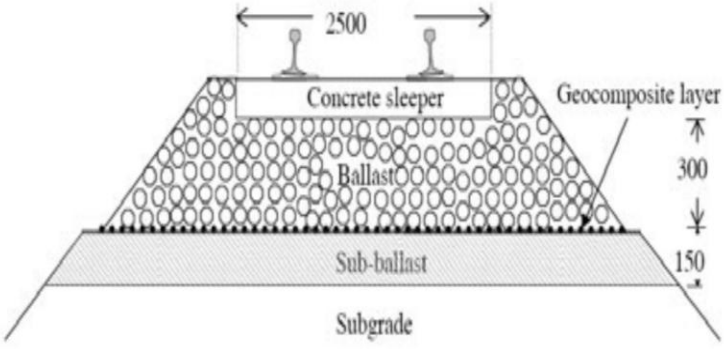

Figure2.11 Section of ballasted track bed with geocomposite layer (modified from Indraratna et al. 2010b)

Chapter Three

Research Scope

This chapter contains summaries of the test setup, instrumentation and scope of material testing of subgrade and ballast.

3.1 Test section design

A full-scale railroad section five feet in length was constructed with and without geogrid reinforcement.

Figures 3.1 and 3.2 illustrate how the lab test sections were constructed. A full-scale trapezoidal cross section of a railroad was built which consisted of a 2 ft deep subgrade that was 4.5 ft wide from centerline of the trapezoid on each side at the top and sloped down on 2:1 slope. The subgrade was covered with 2 feet of ballast 9 feet wide at the top and sloped down on both sides on 2:1 slope. Additional subballast was added at 1.5:1 slope to prevent sieving a large amount of ballast on the sides as shown in Figures 3.1, 3.2 and 3.3.

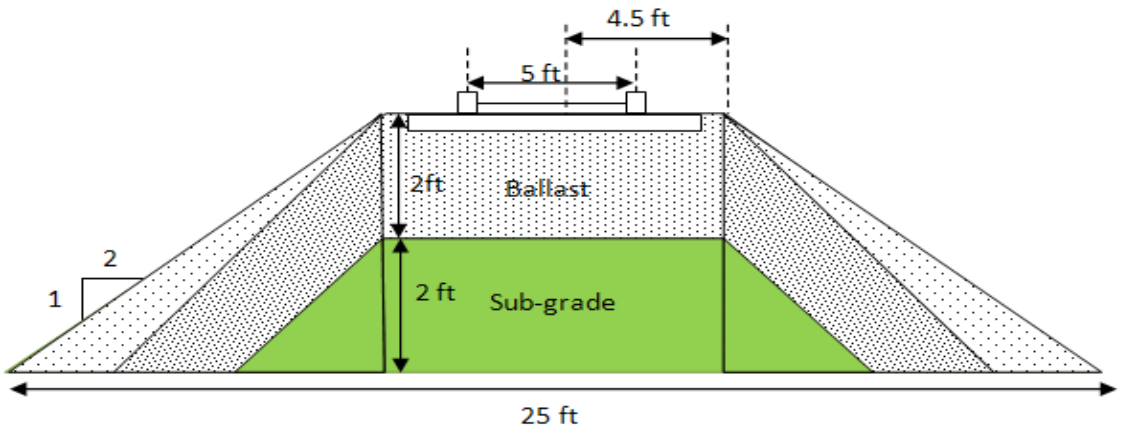

Figure 3.1 Schematic of the unreinforced railroad cross section (not to scale)

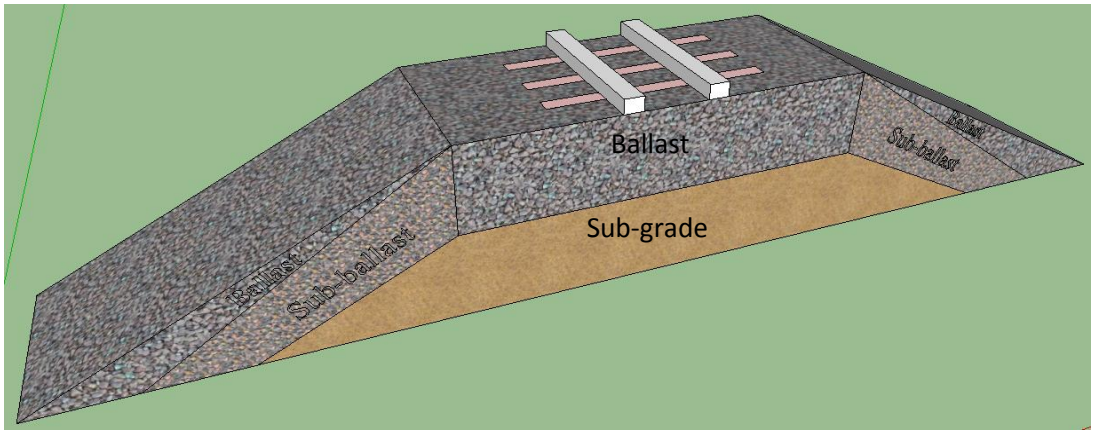

Figure 3.2 3-D view of the test section (not to scale)

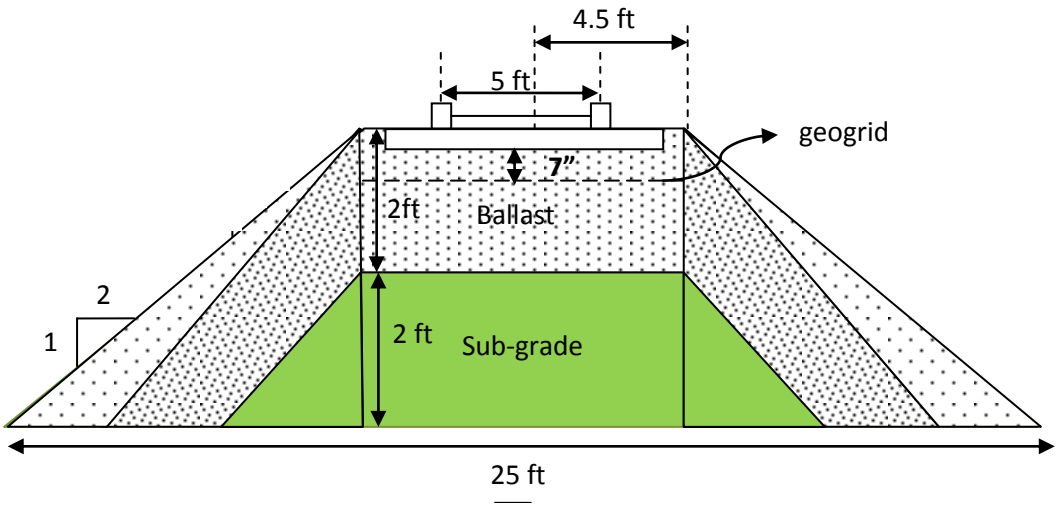

Figure 3.3 Schematic of the railroad cross section (not to scale)

3.1.1 Loading frame

A self-reacting loading frame with a 100,000 lb capacity was constructed and is shown in Figure 3.4. The inside column spacing is 9.5 ft and the clearance between the bottom of the overhead beam and slab is 13 ft. Three reinforced 3 by 5 ft concrete slabs were built and post-tensioned together to construct the self-reacting loading frame. Figure 3.5 shows the loading cylinder with maximum capacity of 104000 lb.

Figure 3.4 Loading frame

Figure 3.5 Loading cylinder

3.1.2 Wooden frames

Two 28 ft long (14’ from center line) wooden frames were added as shown in Figure 3.6 to restrain deformation in the longitudinal direction.

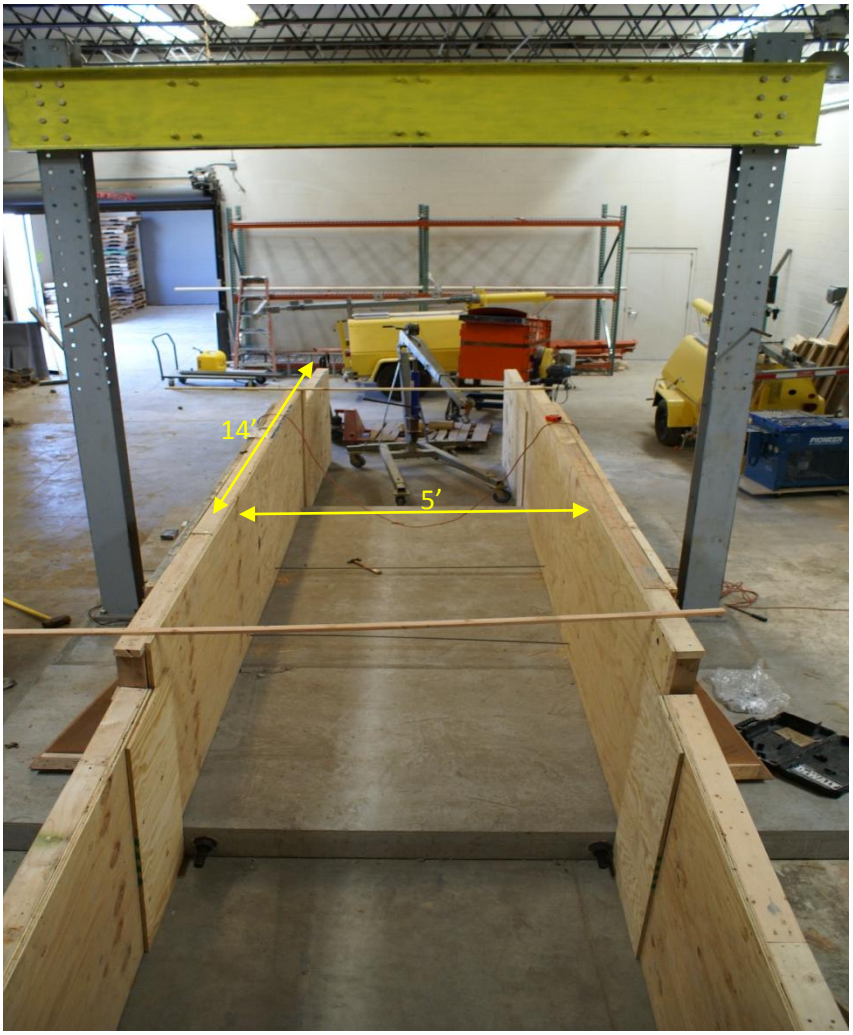

Figure 3.6 Wooden frames

3.2 Subgrade

The source of the subgrade was the yard in front of Learned Hall on the main campus of KU. The soil was characterized in accordance with the tests listed in Table 3.1. The grain size distribution of the subgrade soil is shown in Figure 3.7.

Table 3.1 ASTM Standards

ASTM Standards	Lab Tests
D422.2703-1	Hydrometer Analysis
D2166.14900-1	Unconfined Compression
D3080.2626-1	Direct Shear
D4318.3420-1	Atterberg Limits
D2216-267-1	Moisture Content
D698.23713-1	Proctor Test
D6951/D6951M	DCP Test

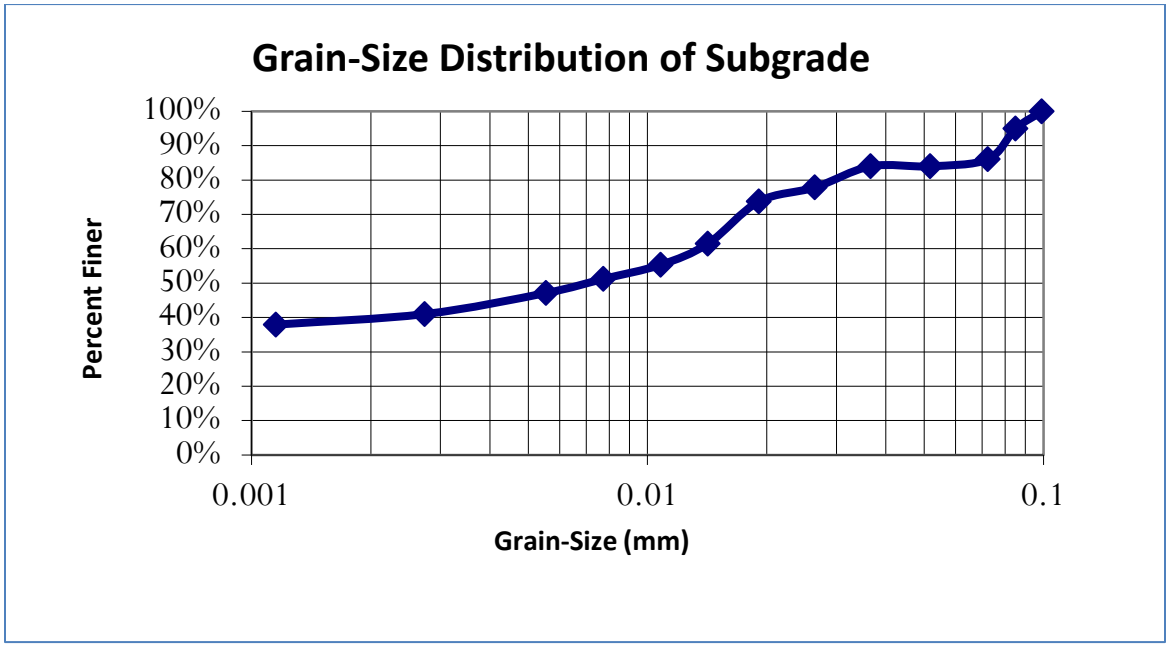

Figure 3.7 Grain size distribution for subgrade

The sub-grade had an optimum moisture content of 23% and maximum dry density of 99.5 lb/ft^3. Figure 3.8 shows the compaction test curve. Results of Atterberg limits testing are shown in Figure 3.9 and Table 3.2. Based on the Atterberg limits and grain size distribution the soil was classified as fat clay (CH).

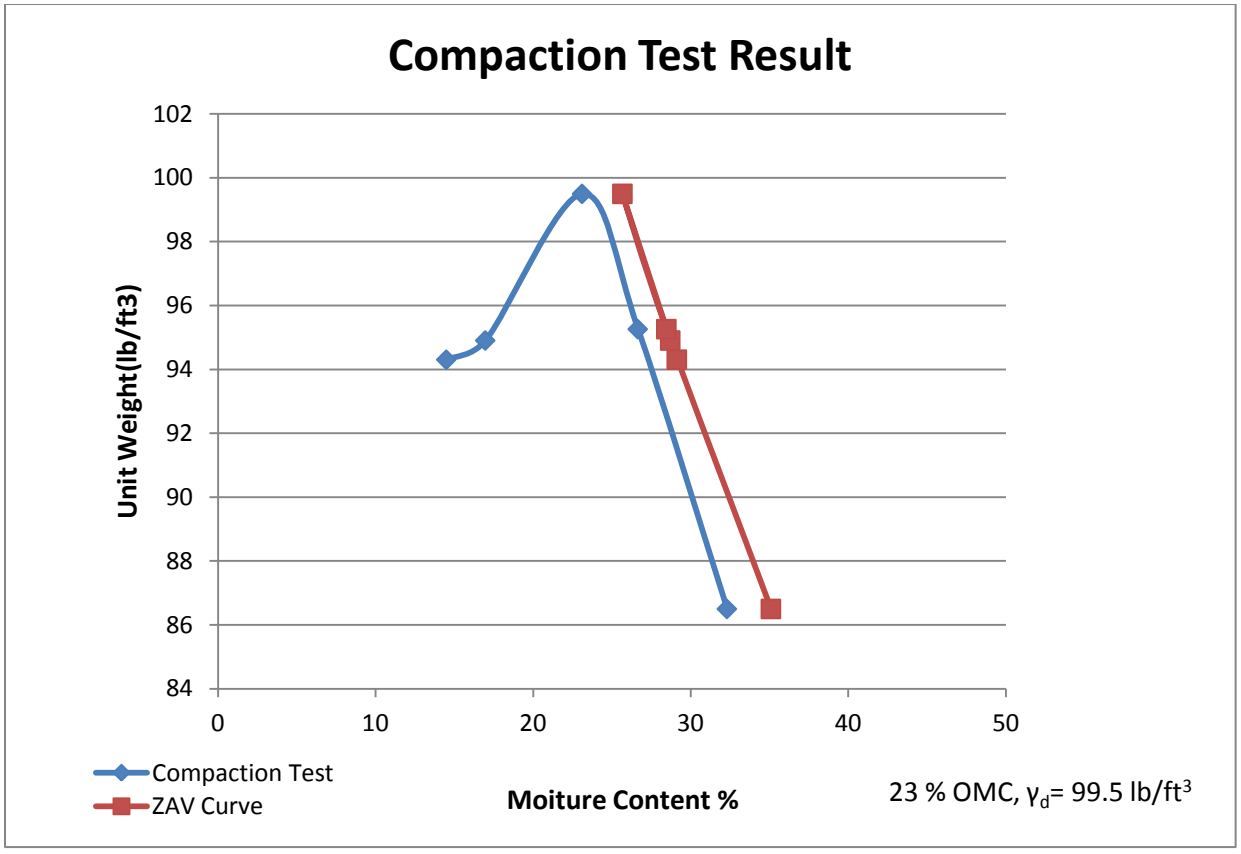

Figure 3.8 Standard proctor compaction curve of the subgrade

Table 3.2 Atterberg Limit

PL=	21
LL=	52
PI=	31

High plasticity clay

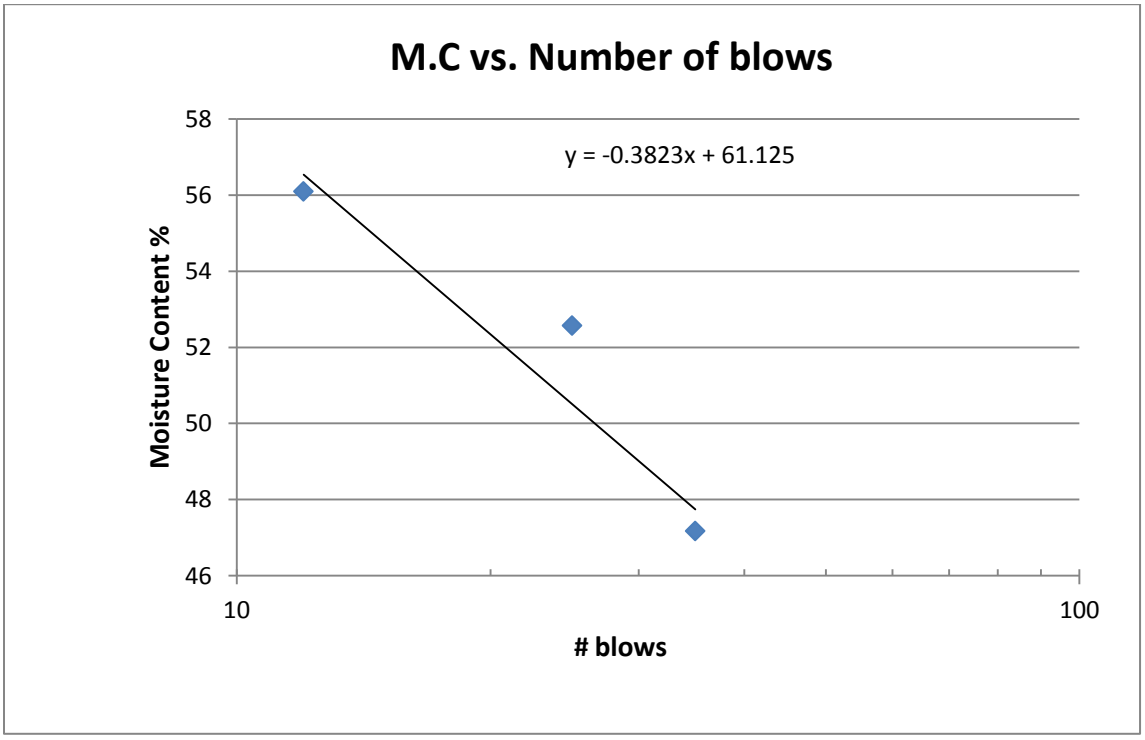

Figure 3.9 Standard Atterberg limit test curve of the subgrade

Unconfined compression tests were conducted to determine the undrained shear strength (Su) of the subgrade. The results are presented in Figure 3.10.

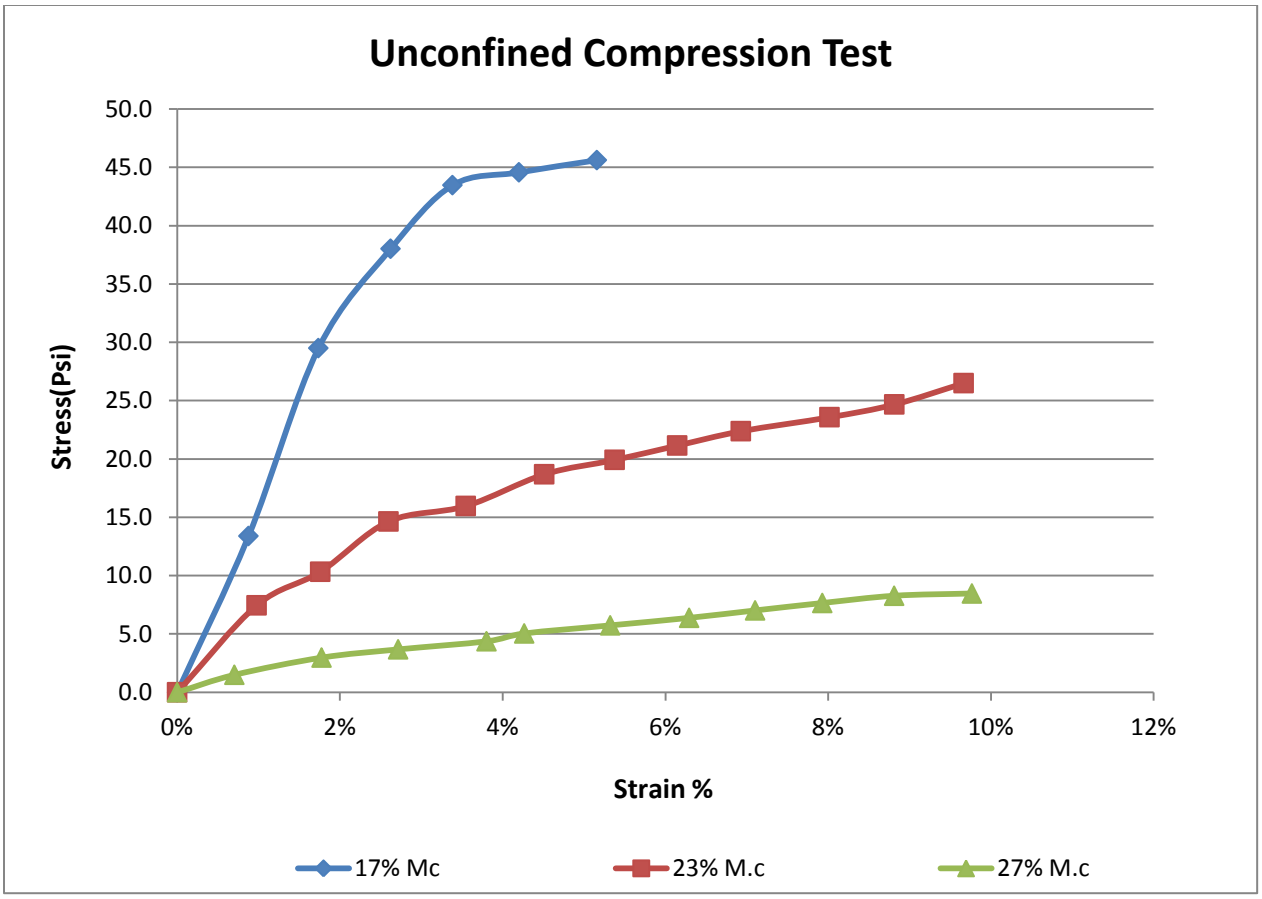

Figure 3.10 Unconfined compression test curves

Table 3.3 Unconfined compression tests on subgrade

Length (in)	Area (in^2)	Mass (lb)	Moisture (%)	q_u (psi)	$S_u=q_u/2$ (psi)	$S_u=q_u/2$ (psf)
2.79	1.343	0.255	19.15	45.45	22.73	3272
2.813	1.341	0.275	22.7	26.93	13.47	1939
2.714	1.335	0.25	28.5	8.78	4.39	632

As shown in Figure 3.11, the subgrade was placed with a skid loader in 6 inch lifts. Each lift was compacted with a vibratory plate compactor as shown in Figure 3.11. Unreinforced and reinforced sections were compacted at 26% moisture content and densities of 91.5 lb/ft^3 dry density and 93 lb/ft^3 dry density respectively.

Figure 3.11 Placing subgrade and compaction

3.3 Instrumentation

3.3.1 Tell-tales

Figure 3.13 Tell-tale

Tell-tales are used to measure vertical deformation in soil profiles at selected depths. As the load is applied to the section, the base plate and the interior pipe move with the soil at the base plate elevation.

The exterior pipe minimizes interference from the soil or ballast above the base plate.

Two tell-tales were set at the subgrade interface with ballast and the other two were set 7 inches below the ties in the unreinforced and reinforced testss. Locations of tell-tales are shown in Figure 3.14.

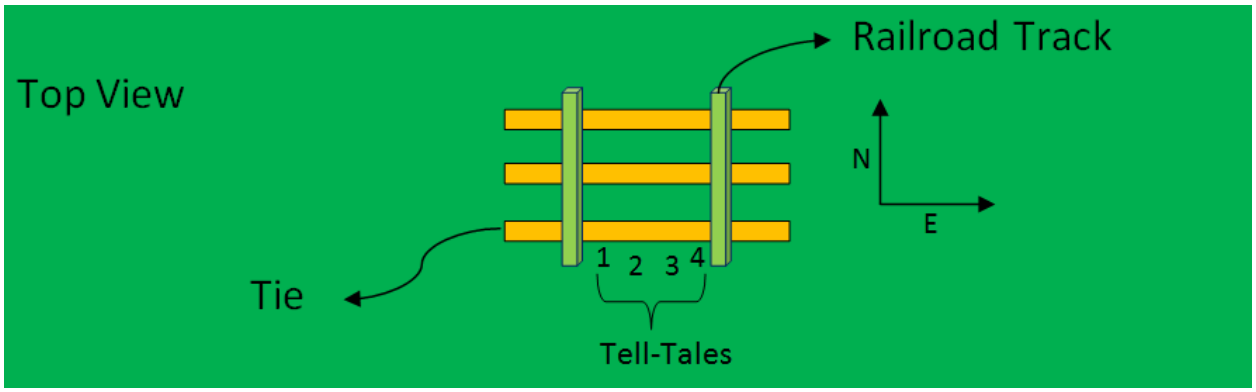

Figure 3.14 Locations of tell-tales

3.3.2 Pressure cells

Model 3515 Geokon pressures cells are heavy duty cells and recommended for railroad applications. Five pressure cells were placed between the subgrade and ballast right beneath the

railroad ties as shown in Figures 3.14 and 3.15. These earth pressure cells have a diameter of 9” and a capacity of 58 psi.

Figure 3.15 Model 3515 circular earth pressure cells during placement

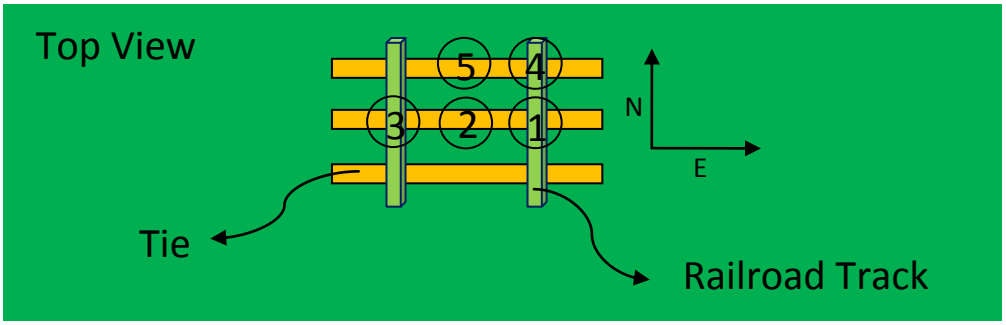

Figure 3.16 Pressure cell locations (not to scale)

3.3.4 Displacement transducers

A total of four displacement transducers were used to instrument the corners of the track panel as shown in Figure 3.17. The displacement transducers were manufactured by Tokyo Sokki Kenkyujo, Co., Ltd., Japan. Two types of displacement transducers, the CDP-100 (100 mm capacity) and CDP-50 (50 mm capacity), were used to measure the surface displacement of railroad track.

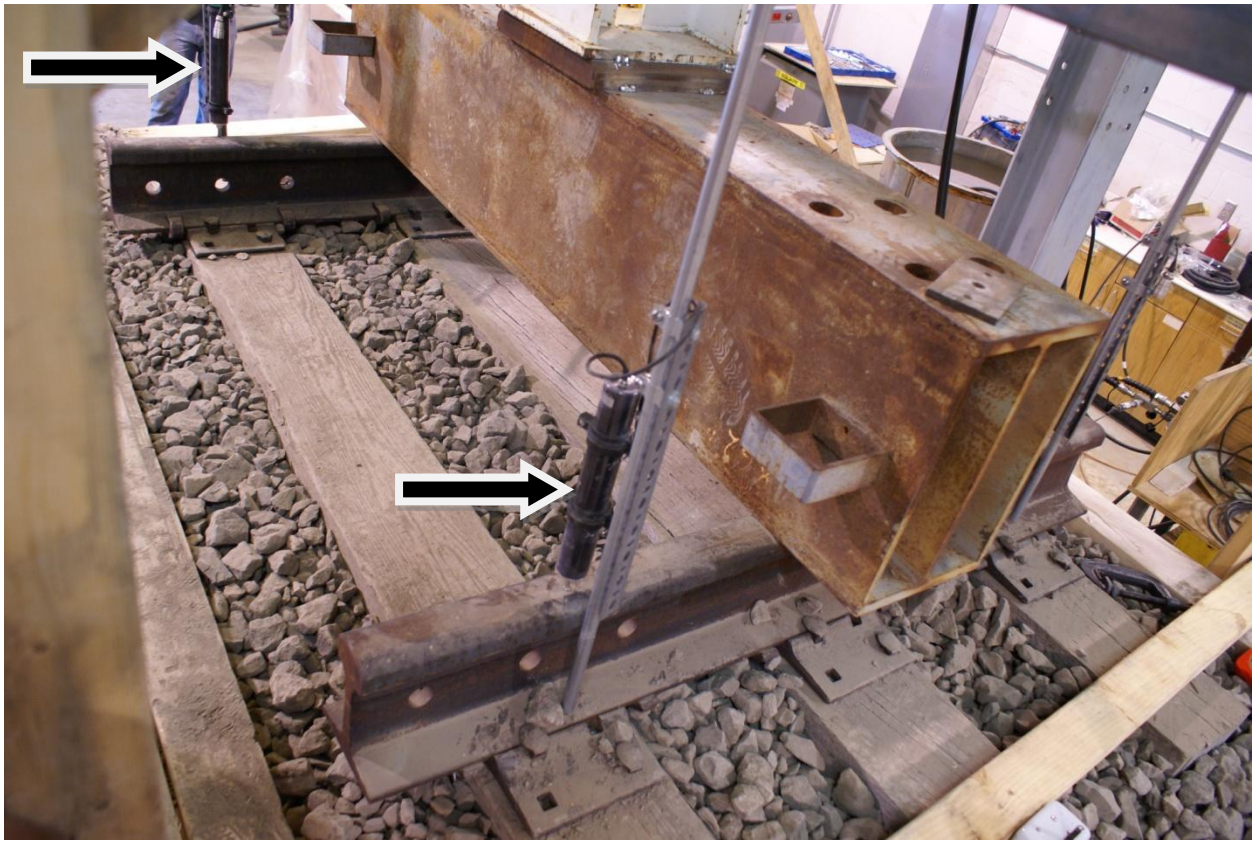

Figure 3.17 Displacement transducer placement

3.3.5 String pots

Two String potentiometers (string pots) with a maximum range of 20 inches were used to measure the displacement of center ties in the railroad section as shown in Figure 3.18.

Figure 3.18 String pot

3.4 Ballast

Recycled Ballast was provided by the BNSF and came from track undergoing maintenance in Gardner, Kansas. It was sieved to remove fouling material and to meet the gradation size of BNSF specification limits (class 1) reported in Table 3.4.1. A picture of the sieved material is shown in Figure 3.19. This ballast is composed of heterogeneous igneous rock. Figure 3.20 presents the washed rock.

Figure 3.19 Recycled ballast after sieve

Figure 3.20 Washed rock

3.4.1 Sieve analysis of ballast:

Table 3.4.1 BNSF Specification Limits (class 1)

Sieve Analysis (ASTM C 136)	
Sieve Size	**BNSF Specification Limits (class 1)**
2 .5 "	100
2"	90-100
1.5"	50-80
1"	10-35
0.75"	0-10
0.5"	0-5

Recycled ballast was sieved with a sieve shaker provided by BNSF as shown in Figure 3.22 to meet the BNSF Specification limits on gradation size.

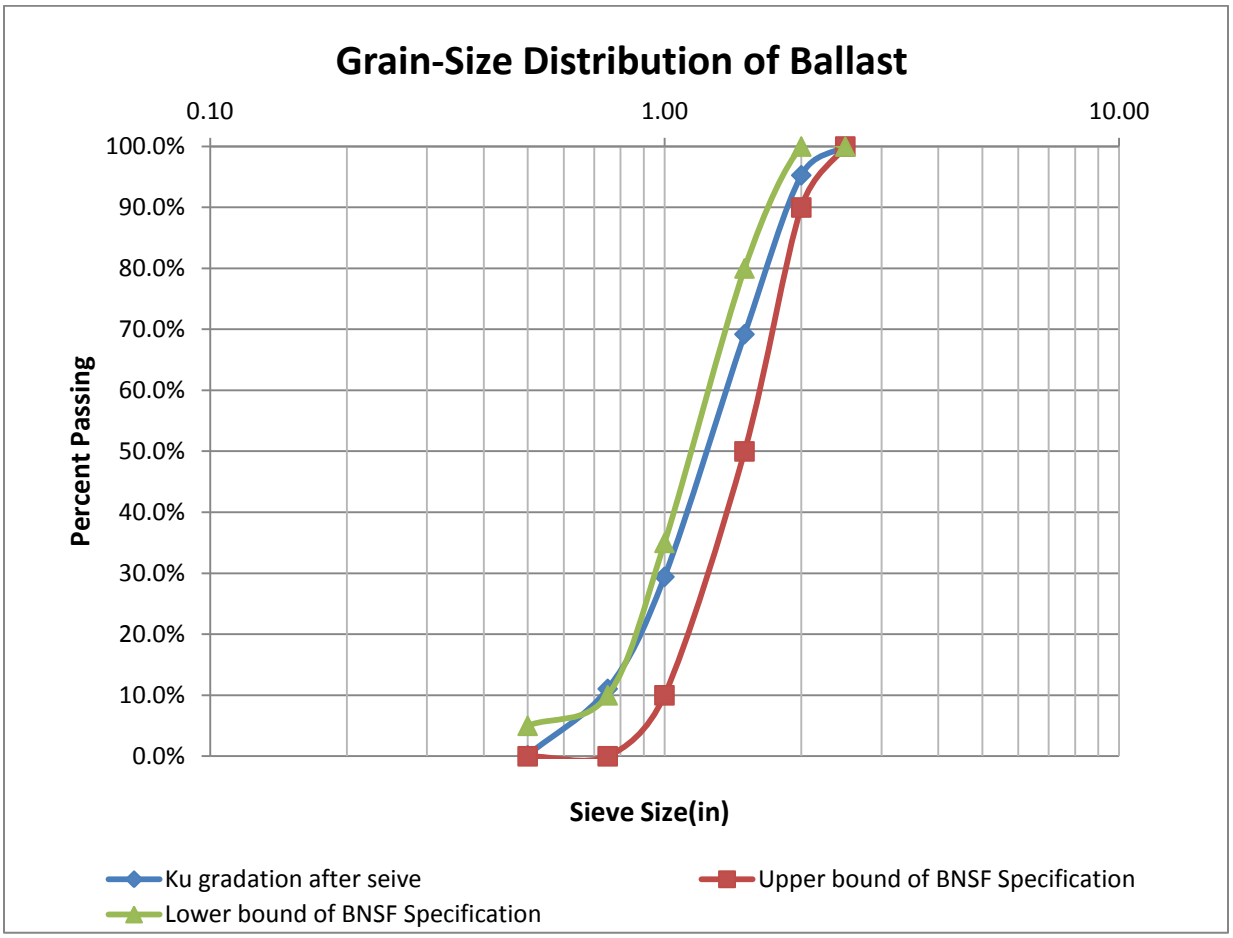

Figure 3.21 Sieve Analysis for ballast.

Table 3.4.2 Sieve Analysis for Ballast

Sieve Opening	Mass Clean Sieve (lb)	Mass Sieve and Soil (lb)	Mass Retained (lb)	% Mass Retained	Cumulative % Retained	% Passing
2.50	22.38	22.38	0	0.0	0.0	100.0
2.00	17.54	20.38	2.84	4.7	4.7	95.3
1.50	21.14	36.84	15.7	26.1	30.8	69.2
1.00	18.3	42.26	23.96	39.8	70.6	29.4
0.75	21.3	32.36	11.06	18.4	88.9	11.1
0.50	22.38	28.94	6.56	10.9	99.8	0.2

Figure 3.22 Sieve shaker for ballast

All sizes were within the range gradation sizes recommended by BNSF except for the 0.75 inch material, which exceeded the limit by 1%. After review, it was the judgment of KU and BNSF

that the sieved ballast was essentially consistent with their specifications and would be accepted for use.

3.5 Track

A track panel five feet in length and with wooden ties(7” x 9” x $8\frac{1}{2}$ ’) was in the test set up as shown in Figure 3.23.

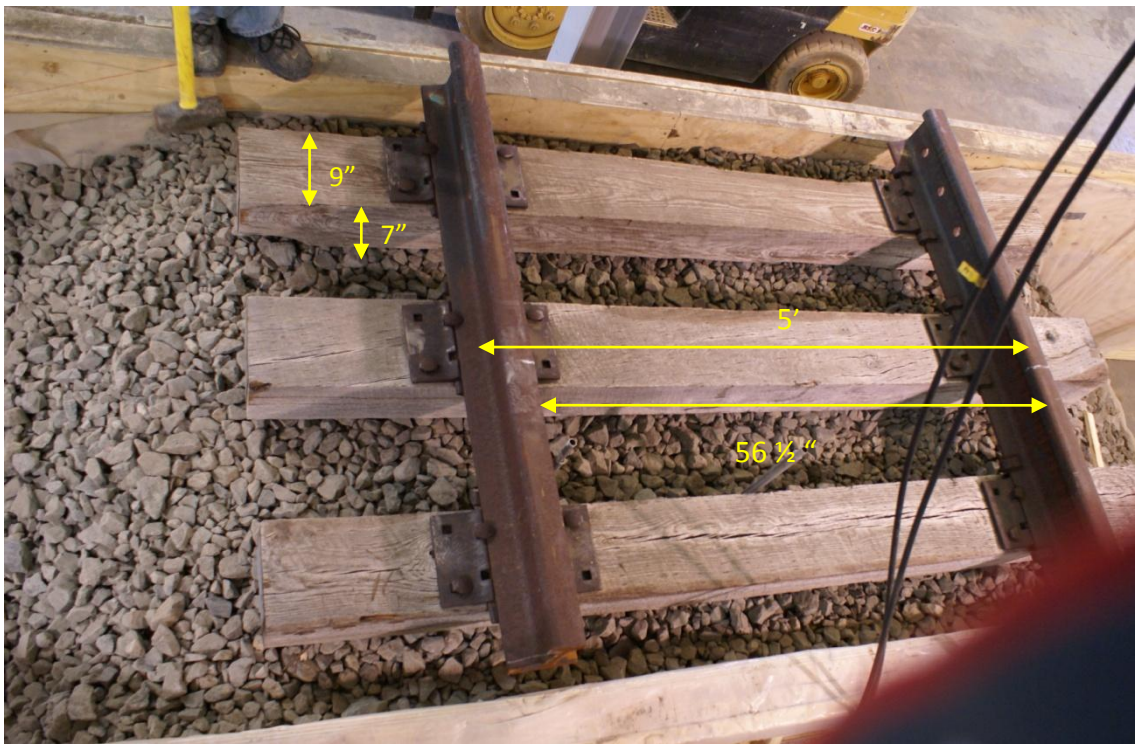

Figure 3.23 A Wooden tie track panel

3.8 Geogrid

Triaxial Geogrid (TX190LA) provided by Tensar Int. Corporation was used to reinforce the ballast section in the reinforced test.

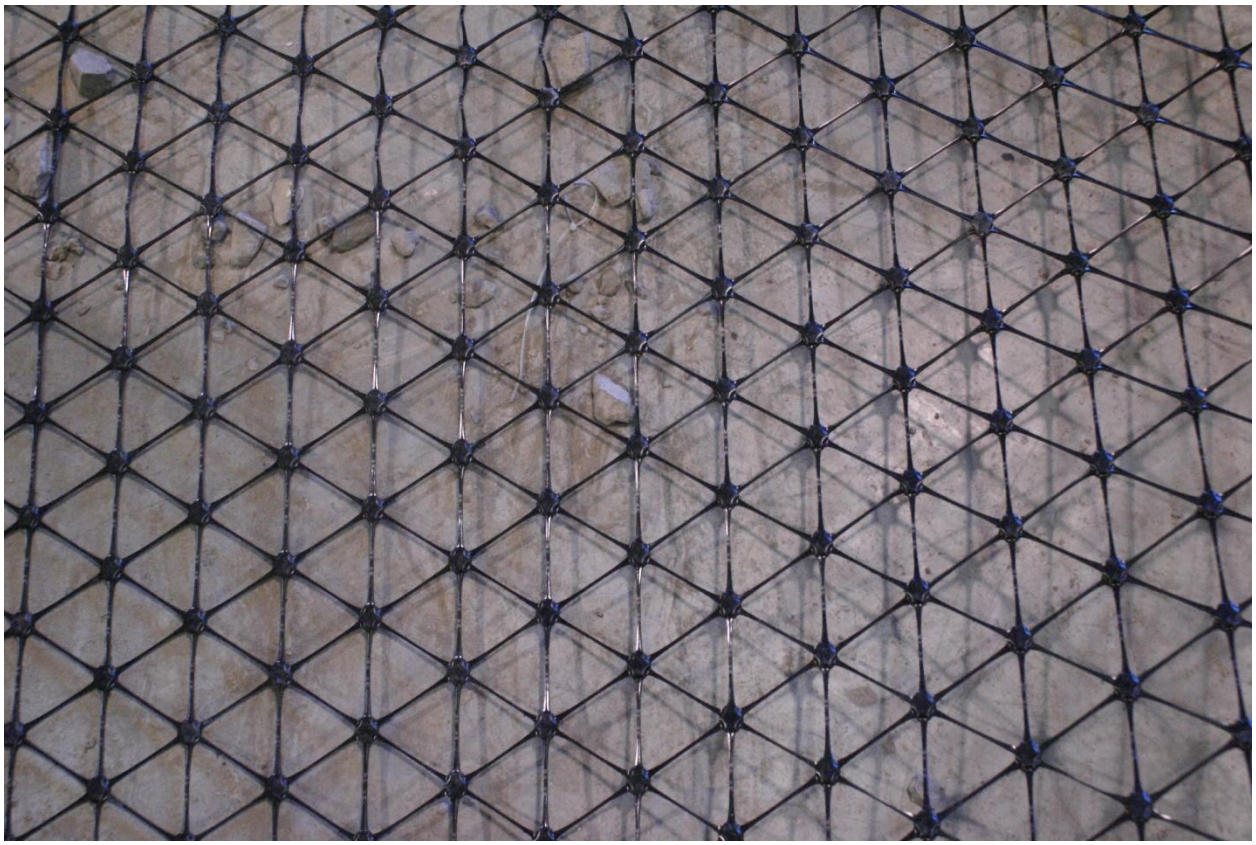

Figure 3.24 Triaxial geogrid used in reinforced test

3.9 Quality control tests

Three sets of quality control tests were performed before and after each test in order to verify the compaction quality, modulus, and CBR (DCP Index) of subgrade.

3.9.1 Light weight deflectometer test (LWD)

LWD is a test method for measuring deflection and compaction quality control during construction. There is acceleration sensor on the loading plate. LWD also measures the degree of compressibility and average settlement of the section. The LWD tests were carried out on the subgrade with the 30 cm plate since this plate is suitable for fine soil. This device has a 10 kg drop hammer with a drop height of 1 meter. In LWD device hammer is released which hits the plate. Acceleration is measured with time and a modulus is calculated based on the force required to generate a given deflection for that soil type. Figure 3.25 shows the LWD.

Fig 3.25 Light weight deflectometer

3.9.2 Density testing by drive tube

Drive tubes were used to determine the level of compaction of the subgrade as shown in Figure 3.18. The average dry unit weight for the subgrade based on an average of four samples was 91.5 lb/ft^{3}for the unreinforced test (92% of Proctor) and 93lb/ft^{3}for reinforced case (93% of Proctor).

Figure 3.26 Drive tube and sampler driver.

3.9.3 DCP (Dynamic Cone Penetrometer)

The DCP was used to measure the in-situ strength of subgrade before and after each test.

Results from DCP were then converted to CBR (California bearing ratio) values using the following correlation:

$$CBR\% = 292/(DPI)^{1.12}$$ DPI- (mm/blow)

Chapter Four

Test Results

Two dynamic loading tests were conducted on full scale railroad sections to investigate the effects of triaxial geogrid on reducing settlement and ballast degradation. The first test was conducted on an unreinforced control section. The second test was conducted with reinforcement using triaxial geogrid. Figure 4.1 shows the unreinforced section prior to placement of the track panel and Figure 4.2 shows the reinforced section with geogrid in place. Figure 4.3 shows the test setup with loading frame.

Figure 4.1 Unreinforced Test section

Figure 4.2 Geogrid after replacement in the reinforced test

Figure 4.3 Test during dynamic loading

4.1 Loading sequence for the unreinforced test

For this test dynamic loading was conducted in five steps (23194 lb, 53407 lb, 79116 lb, 97500 lb dry and 104000 lb soaked)

Table 4.1.1 Number of cycles, loading rate, loading sequences, target supply pressure, total load and tie bearing pressure

Load Step	cycles	Loading Rate(Sec/Cycle)	Target Supply Pressure(psi)	Total Load (lb)	Tie Bearing Pressure (psi)
1	79	5.5	1100	23194	9
2	116	7	2500	53407	21
3	52	19	3500	79116	31
4	100	21	4500 (dry)	97500	38
5	100	22	4500 (soaked)	104000	40

4.1.1 East string pot

Figure 4.1.1 shows the deformation with dynamic loading on the east side of the middle tie.

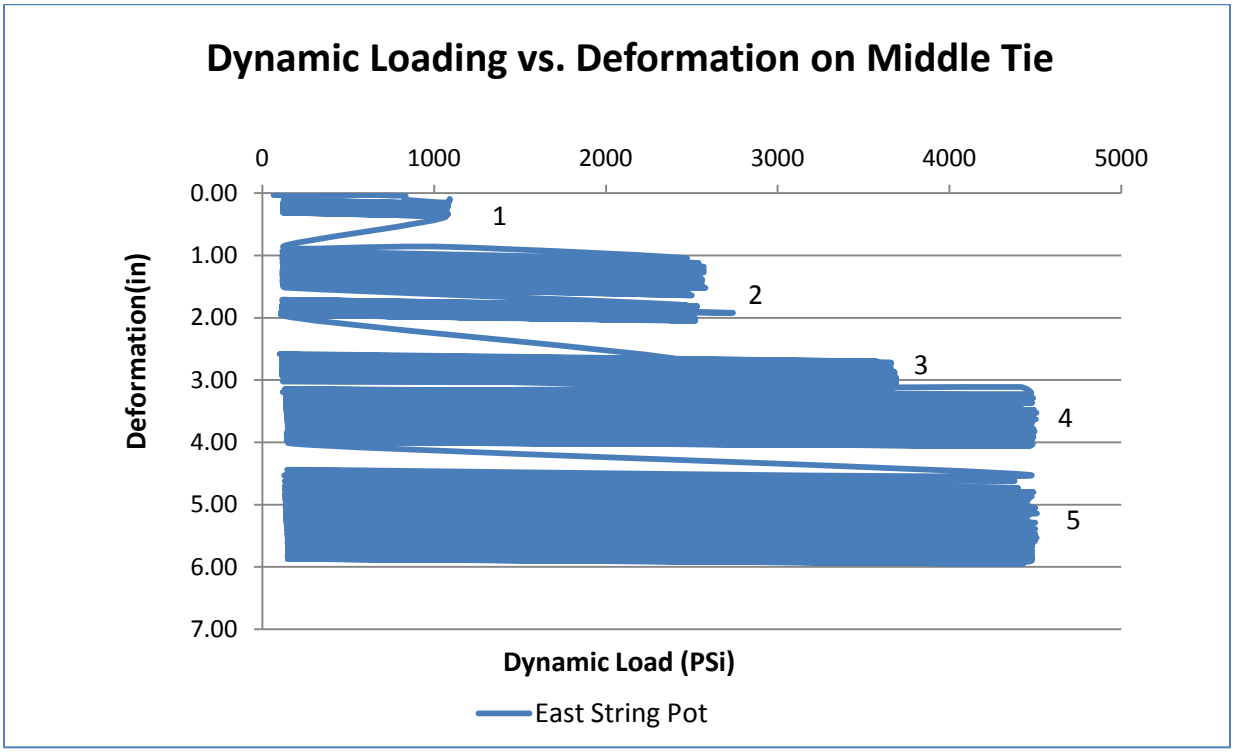

Figure 4.1.1 Dynamic loading vs. deformation. (East String Pot)

4.1.2 East string pot versus dynamic loading at 1100 psi (9 psi tie bearing pressure)

Seventy-nine cycles were applied on the railroad section at 1100 psi, resulting in a total accumulated deformation after seventy-nine cycles of 0.37 in. Figure 4.1.2 shows deformations (settlement) recorded by the East String Pot for a dynamic loading of 1100 psi.

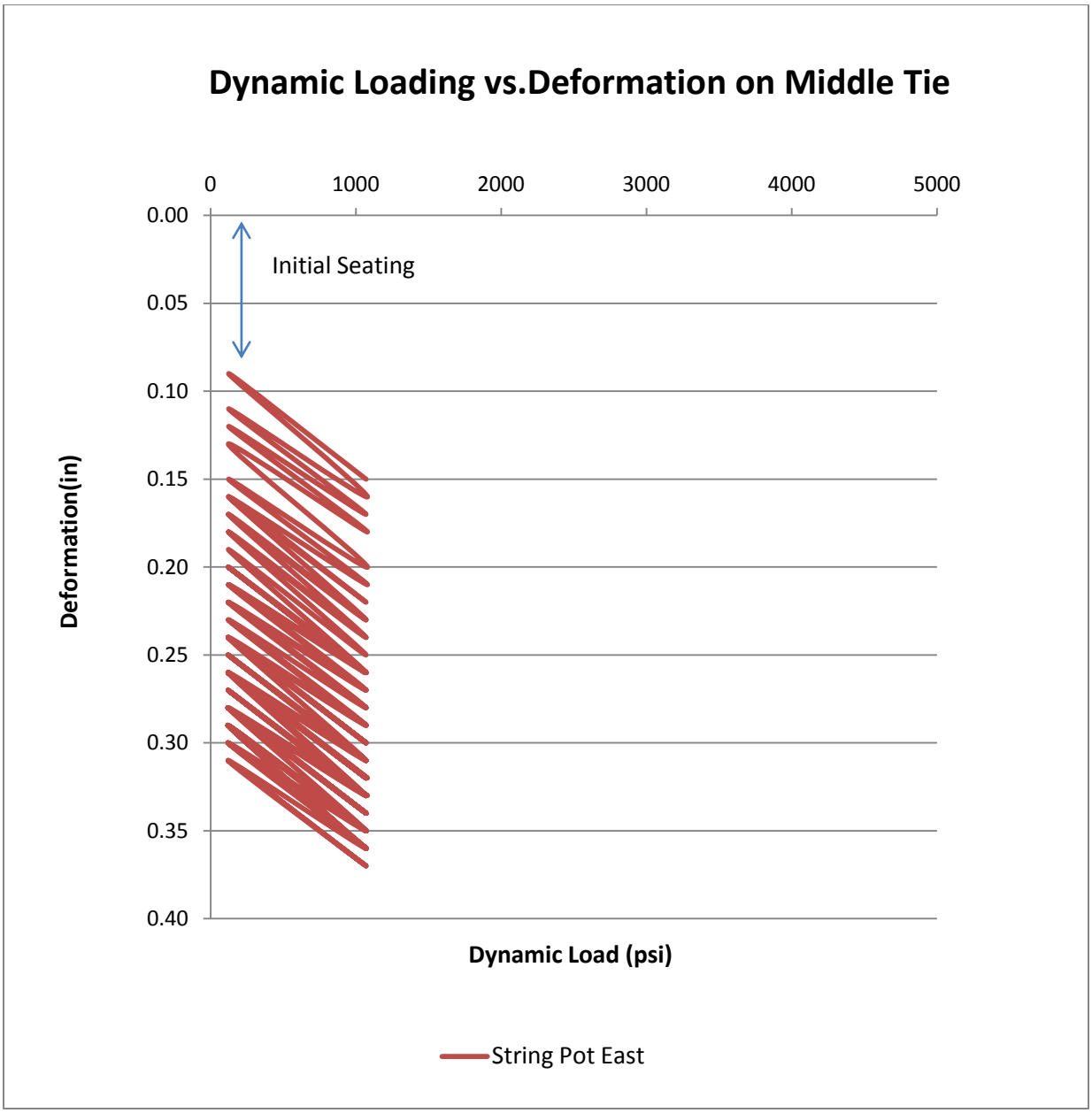

Figure 4.1.2 East string pot deformations versus dynamic loading at 1100 psi

4.1.3 East string pot versus dynamic loading at 2500 psi (21 psi tie bearing pressure)

One hundred sixteen cycles were applied to the railroad section at 2500 psi. The total accumulated deformation after one hundred sixteen cycles was 2.0 in. More permanent deformation was observed during the early cycles of each step. As number of cycle increased, a

higher percentage of the deformation was elastic. Figure 4.1.3 shows the East String Pot reading versus dynamic loading at 2500 psi.

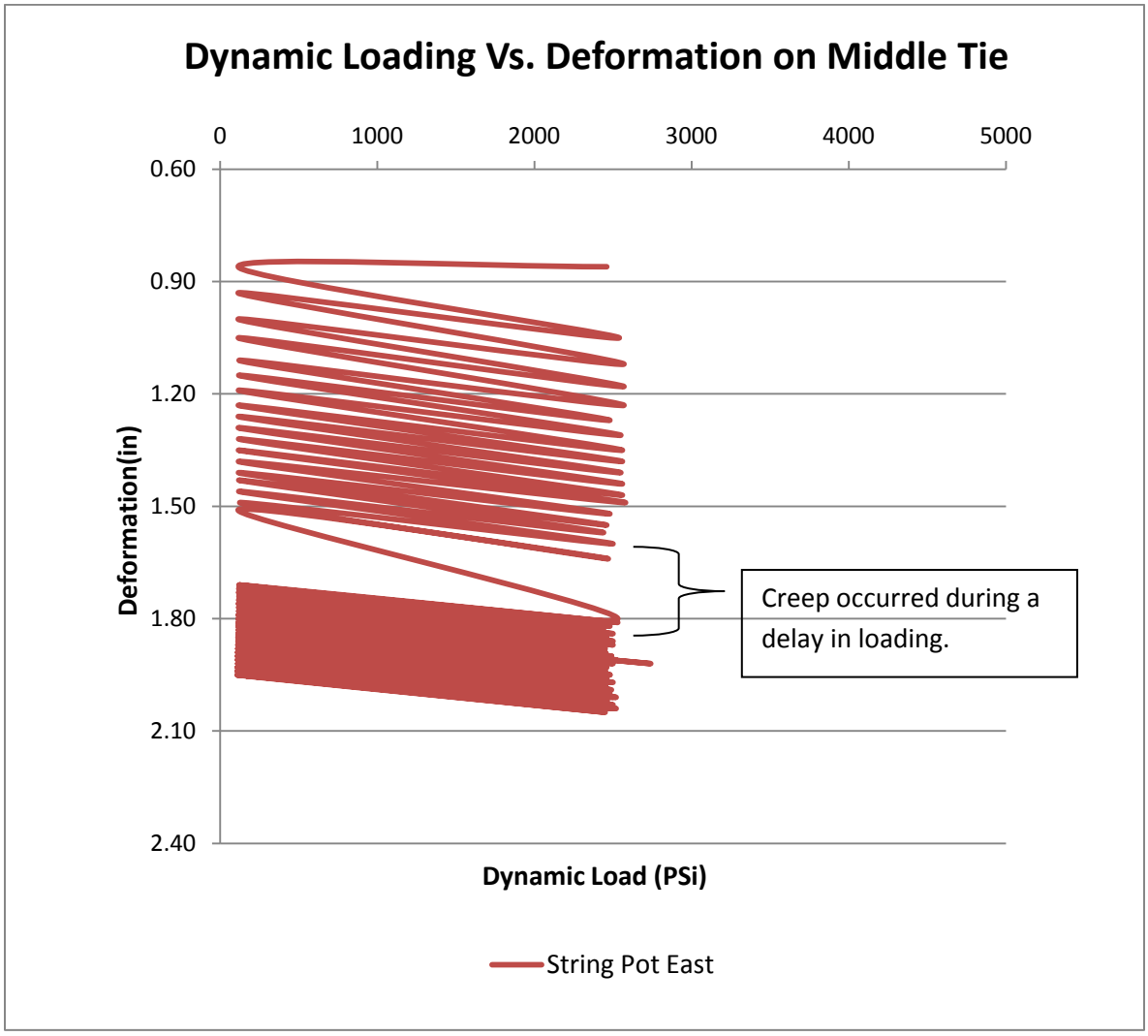

Figure 4.1.3 East string pot versus dynamic loading at 2500 psi

4.1.4 East string pot versus dynamic loading at 3500 psi (31 psi tie bearing pressure)

Fifty-two cycles were applied to the railroad section at 3500 psi for a total accumulated deformation after fifty two cycles of 3.05 in. Figure 4.1.4 shows the East String Pot reading versus dynamic loading at 3500 psi.

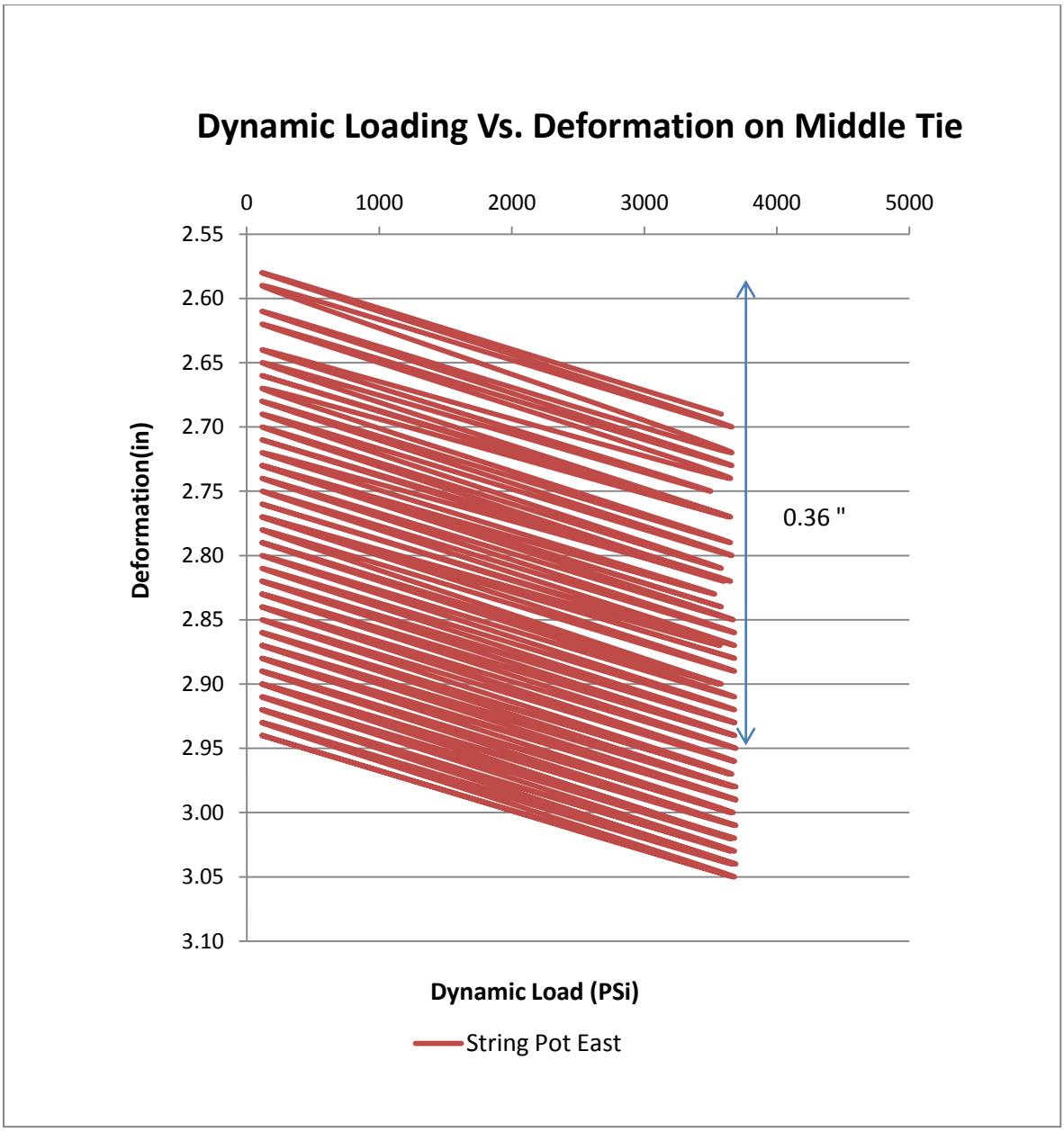

Figure 4.1.4 East string pot versus dynamic loading at 3500 psi

4.1.5 East string pot versus dynamic loading at 4500 psi (38 psi tie bearing pressure)

One hundred cycles were applied to the railroad section at 4500 psi. The total accumulated deformation after one hundred cycles was 4.05 in. Figure 4.1.5 shows the east string pot reading versus dynamic loading at 4500 psi. More permanent deformation was observed for the early cycles. As the number of cycles increased, more elastic deformation was observed.

As Figure 4.1.5 shows, at the beginning of the loading step the total deformation is the difference between number 1 on Figure 4.1.5 and number 2, which is about 0.12 in. On the same graph the difference between numbers 1 and 3 is the permanent deformation for the same cycle, which is 0.04 in. while the difference between points 2 and 3 is the elastic deformation. This elastic deformation is 0.08 in. As the number of cycles increases the permanent and total deformations per cycle decrease and a higher percentage of the deformation is elastic.

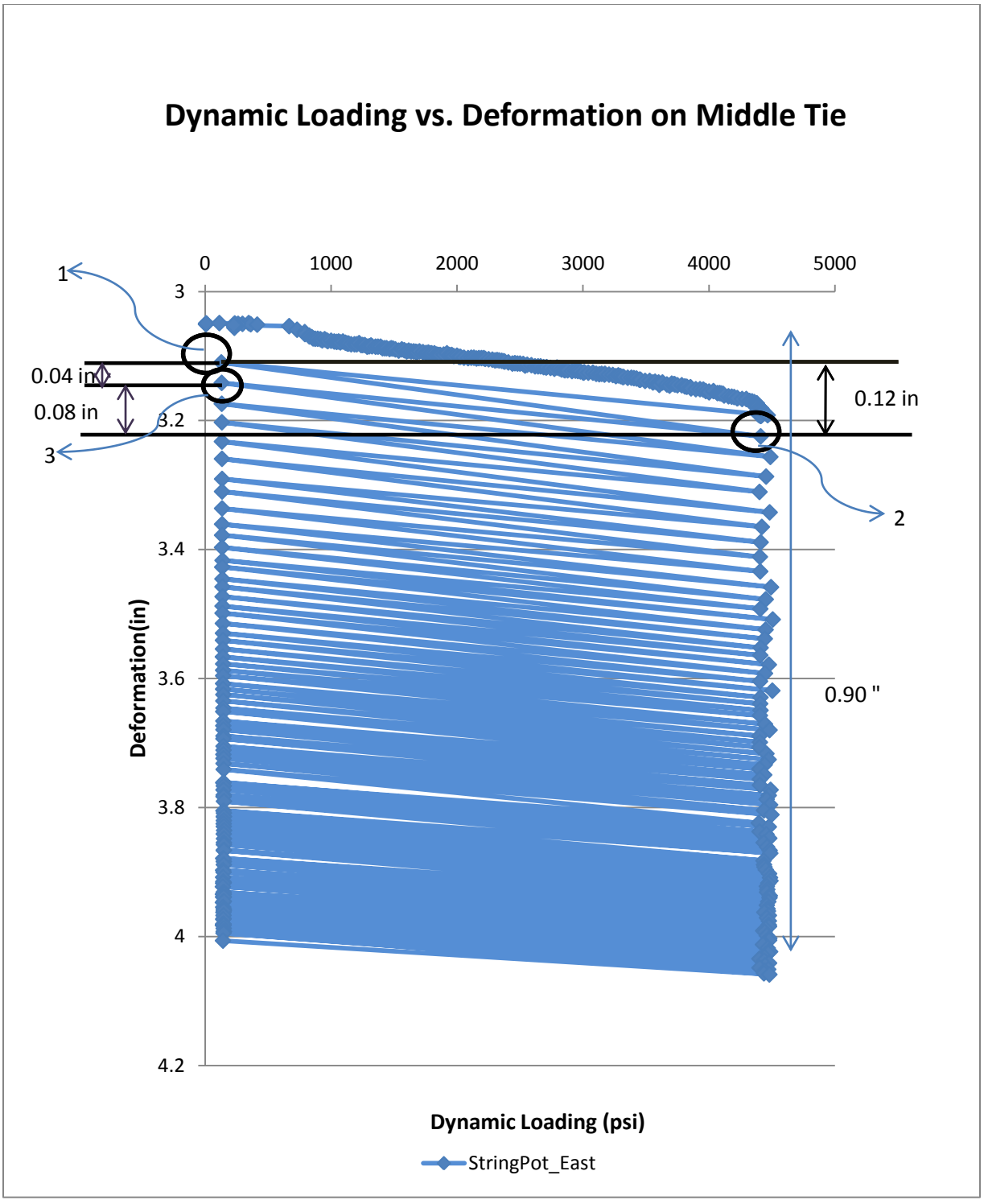

Figure 4.1.5 East string pot versus dynamic loading at 4500 psi (not soaked)

4.1.6 East string pot versus dynamic loading at 4500 psi (soaked) (40 psi tie bearing pressure)

Fifty gallons of water was added to the section by garden hose over period of 15 minutes. The section was left overnight for water to penetrate into the soil. One hundred cycles were applied to the railroad section at 4500 psi the following day. The total accumulated deformation after one hundred cycles was 5.95 in. As with the earlier steps the beginning cycles resulted in more permanent deformation per cycle. As the number of cycles increased more elastic deformation was observed. Figure 4.1.6 shows the east string pot reading versus dynamic loading at 4500 psi soaked.

As Figure 4.1.6 shows, at the beginning of the loading step the difference between number 1 on Figure 4.1.6 and number 2 was the total deformation, or 0.18 in which was 50% more than was observed during the initial cycles when loading the section to 4500 psi without soaking and 40% more than was observed at the end of the end of unsoaked loading. Most of the additional deformation per cycle was permanent. On the same graph difference between numbers 1 and 3 was the permanent deformation for the same cycle, which was 0.09 in. The elastic deformation is shown on the same graph and was also 0.09 in. As with the previous loading step the permanent and total deformations per cycle decreased as the number of cycles increased and a higher percentage of the deformation was elastic.

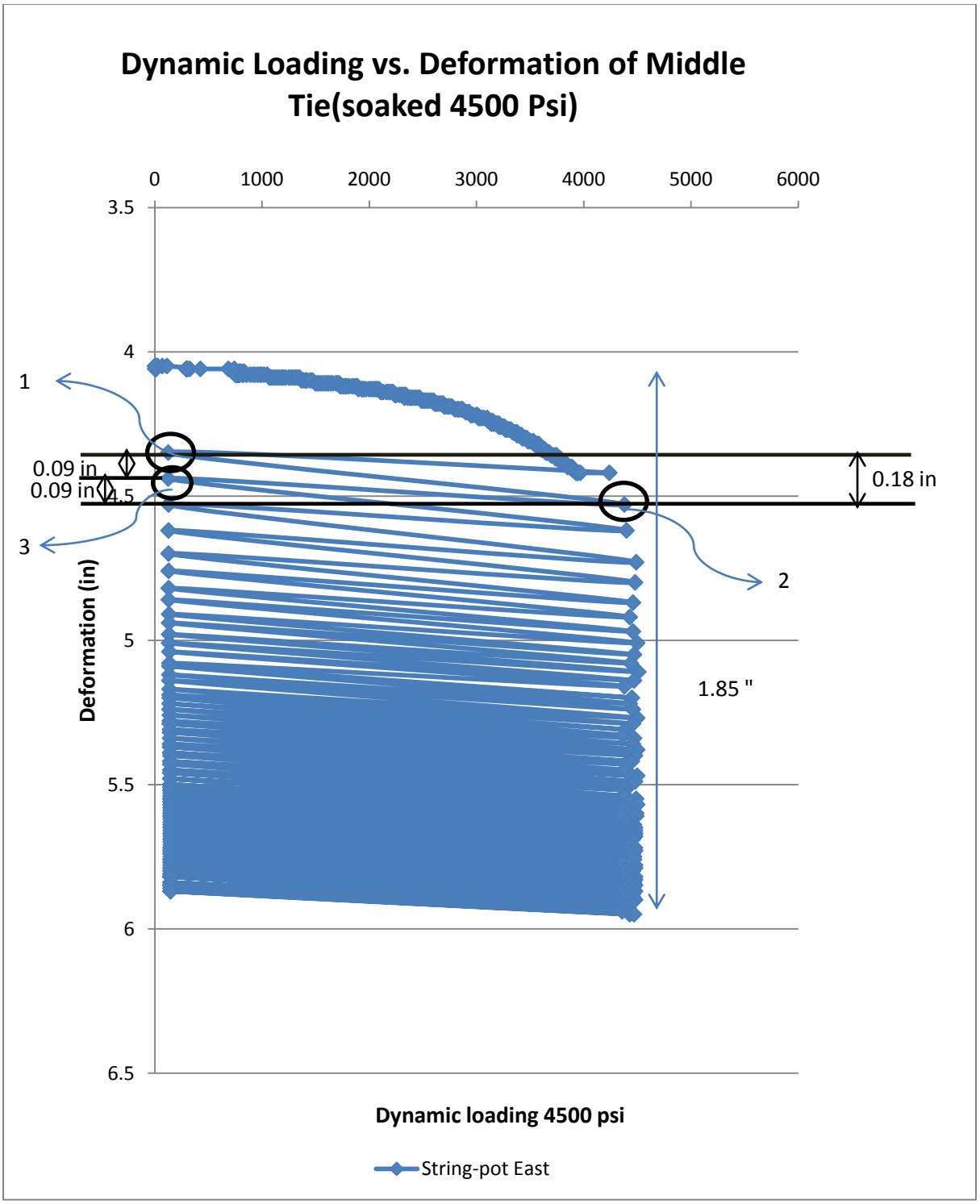

Figure 4.1.6 East string pot reading versus dynamic loading at 4500 psi soaked.

4.2 Unreinforced test

4.2.1 West string pot

Figure 4.2.1 through Figure 4.2.6 show the recorded values on the west string pot. These deformations were generally consistent with those from the east string pot.

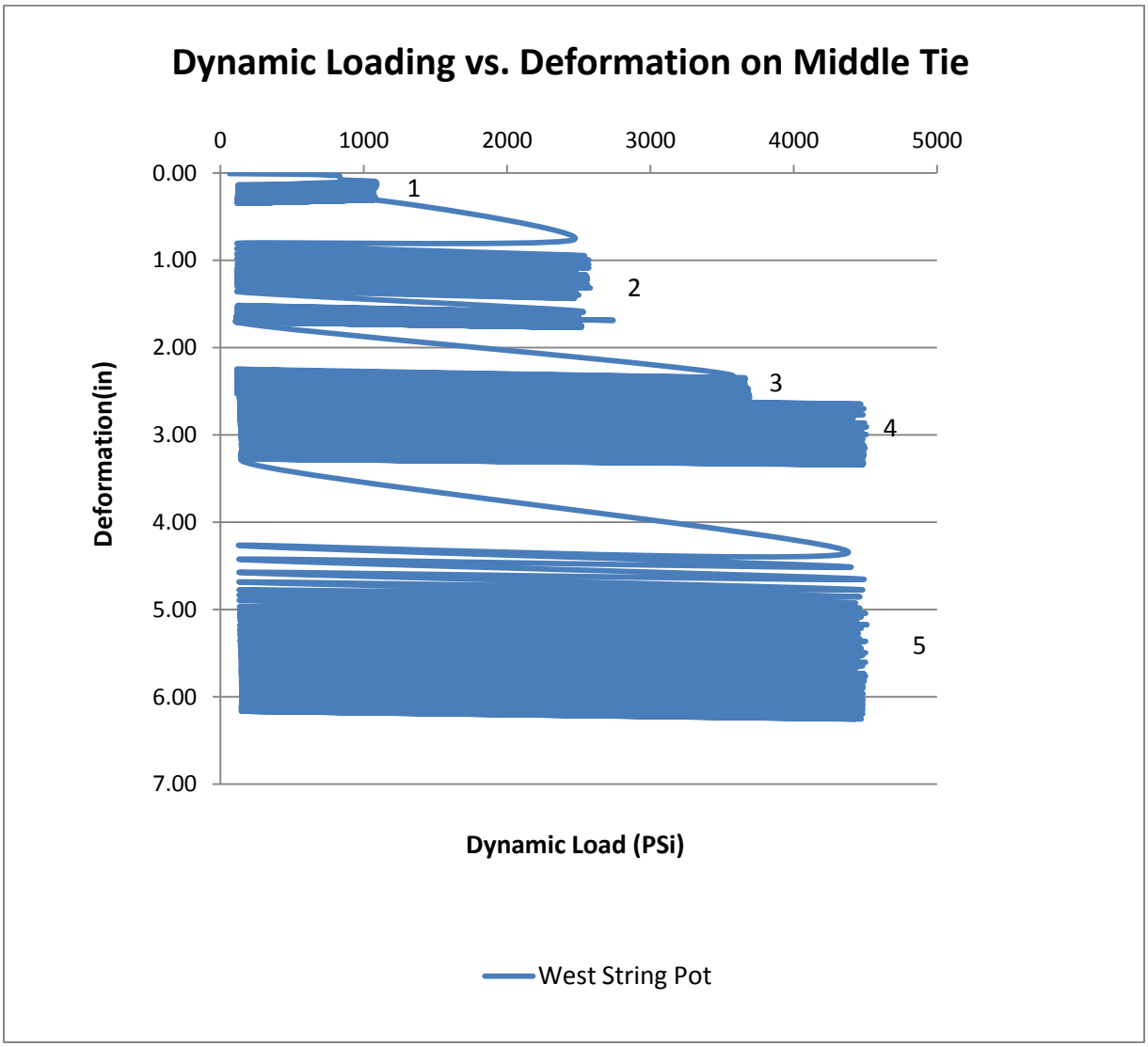

Figure 4.2.1 Dynamic loading vs. deformation. (West String Pot)

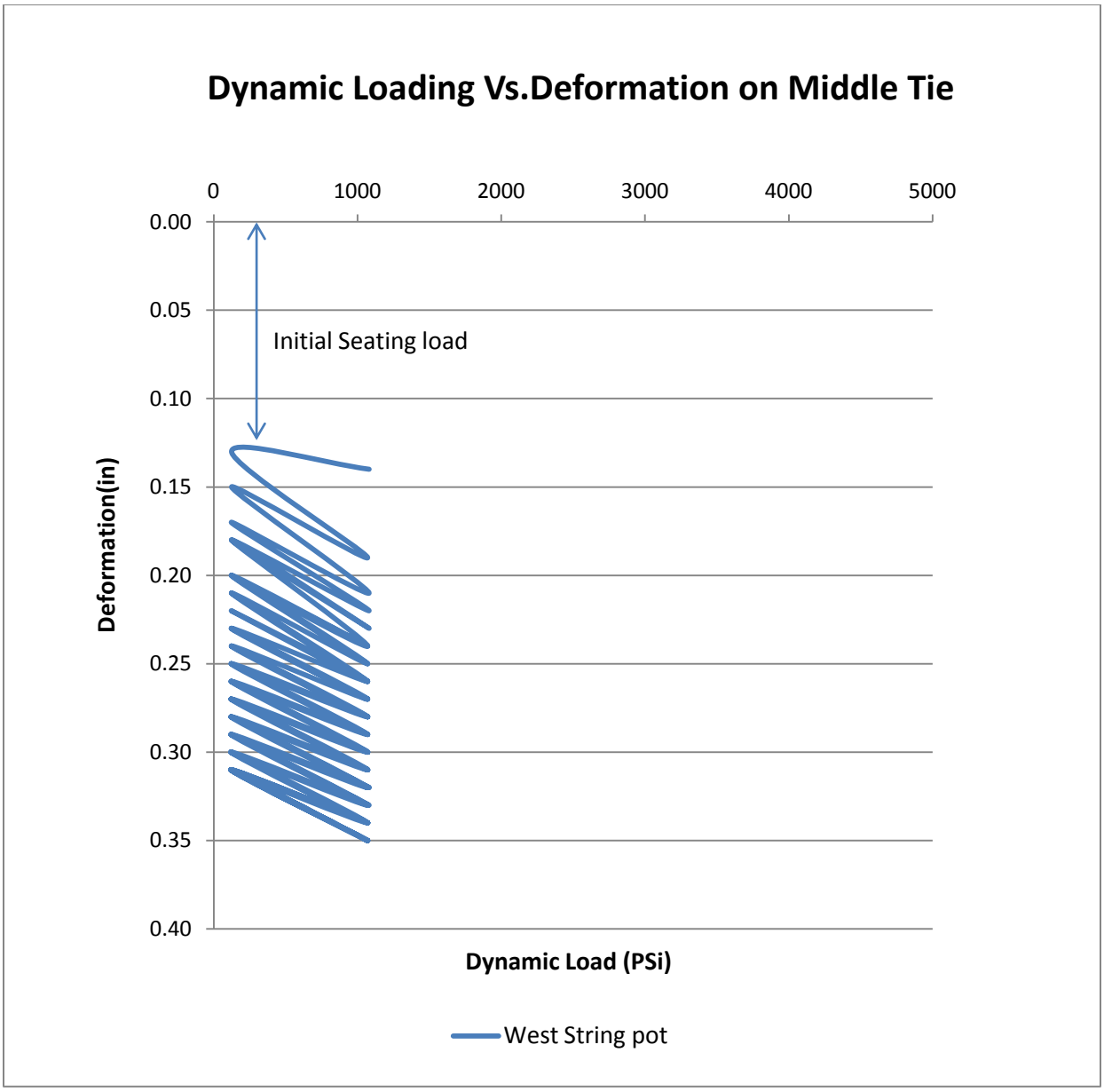

Figure 4.2.2 West string pot versus dynamic loading at 1100 psi

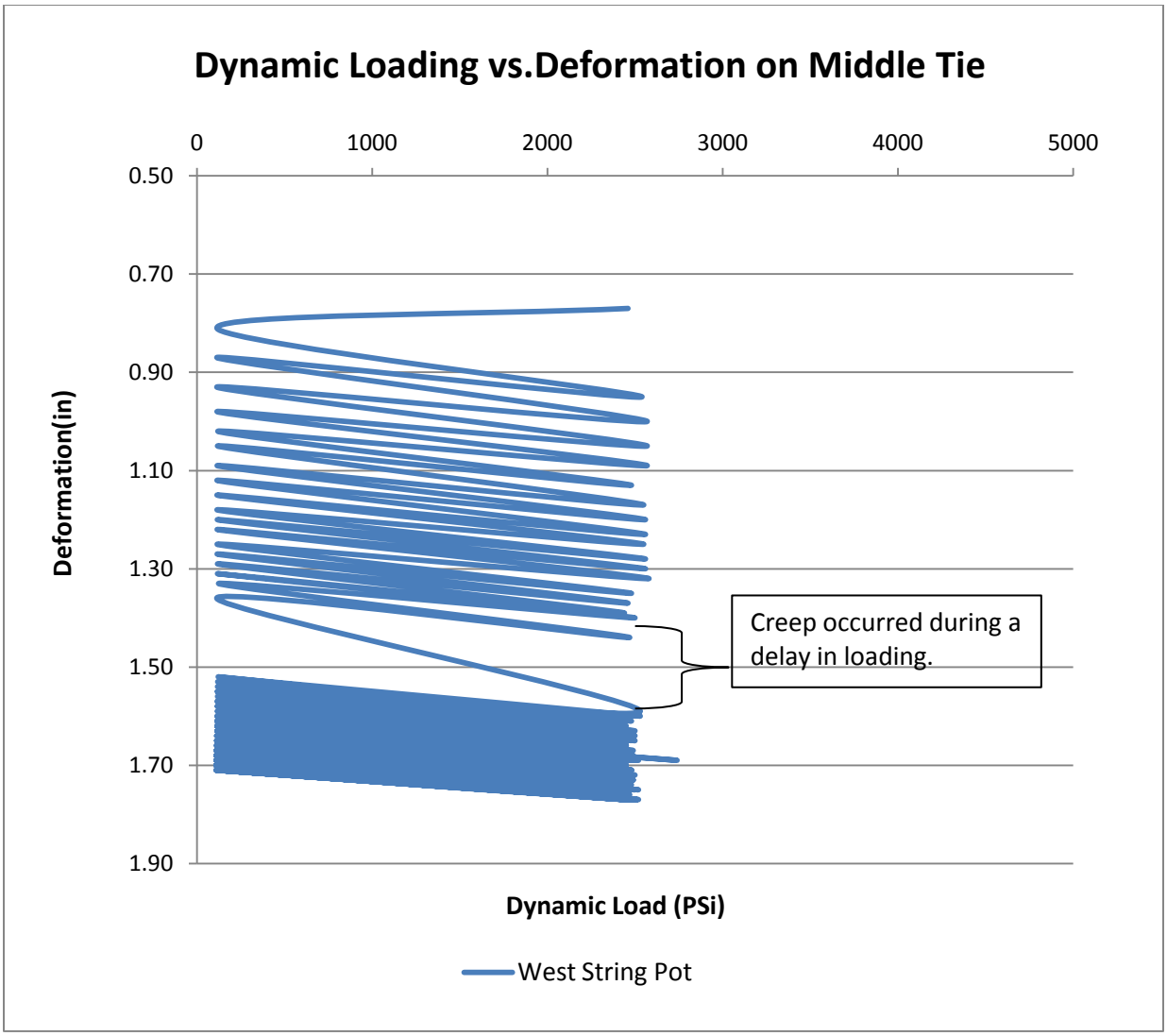

Figure 4.2.3 West string pot versus dynamic loading at 2500 psi

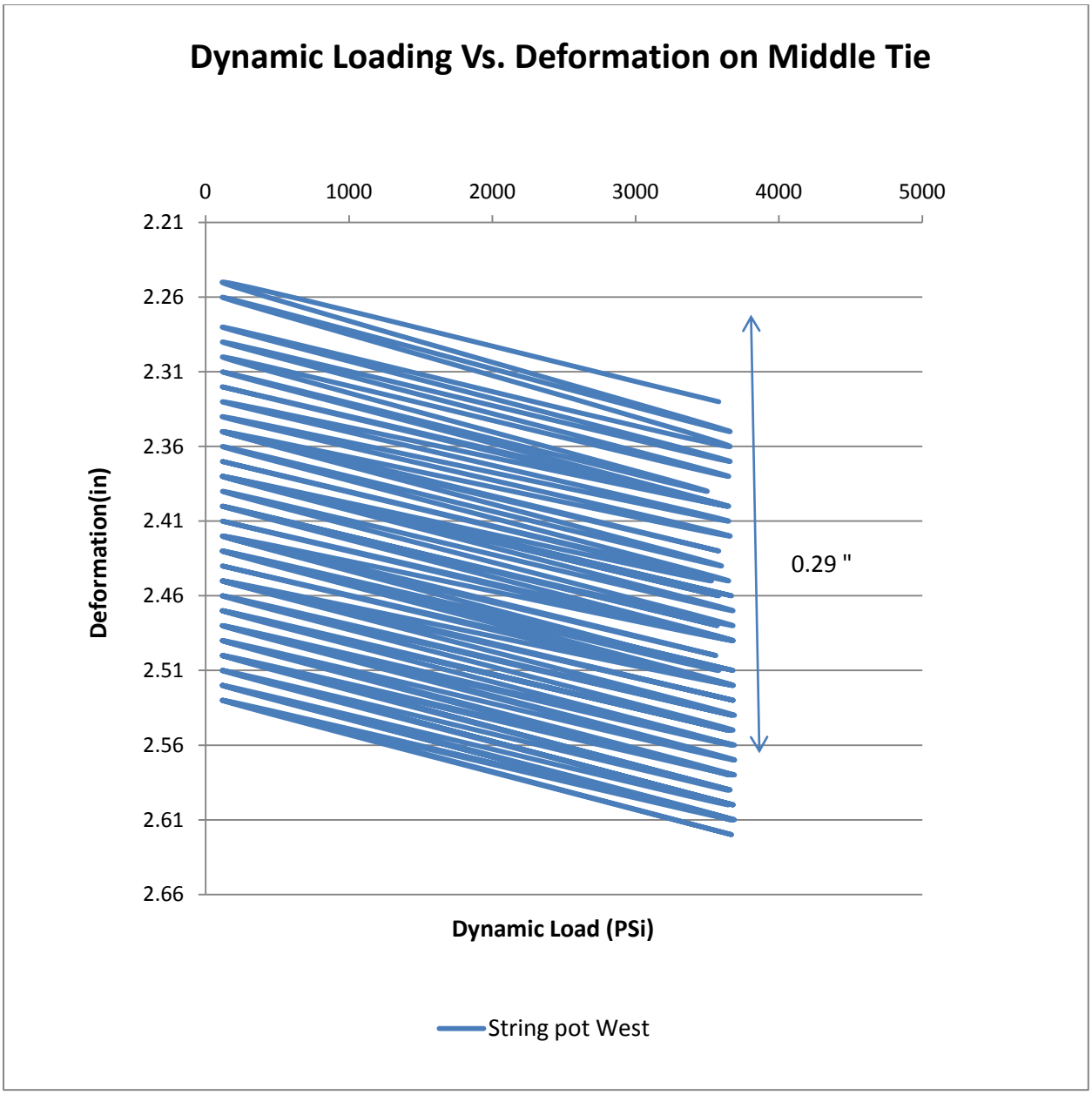

Figure 4.2.4 West string pot versus dynamic loading at 3500 psi

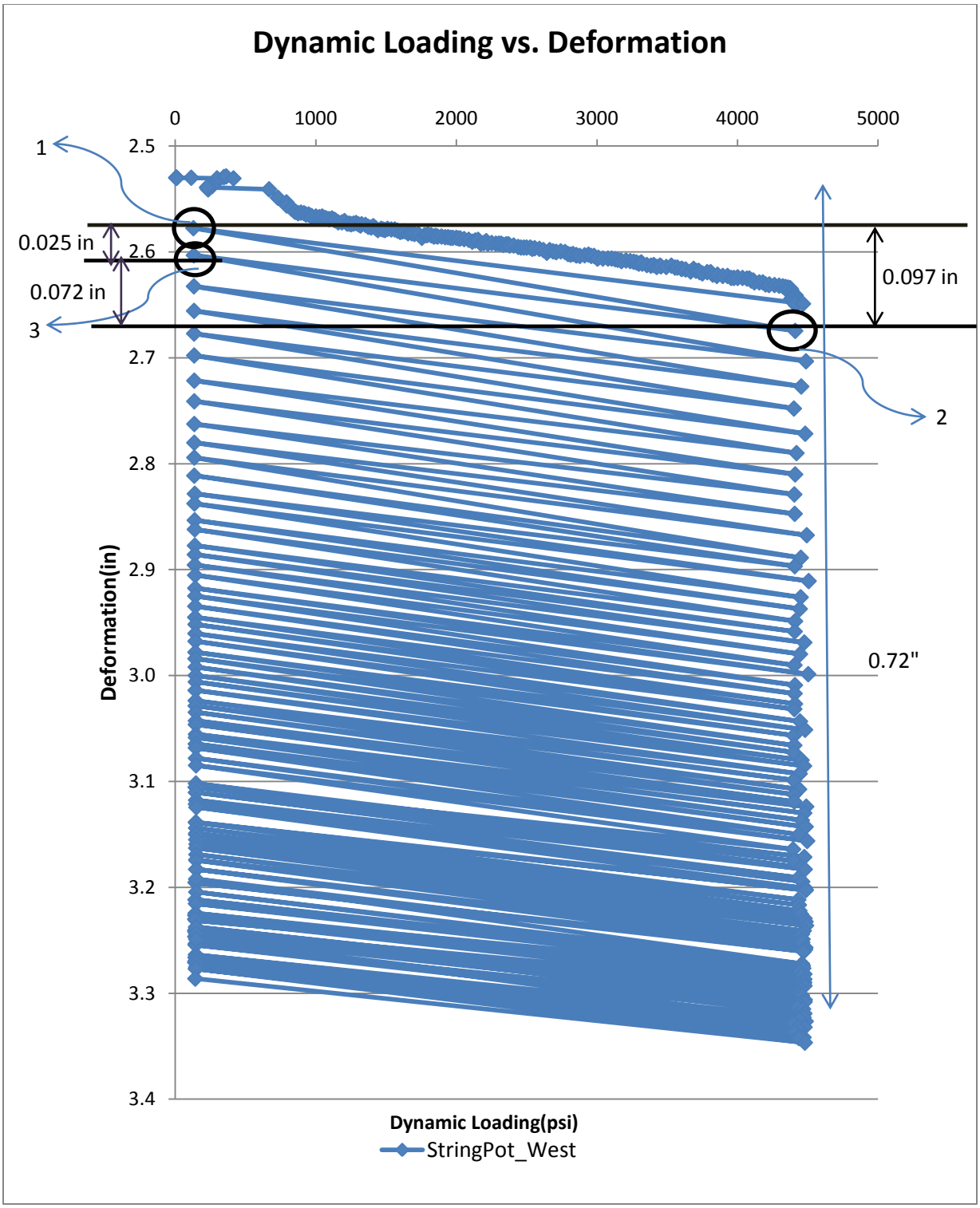

Figure 4.2.5 West string pot versus dynamic loading at 4500 psi (not soaked)

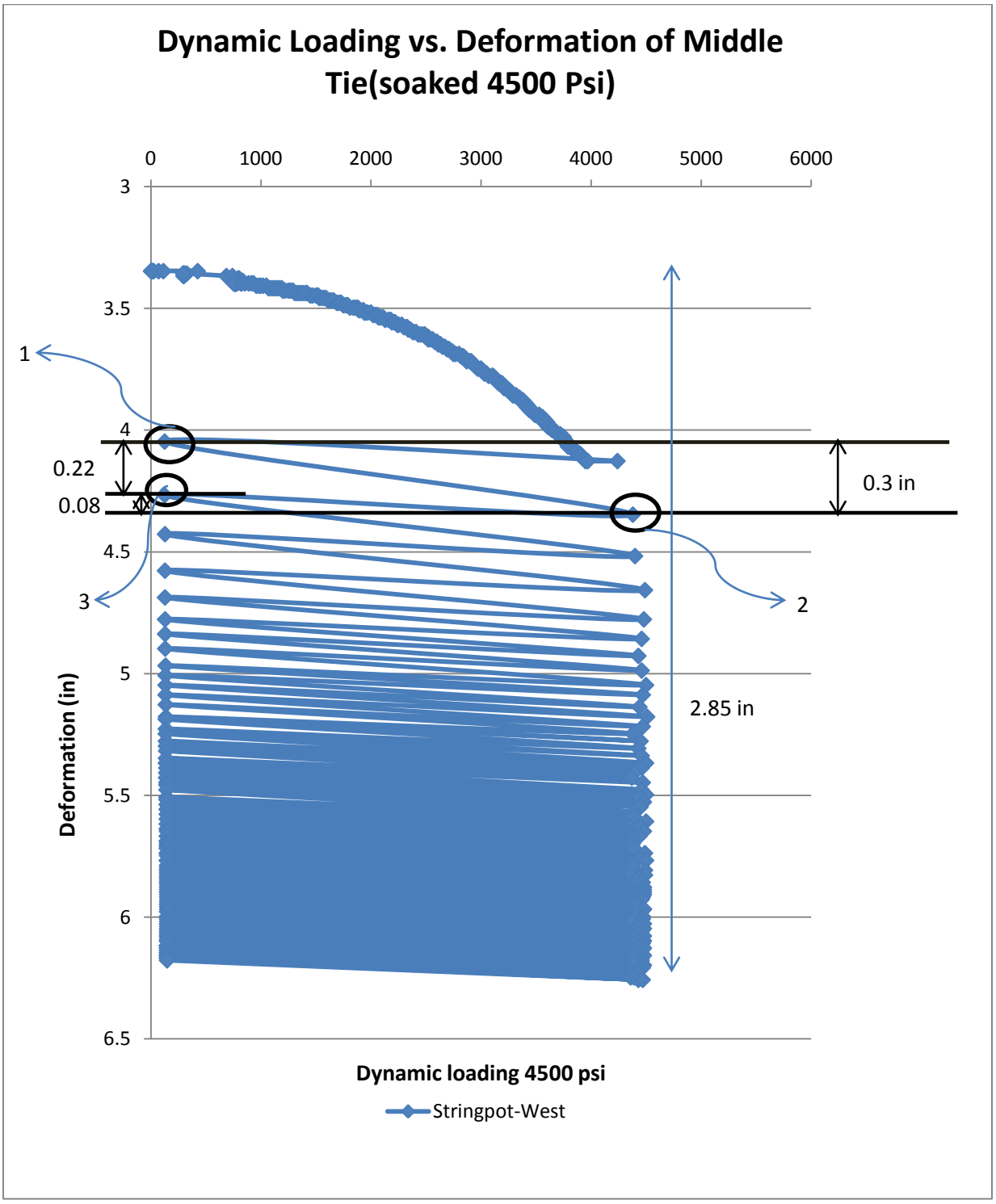

Figure 4.2.6 West string pot versus dynamic loading at 4500 psi (soaked)

4.3 Unreinforced test (Displacement Transducers)

Four displacement transducers were installed on the railroad track to measure the deformation near the ends of each rail on the track panel. Figure 4.3 shows the transducer locations. Some sliding of transducer ends resulted in measurements that were not reliable and these results are not included in the analysis.

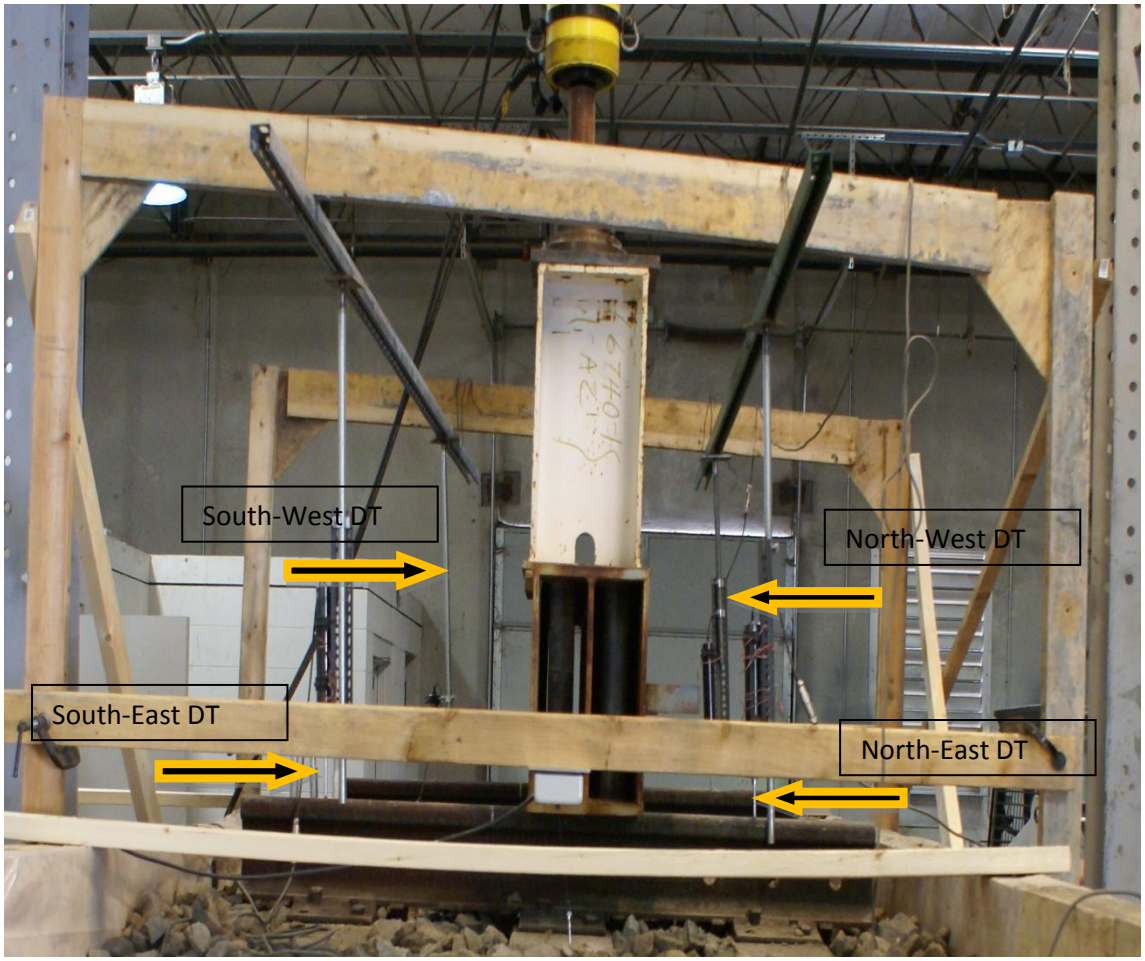

Figure 4.3 Displacement transducers

4.3.1 Displacement Transducers at 1100 psi (South-East) (9 psi tie bearing pressure)

Seventy nine cycles were applied to the railroad section at 1100 psi. The total deformation accumulated after seventy-nine cycles was 0.41 in. Figures 4.3.1 through 4.3.4 shows DT reading versus dynamic loading at 1100 psi.

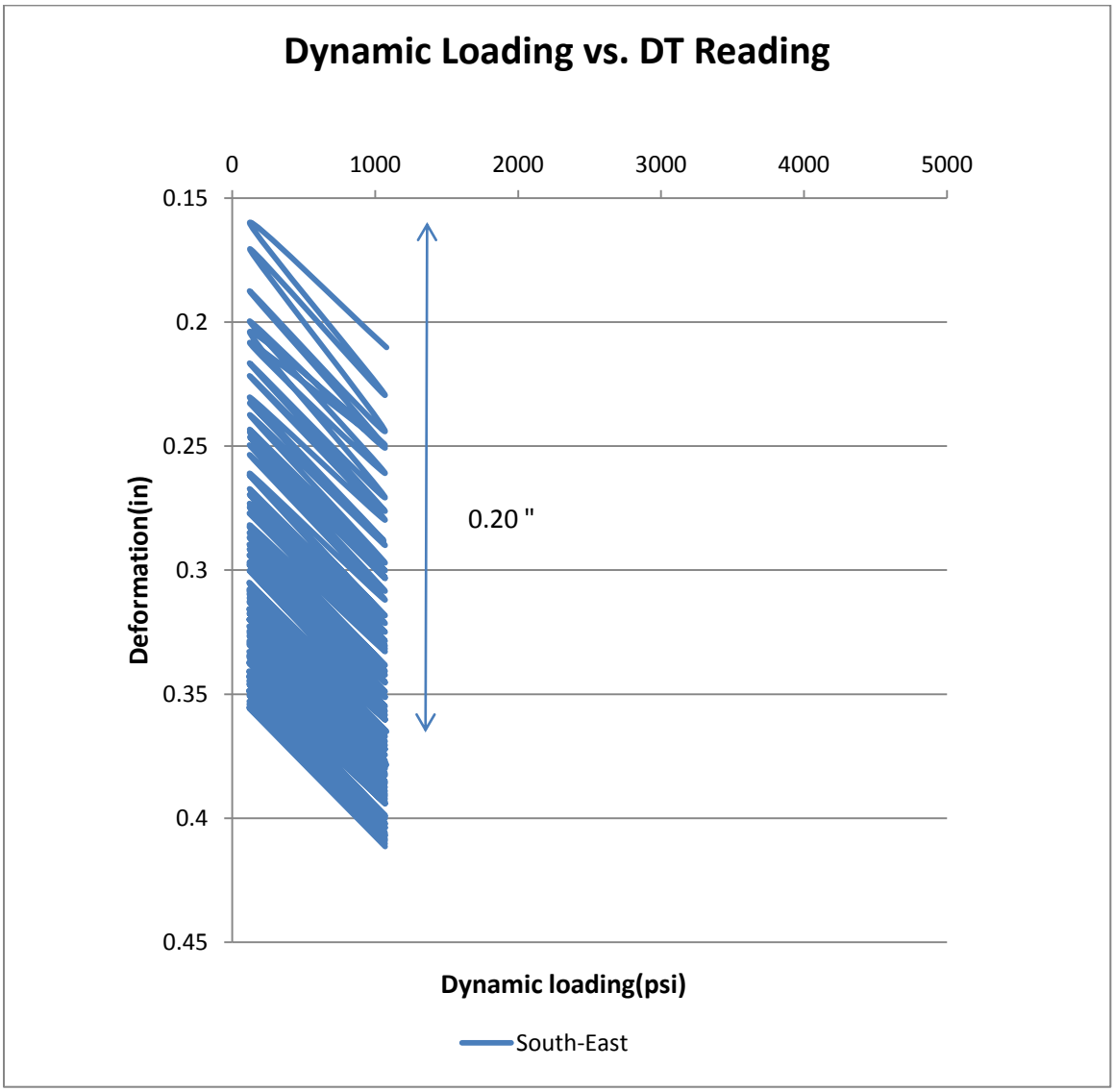

Figure 4.3.1 Displacement transducer reading at 1100 psi (South-East)

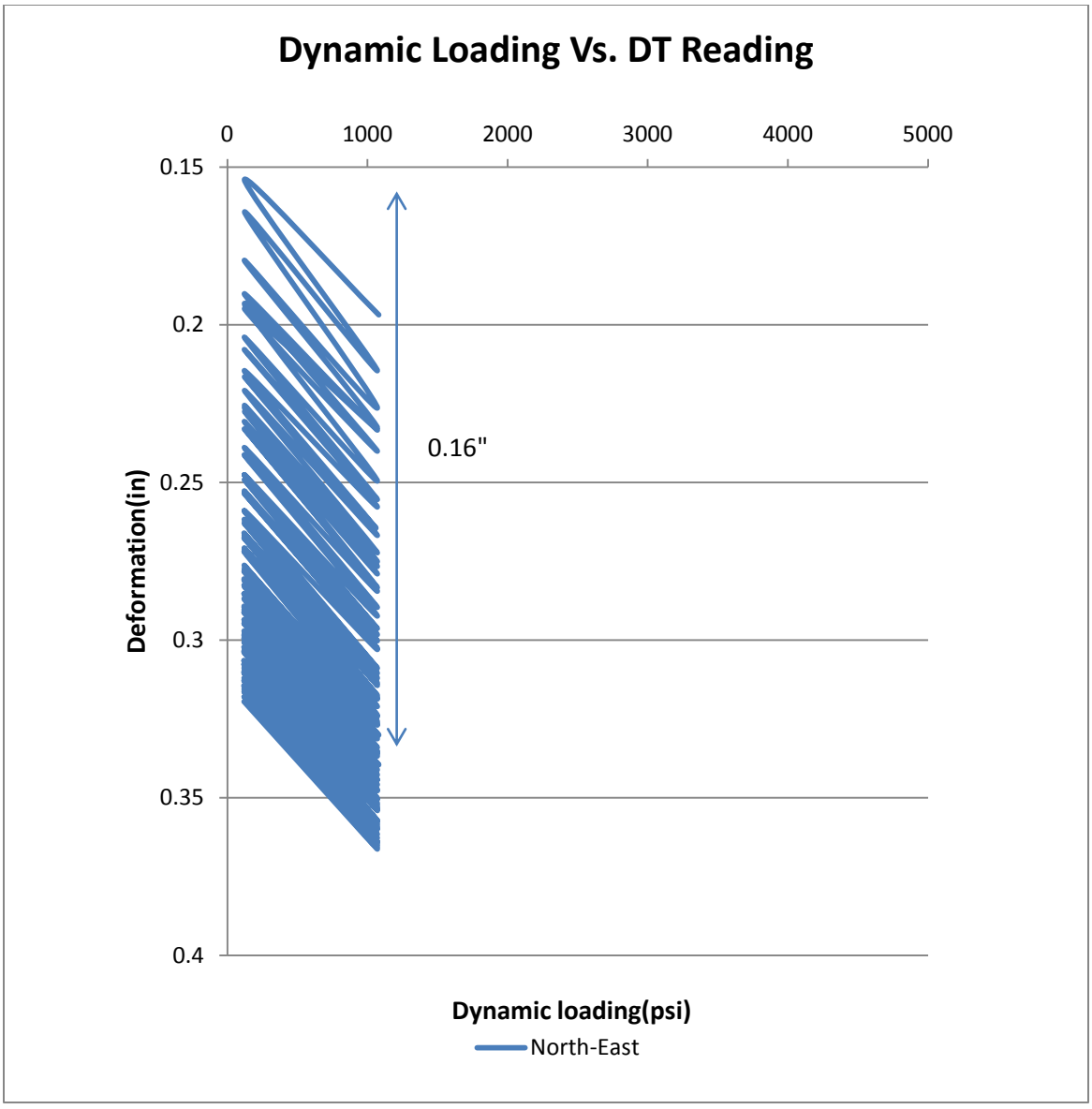

Figure 4.3.2 Displacement transducer reading at 1100 psi (North-East)

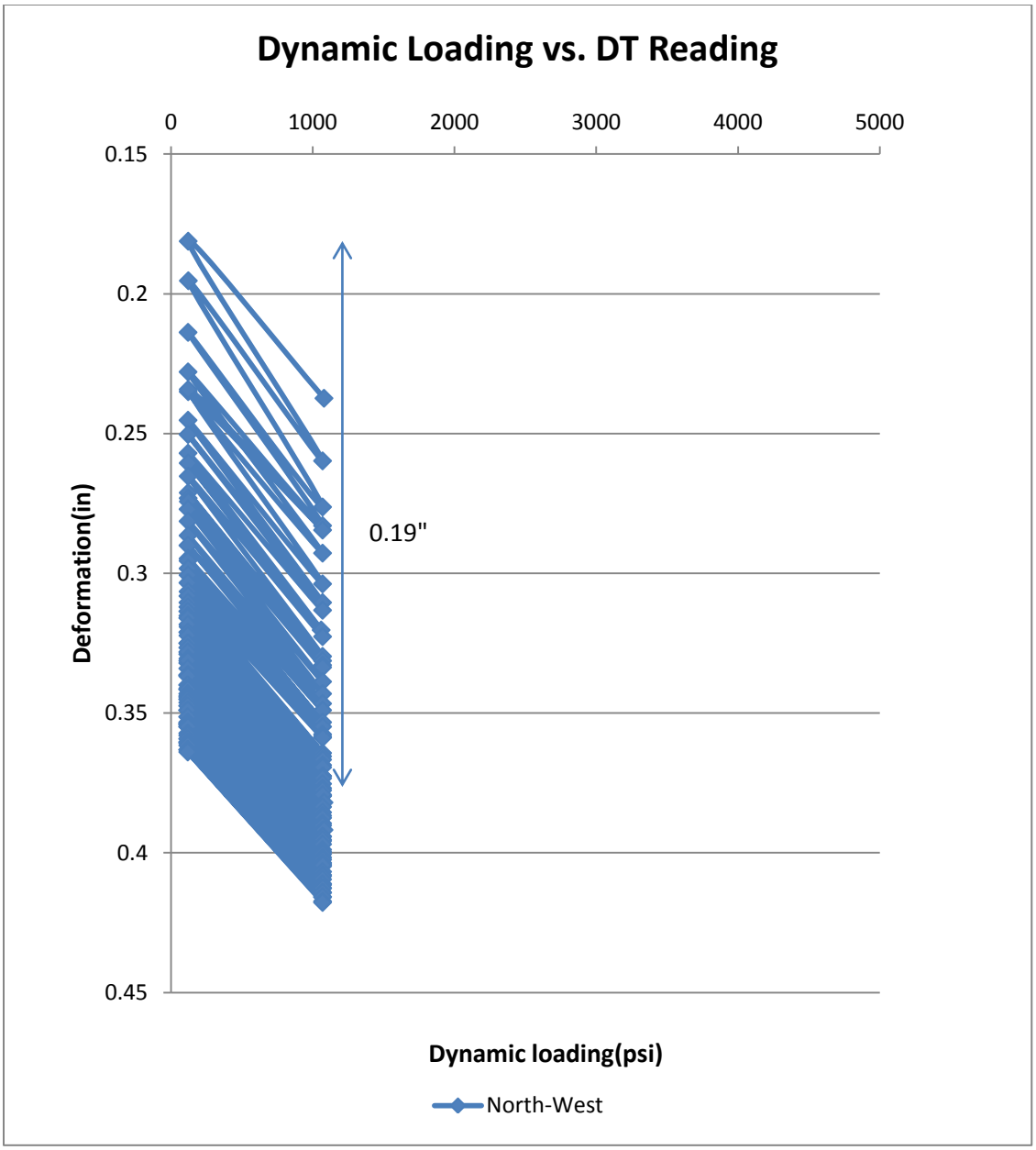

Figure 4.3.3 Displacement transducer reading at 1100 psi (North-West)

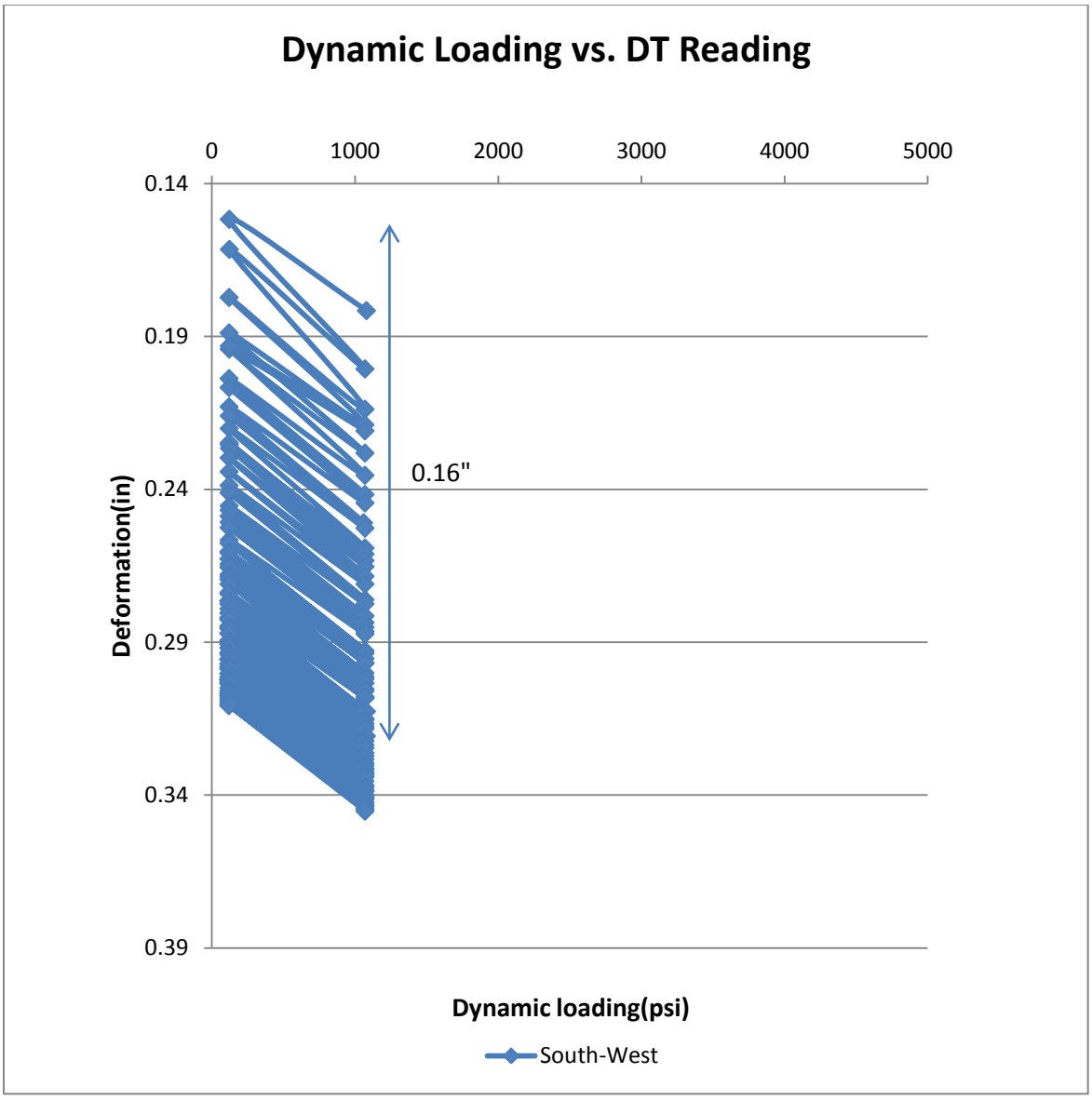

Figure 4.3.4 Displacement transducer reading at 1100 psi (South-West)

Due to slippage of the displacement transducers, data for the 2500 psi and 3500 psi load levels are not reliable and not included.

4.3.5 Displacement transducers at 4500 psi dry (South-East)

One hundred cycles were applied to the railroad section at 4500 psi unsoaked resulting in a total accumulated deformation after one hundred cycles of 3.7 in. Permanent deformations were large during early cycles in the load step. As the number of cycle increased total deformation per cycle decreased and a higher percentage of the deformation was elastic. Deformations at each of the four corners of the track panel are shown in Figures 4.3.5 through 4.3.8.

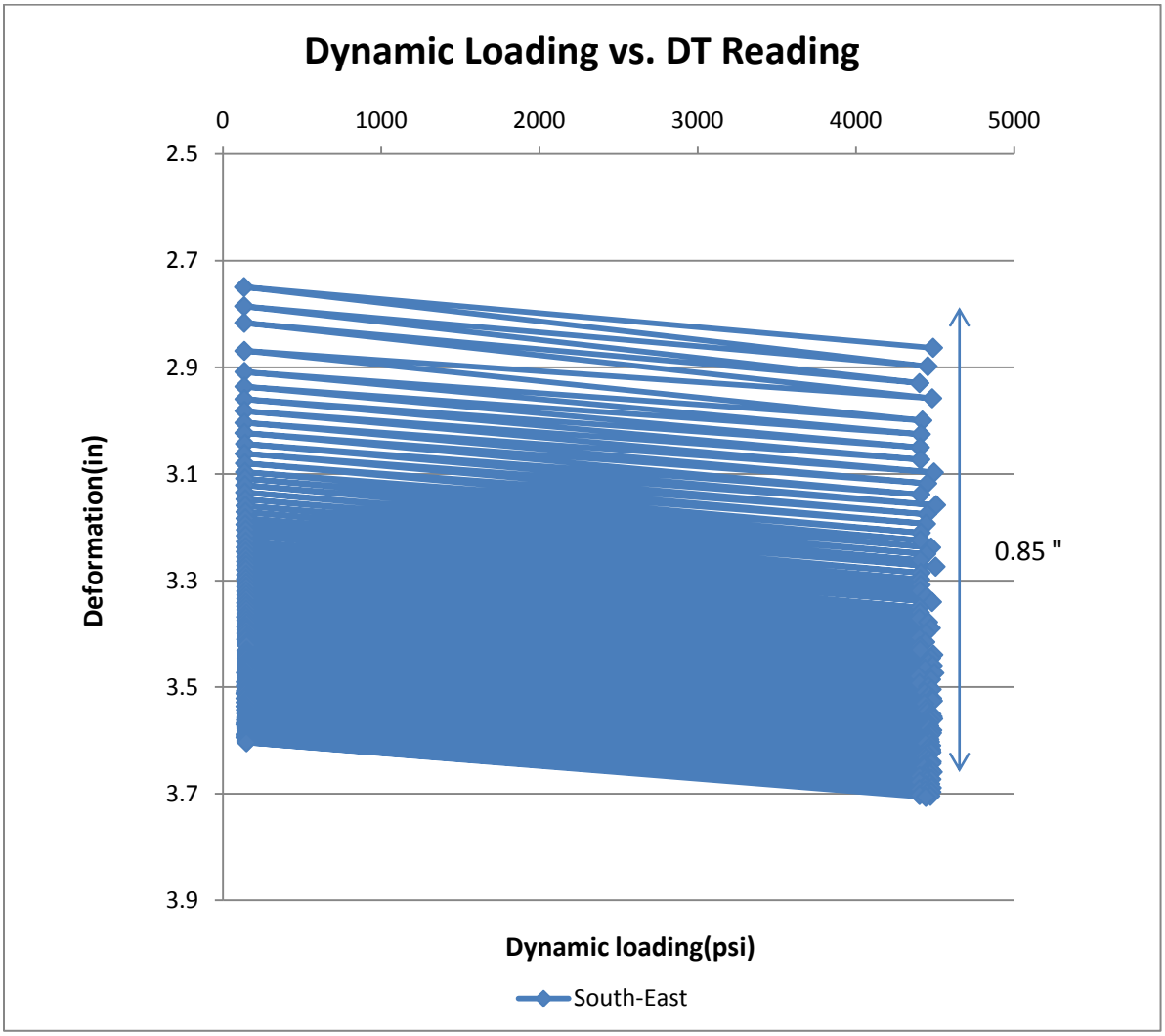

Figure 4.3.5 Displacement transducer reading at 4500 psi not soaked (South-East)

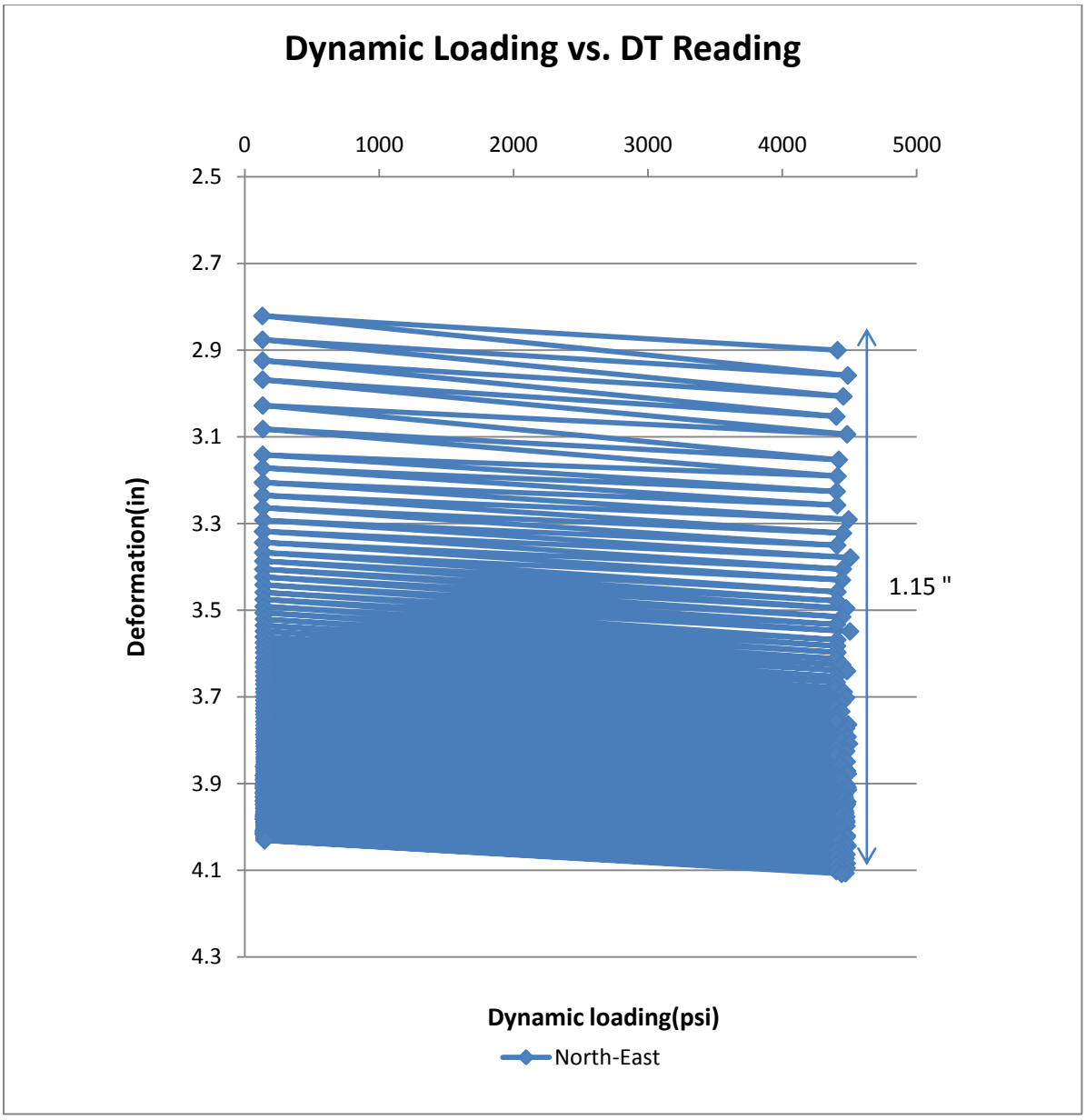

Figure 4.3.6 Displacement transducer reading at 4500 psi not soaked (North-East)

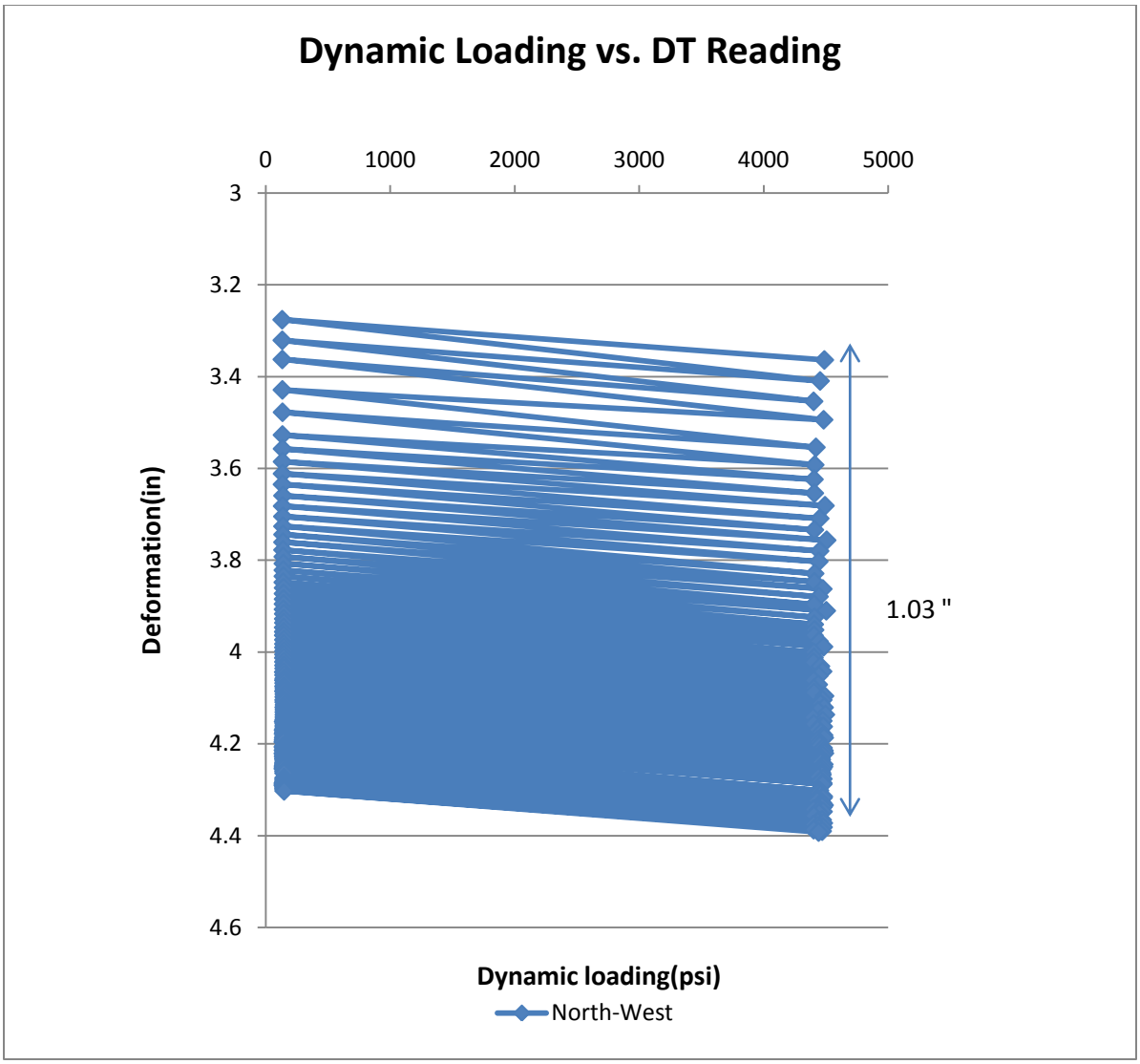

Figure 4.3.7 Displacement transducer reading at 4500 psi not soaked (North-West)

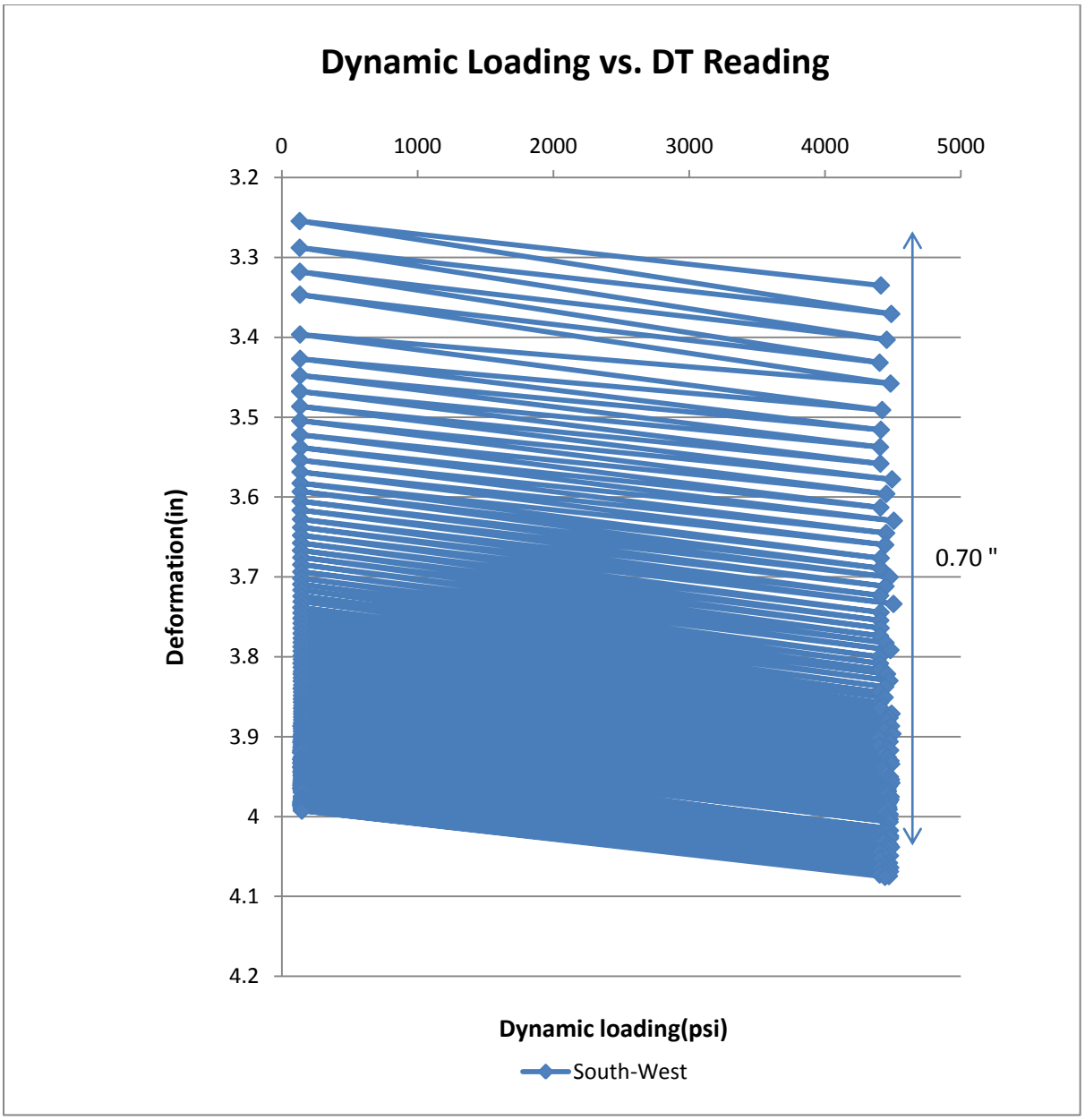

Figure 4.3.8 Displacement transducer reading at 4500 psi not soaked (South-West)

4.3.9 Displacement transducers at 4500 psi soaked (40 psi tie bearing pressure)

After completion of the 4500 psi (unsoaked) loading step, 50 gallons of water were added to the section and allowed to soak in overnight. One hundred cycles were then applied to the railroad section at 4500 psi dry total deformation accumulated after one hundred cycles was 5.85 in. Deformations were larger during the early cycles of the load step. As the number of cycles increased a higher percentage of the deformations were elastic. Deformations at each of the four corners of the track panel are shown in Figures 4.3.9 through 4.3.12.

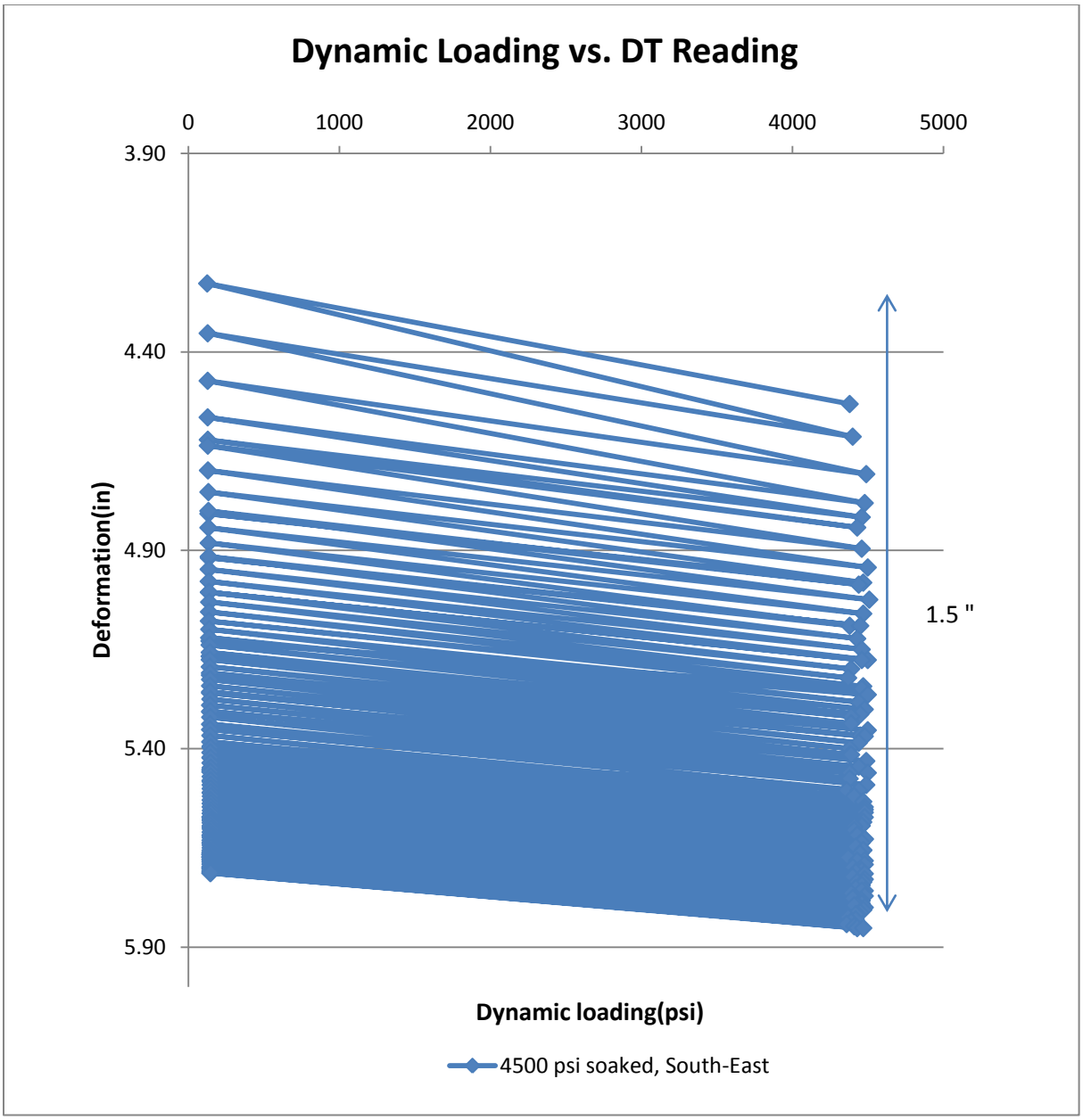

Figure 4.3.9 Displacement transducer reading at 4500 psi soaked (South-East)

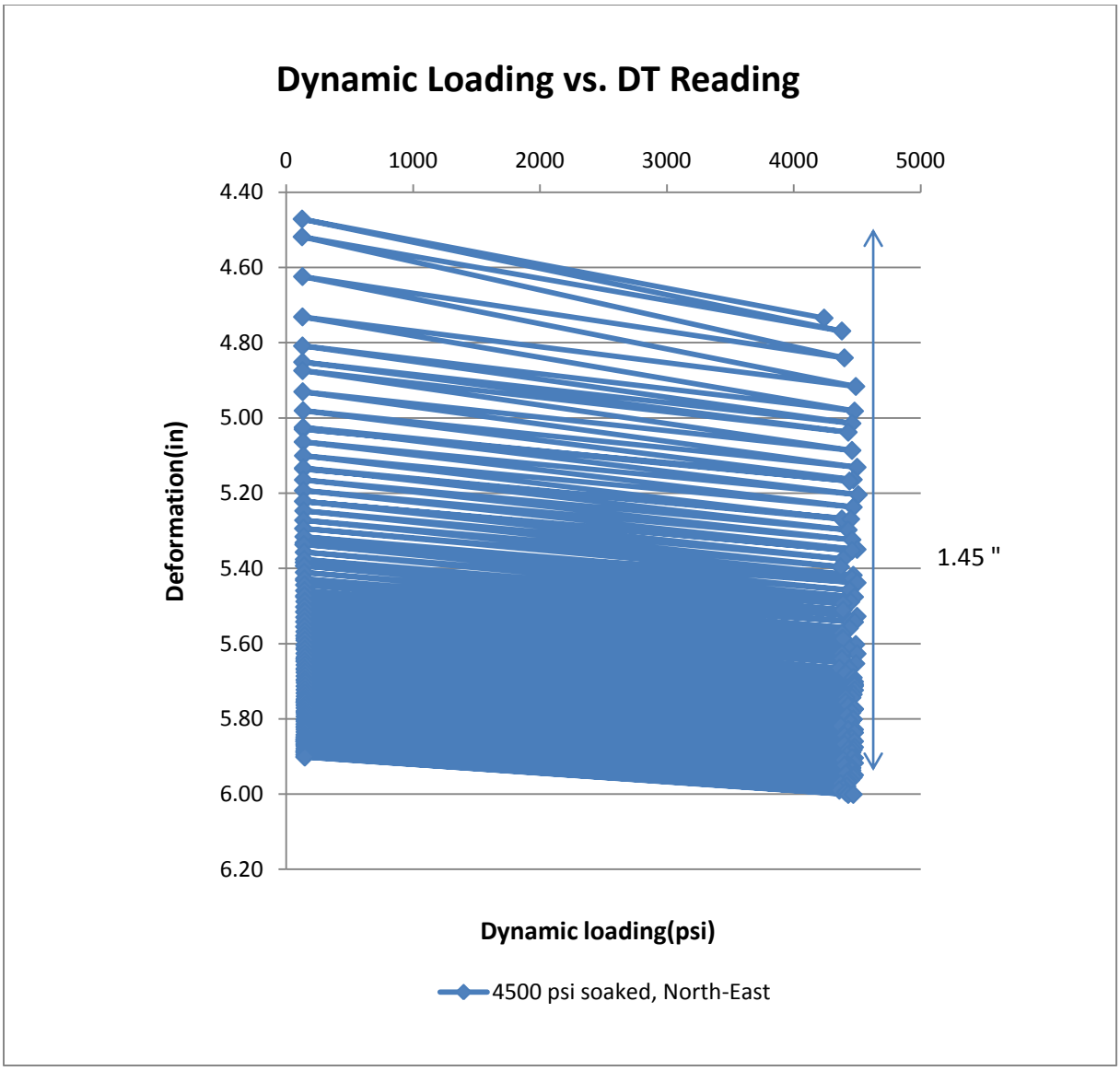

Figure 4.3.10 Displacement transducer reading at 4500 psi soaked (North-East)

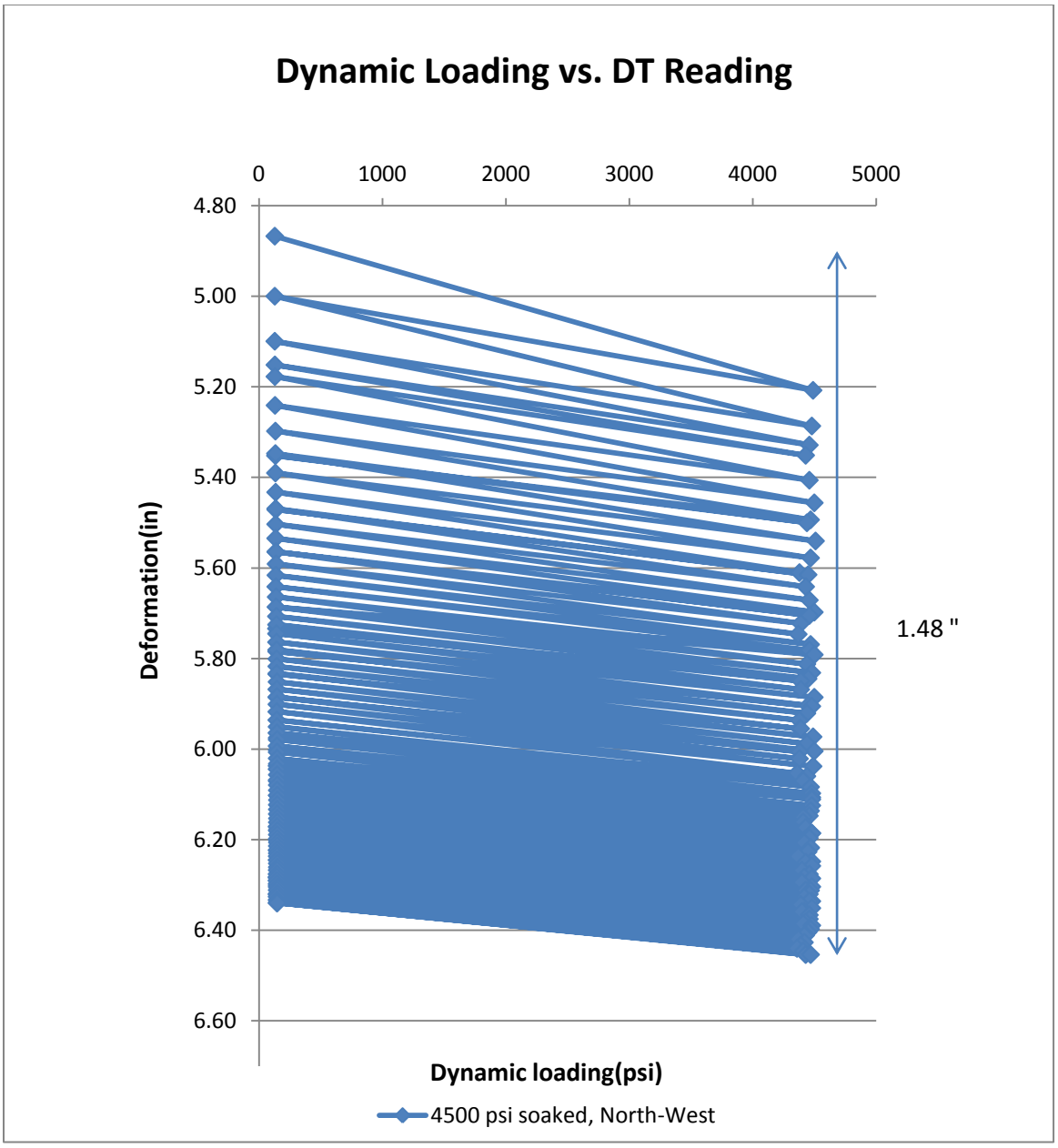

Figure 4.3.11 Displacement transducer reading at 4500 psi soaked (North-West)

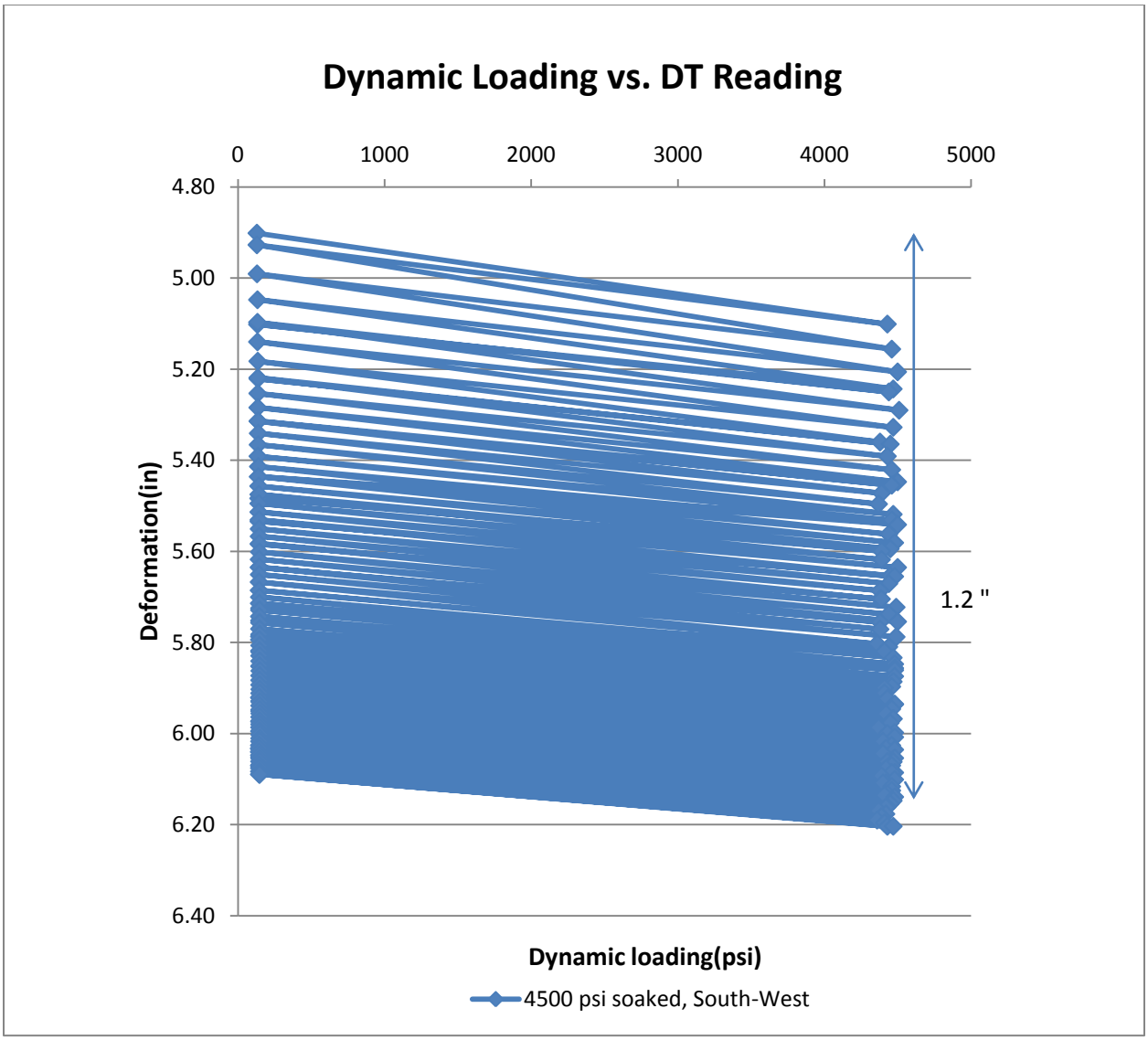

Figure 4.3.12 Displacement transducer reading at 4500 psi soaked (South-West)

4.4.1 Pressure cell results for unreinforced test

Five pressure cells were installed as shown in Figure 4.4.1. Pressure cells 1, 2 and 3 were installed at the interface of subgrade and ballast under the middle tie (1 and 3 were right below the rails). Pressure cells 4 and 5 were installed under the right tie with Cell 4 beneath the rail and Cell 5 beneath the center of the tie.

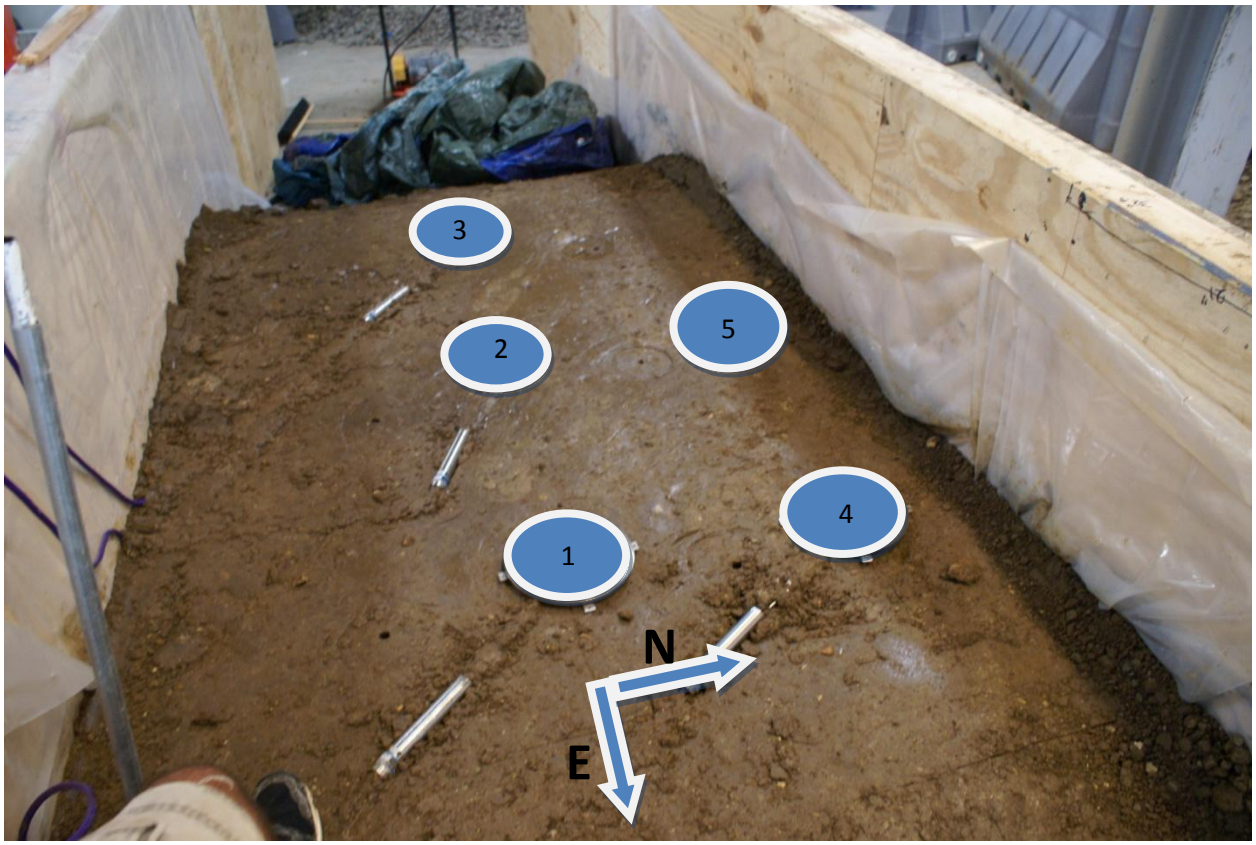

Figure 4.4.1 Pressure cells

Figure 4.4.2 shows pressure cells versus hydraulic pressure in the jack. Pressure cell 1 measured the highest vertical stress observed of 19 psi. When subgrade pressure at the location of pressure cell 1 reached 18 psi the subgrade began to yield (fail). Pressure cell 4 experienced subgrade failure at pressure of 12 psi. The soil beneath these pressure cells began to yield as the hydraulic pressure was increased to 4500 psi. The subgrade did not experience failure at the locations of pressure cells 2, 3 and 5 until it was soaked with 50 gallons of water and reloaded. Pressure cell 3 experienced lower pressure due do the movement of the tie or the pressure cell itself. Figure 4.4.3 shows the same plot with tie bearing pressure at the x- axis. (actual pressure).

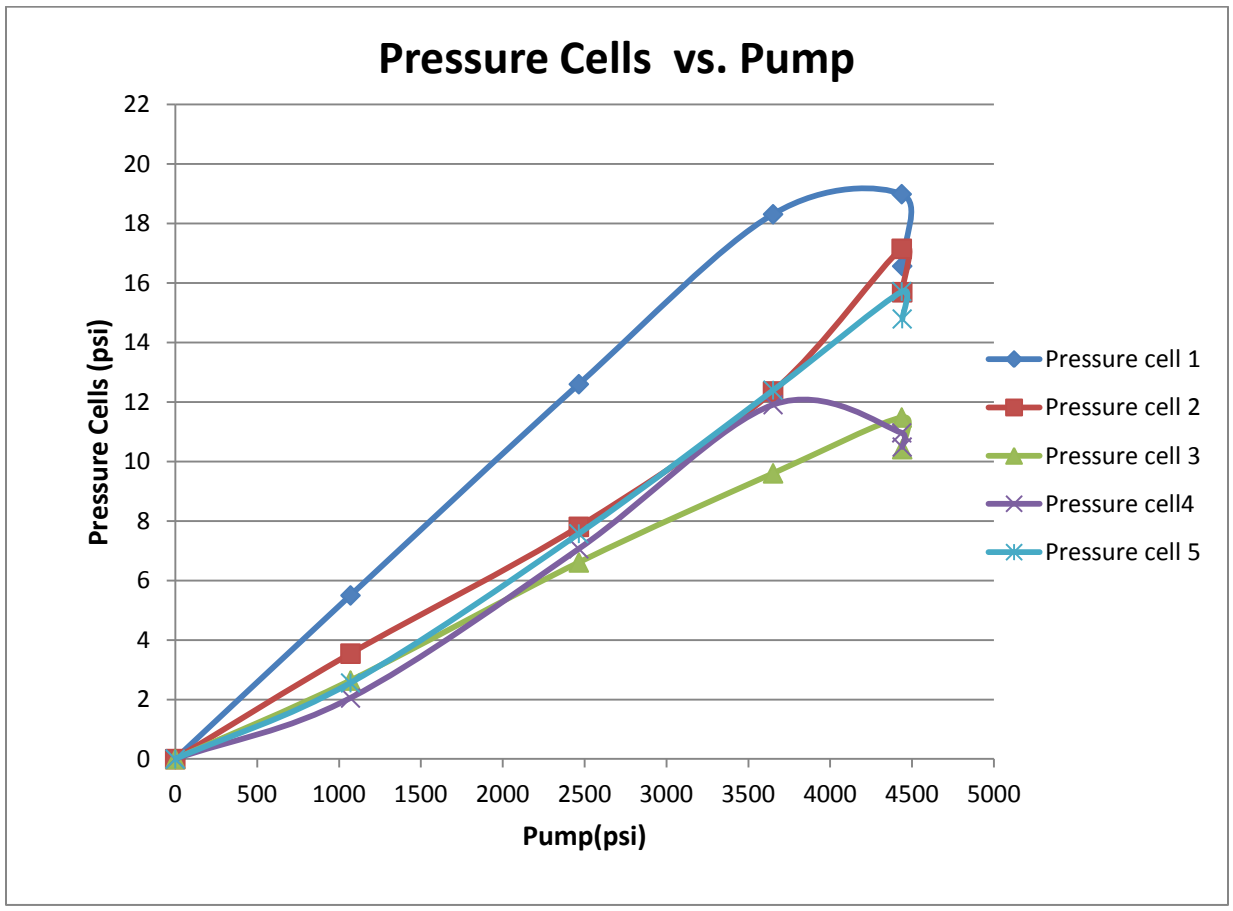

Figure 4.4.2 Pressure cells vs. pump pressure at subgrade level (target pressure)

Table 4.4.2 Pressure cells vs. pump pressure at subgrade level (unreinforced test)

Load (lb)	Pressure Transducer(psi)	Pressure cell 1(psi)	Pressure cell 2(psi)	Pressure cell 3(psi)	Pressure cell 4(psi)	Pressure cell 5(psi)
0	0	0	0	0	0	0
23194	1071	5.50	3.55	2.64	2.05	2.56
53407	2465	12.60	7.81	6.61	7.07	7.58
79116	3652	18.32	12.36	9.61	11.91	12.40
97500	4437	18.99	17.16	11.49	10.97	15.72
104000	4440	16.57	15.70	10.42	10.49	14.80

4.4.2 Pressure cells results under ties

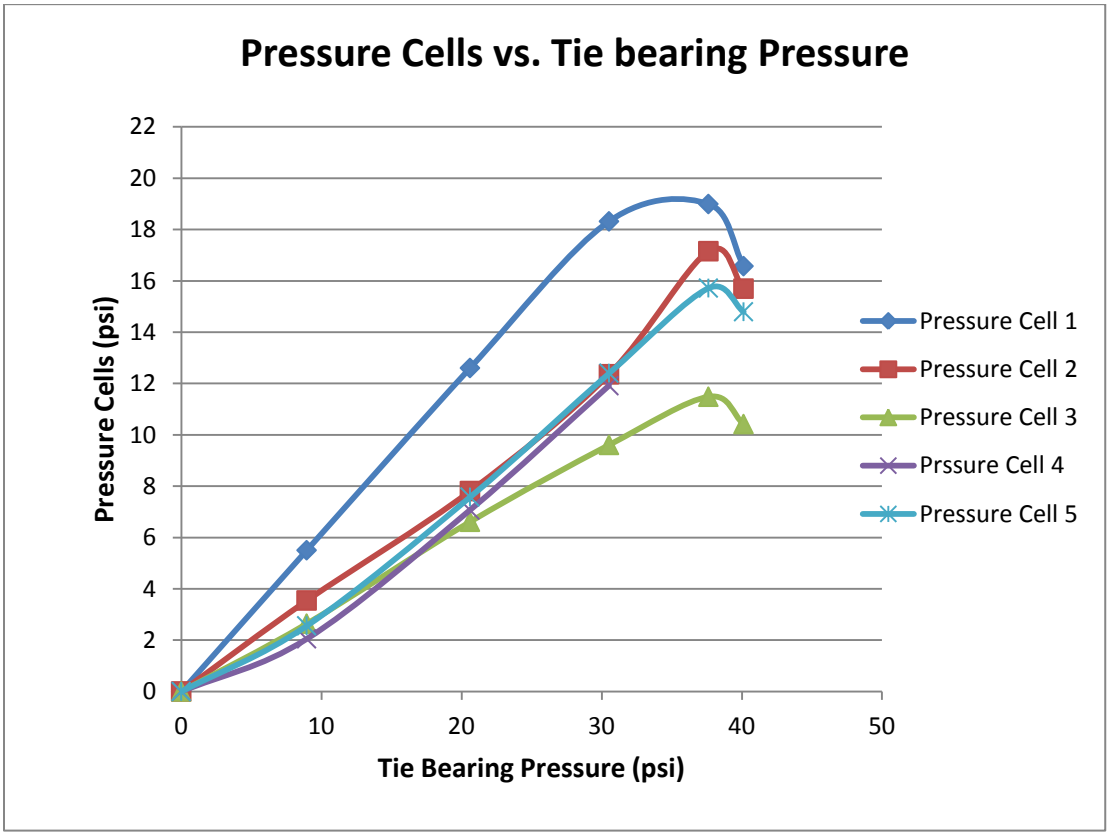

Figure 4.4.3 Pressure cells vs. tie bearing pressure on ballast

Table 4.4.3 Pressure cells vs. tie bearing pressure

Right below ties						
Load (lb)	**Tie Bearing Pressure (psi)**	**Pressure cell 1 (psi)**	**Pressure cell 2 (psi)**	**Pressure cell 3 (psi)**	**Pressure cell 4 (psi)**	**Pressure cell 5 (psi)**
0	**0**	**0**	**0**	**0**	**0**	**0**
23194	9	5.50	3.55	2.64	2.05	2.56
53407	21	12.60	7.81	6.61	7.07	7.58
79116	31	18.32	12.36	9.61	11.91	12.40
97500	38	18.99	17.16	11.49	10.97	15.72
104000	40	16.57	15.70	10.42	10.49	14.80

4.5 Loading sequence for the reinforced section

For the reinforced section dynamic loading was conducted in five steps (1100 psi, 2500 psi, 3500 psi, 4500 psi dry and 4500 psi soaked) while using triaxial geogrid to reinforce the ballast section. The number of cycles for each test matches number used for the unreinforced section.

Table 4.5.1 contains the loading information.

Table 4.5.1 Loading information for reinforced test

Load Step	Cycles	Loading Rate(Sec/Cycle)	Target Supply Pressure(psi)	Total Load (lb)	Tie Bearing Pressure (psi)
1	79	5	1100	24356	9
2	116	6	2500	54340	21
3	52	20	3500	76351	29
4	100	22	4500 (dry)	102245	39
5	100	24	4500 (soaked)	104000	39

4.5.1 East string pot (reinforced test)

Figure 4.5.1 shows the dynamic loading at different loading steps versus deformation.

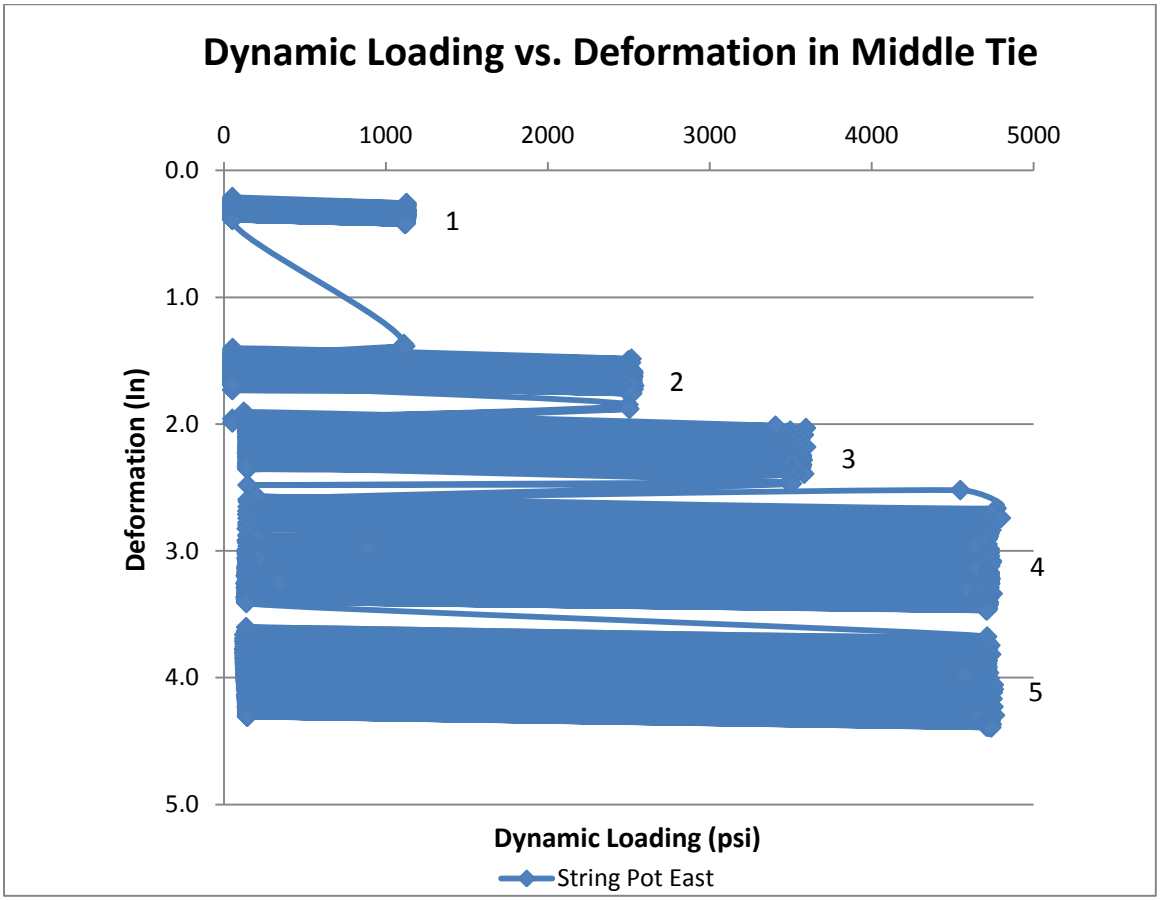

Figure 4.5.1 Dynamic loading vs. deformation. (reinforced test)

4.5.2 East string pot versus dynamic loading at 1100 psi – reinforced (9 psi tie bearing pressure)

Seventy nine cycles were applied on the railroad section at 1100 psi, resulting in a total accumulated deformation after seventy-nine cycles of 0.42 in. Figure 4.5.2 shows deformations (settlement) recorded by the east string pot for a dynamic loading of 1100 psi.

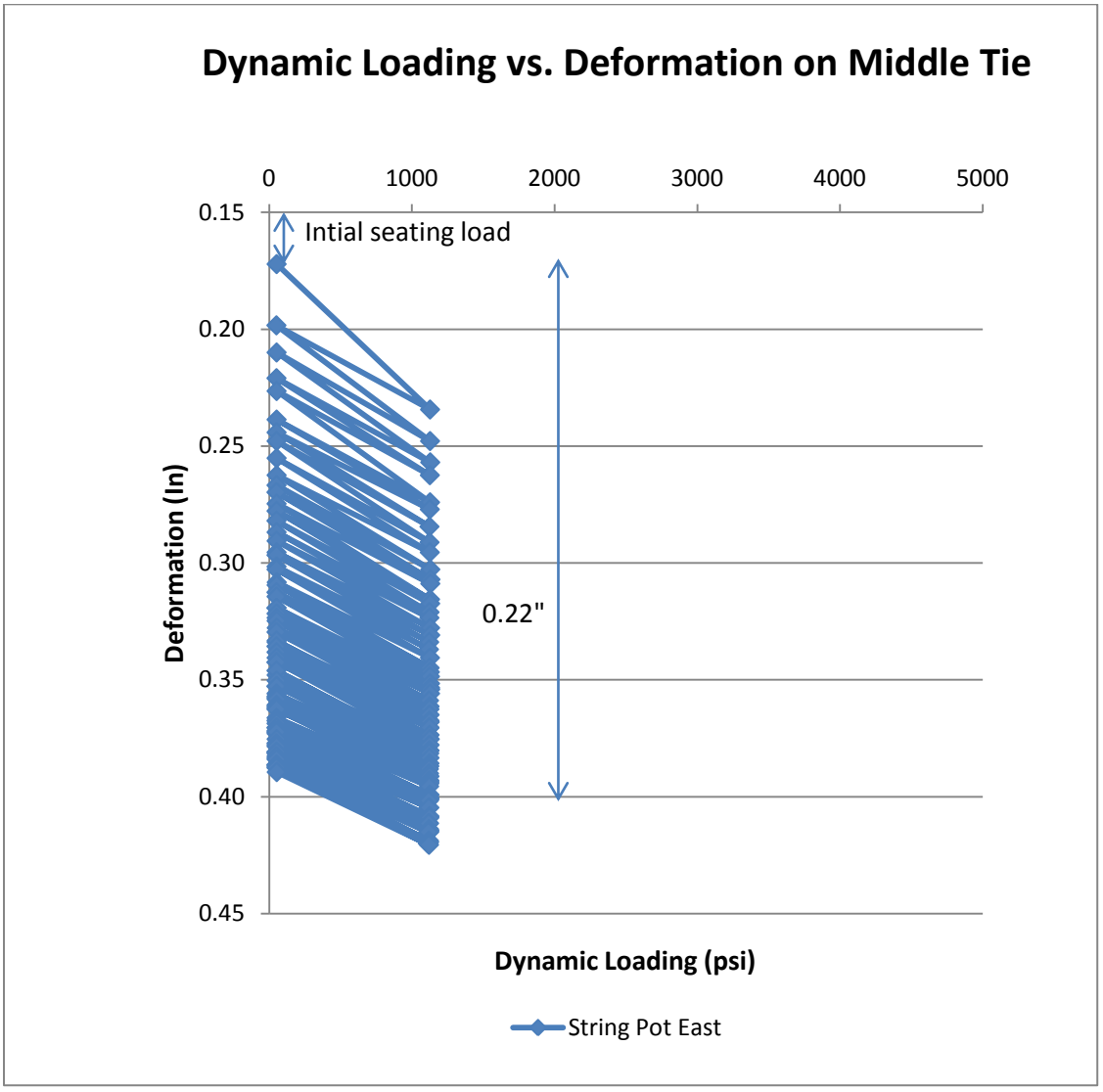

Figure 4.5.2 East string pot deformations versus dynamic loading at 1100 psi

4.5.3 East string pot versus dynamic loading at 2500 psi – reinforced (21 psi tie bearing pressure)

One hundred sixteen cycles were applied on the railroad section at 2500 psi. The total deformation accumulated after one hundred and sixteen cycles was 1.79 in. More permanent deformation per cycle was observed for the early cycles. As the number of cycle increased a greater percentage of the total deformation per cycle was elastic deformation. Figure 4.5.3 shows East string pot reading versus dynamic loading at 2500 psi.

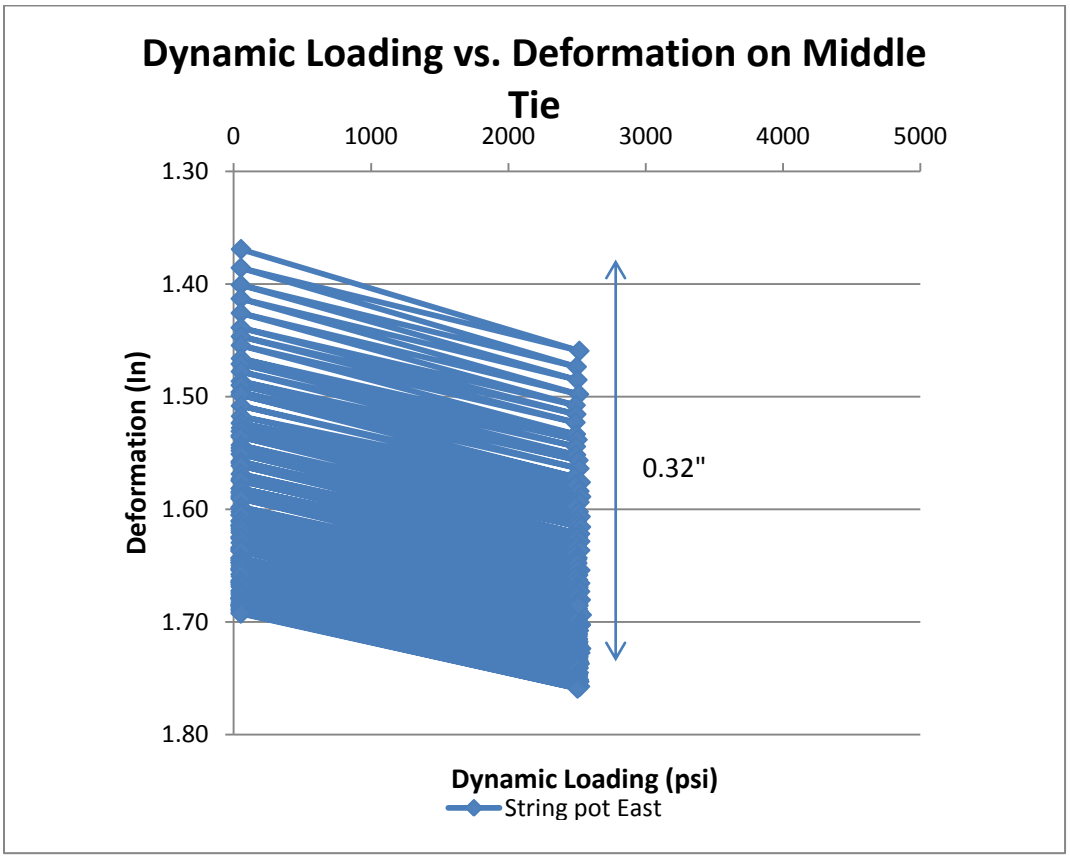

Figure 4.5.3 East string pot deformations versus dynamic loading at 2500 psi

4.5.4 East string pot versus dynamic loading at 3500 psi – reinforced (29 psi tie bearing pressure)

Fifty two cycles were applied to the railroad section at 3500 psi for a total accumulated deformation after 52 cycles of 2.4 in. Figure 4.5.4 shows the east string pot reading versus dynamic loading at 3500 psi.

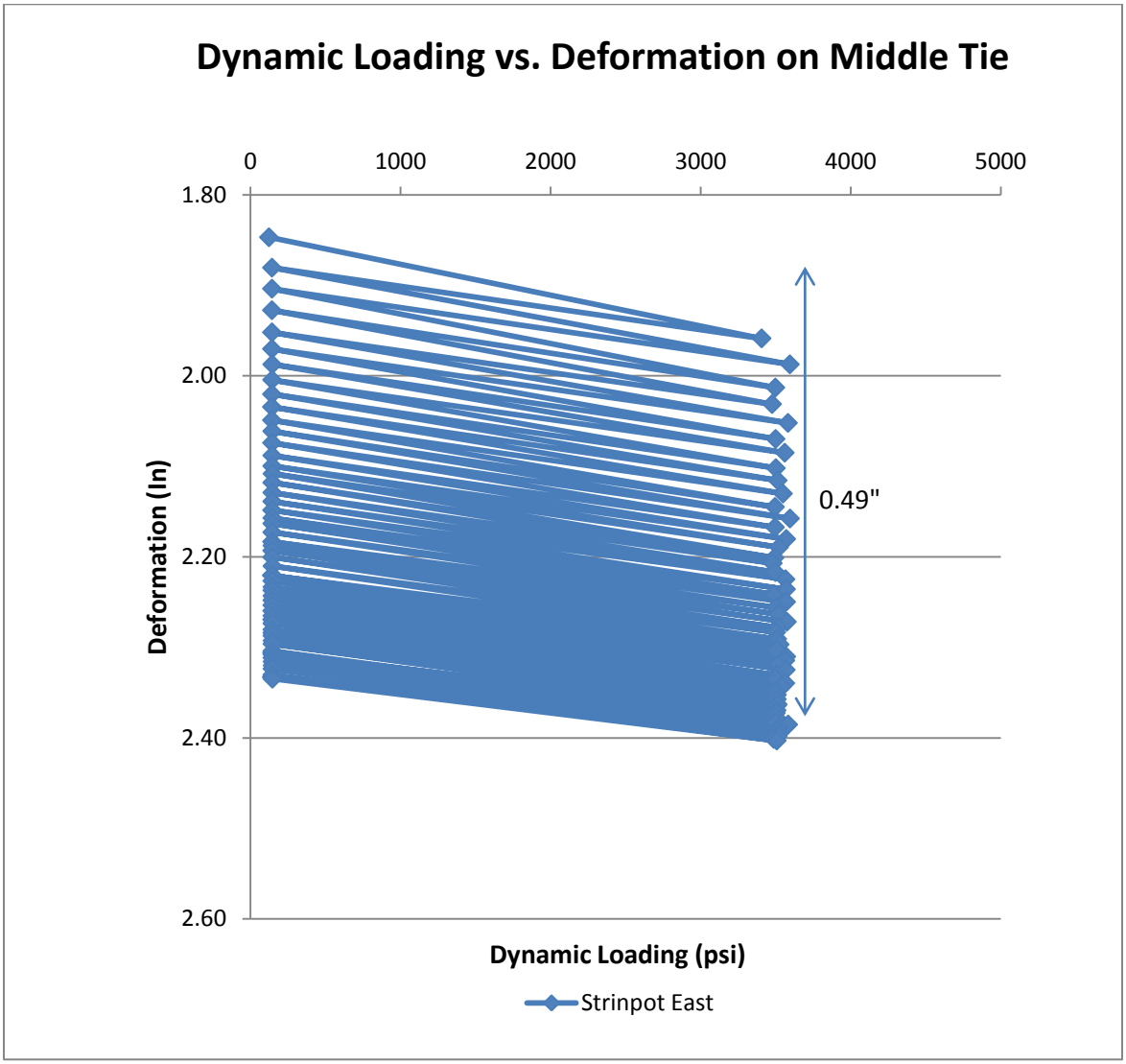

Figure 4.5.4 East string pot deformations versus dynamic loading at 3500 psi

4.5.5 East string pot versus dynamic loading at 4500 psi – reinforced (not soaked, 39 psi tie bearing pressure)

One hundred cycles were applied to the railroad section at 4500 psi. The total accumulated deformation after one hundred cycles was 3.46 in. Figure 4.5.5 shows the east string pot reading versus dynamic loading at 4500 psi. More permanent deformation was observed for the early cycles. As the number of cycles increased, more elastic deformation was observed.

As Figure 4.5.5 shows, at the beginning of the loading step the total deformation is the difference between number 1 on Figure 4.5.5 and number 2, which is about 0.124 in. On the same graph the difference between numbers 1 and 3 is the permanent deformation for the same cycle, which is 0.043 in, while the difference between points 2 and 3 is the elastic deformation. This elastic deformation is 0.081 in. As the number of cycles increases the permanent and total deformations per cycle decrease and a higher percentage of the deformation is elastic.

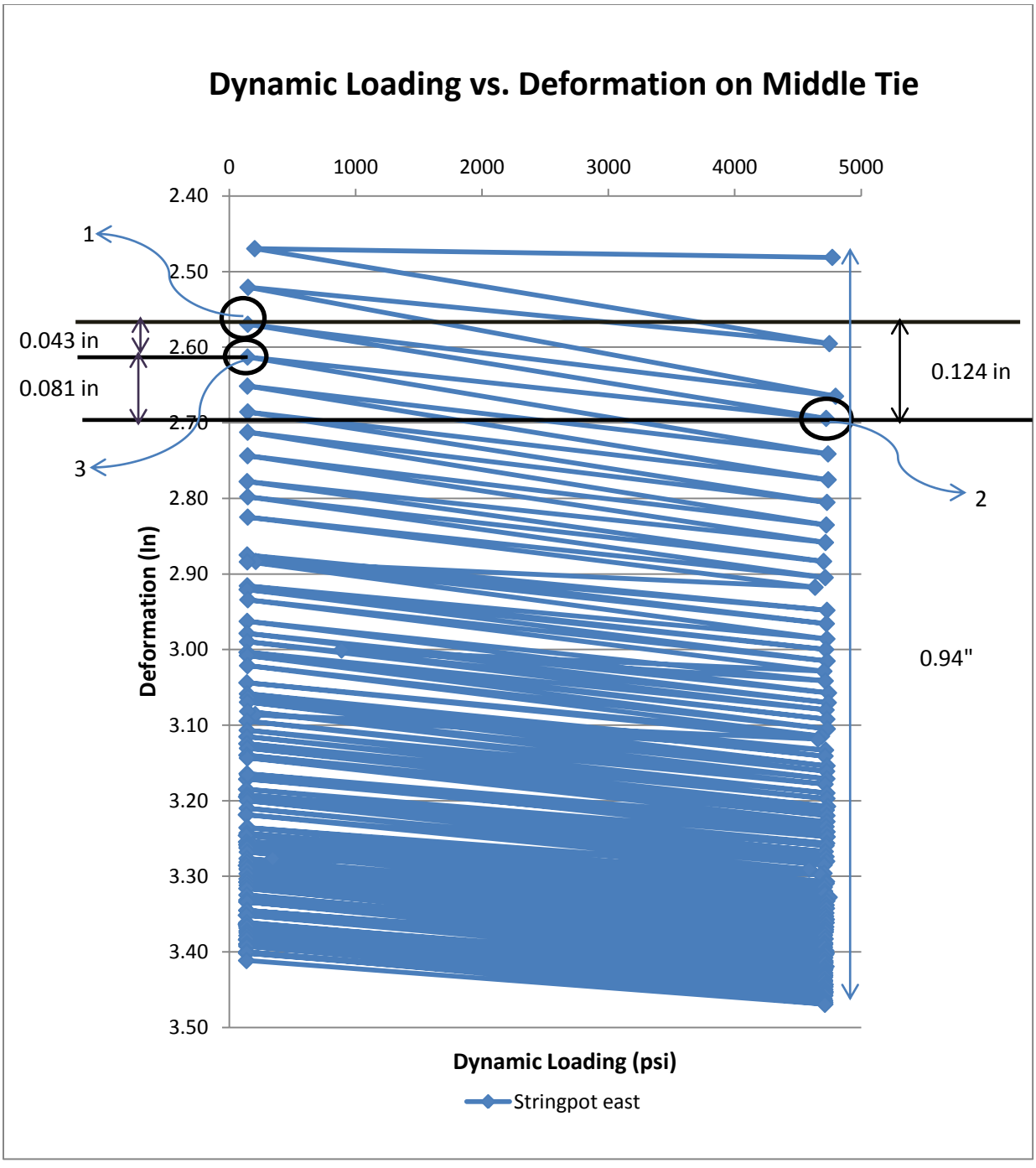

Figure 4.5.5 East String Pot versus dynamic loading at 4500 psi (not soaked)

4.5.6 East string pot versus dynamic loading at 4500 psi – reinforced (soaked, 39 psi tie bearing pressure)

Fifty gallons of water was added to the section by garden hose over period of 15 minutes. The section was left overnight for water to penetrate into the soil. One hundred cycles were applied to the railroad section at 4500 psi the following day. The total accumulated deformation after one hundred cycles was 4.39 in. As with the earlier steps the beginning cycles resulted in more permanent deformation per cycle. As the number of cycles increased a higher percentage of the deformation was elastic. Figure 4.5.6 shows the east string pot reading versus dynamic loading at 4500 psi soaked.

As Figure 4.5.6 shows, at the beginning of the loading step the difference between number 1 on Figure 4.5.6 and number 2 was the total deformation, which was 0.11 in which was 50% more than was observed during the initial cycles when loading the section to 4500 psi without soaking and 40% more than was observed at the end of the end of unsoaked loading. Most of the additional deformation per cycle was permanent. On the same graph the difference between number 1 and 3 was the permanent deformation for the same cycle which was 0.08 in. The elastic deformation is shown on the same graph and was 0.03 in. As with the previous loading step the permanent and total deformations per cycle decreased and a higher percentage of the deformation was elastic.

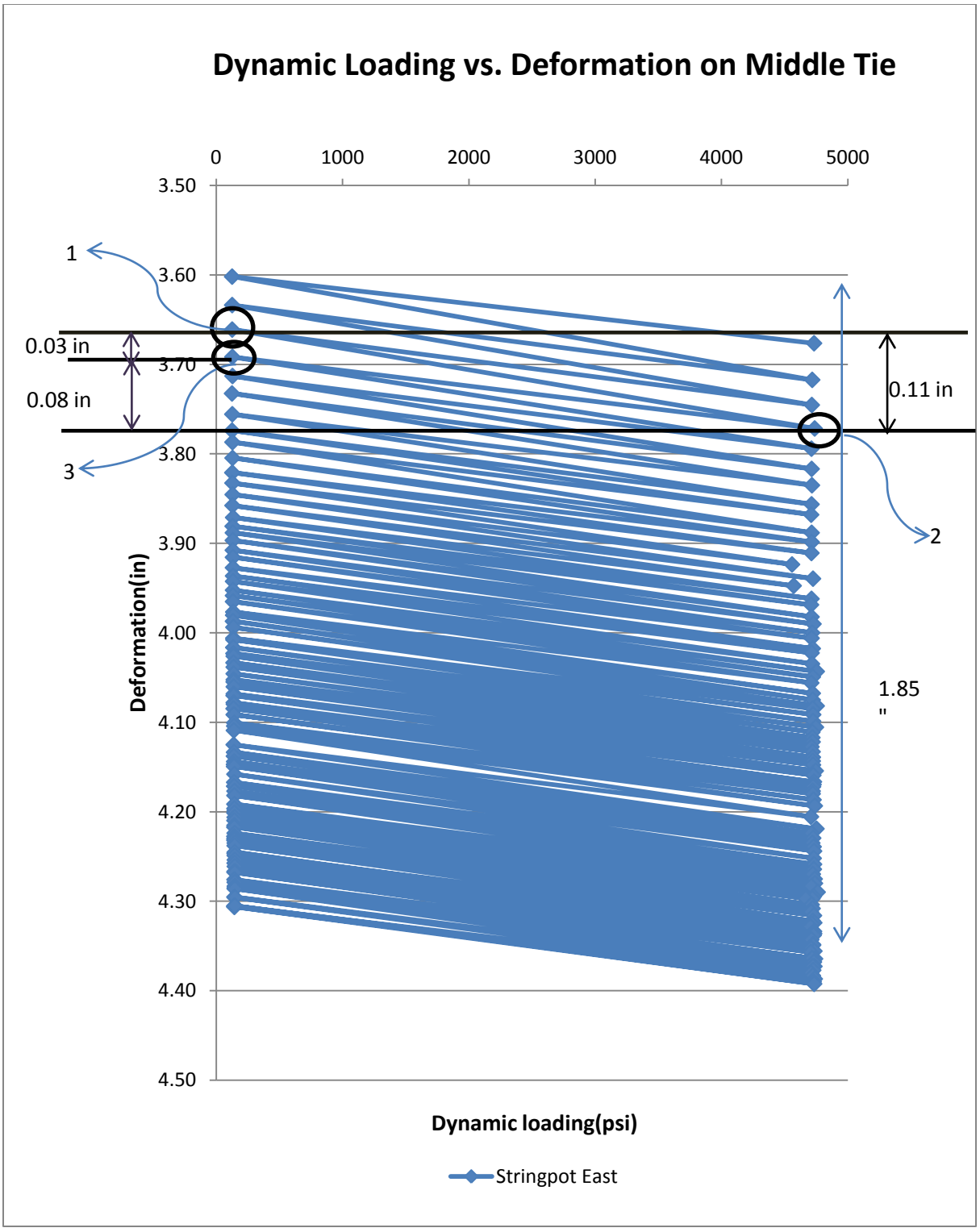

Figure 4.5.6 East String Pot versus dynamic loading at 4500 psi (soaked)

4.6 Reinforced test

4.6.1 West string pot (reinforced test)

Figure 4.6.1 through Figure 4.6.6 show the recorded values on the west string pot.

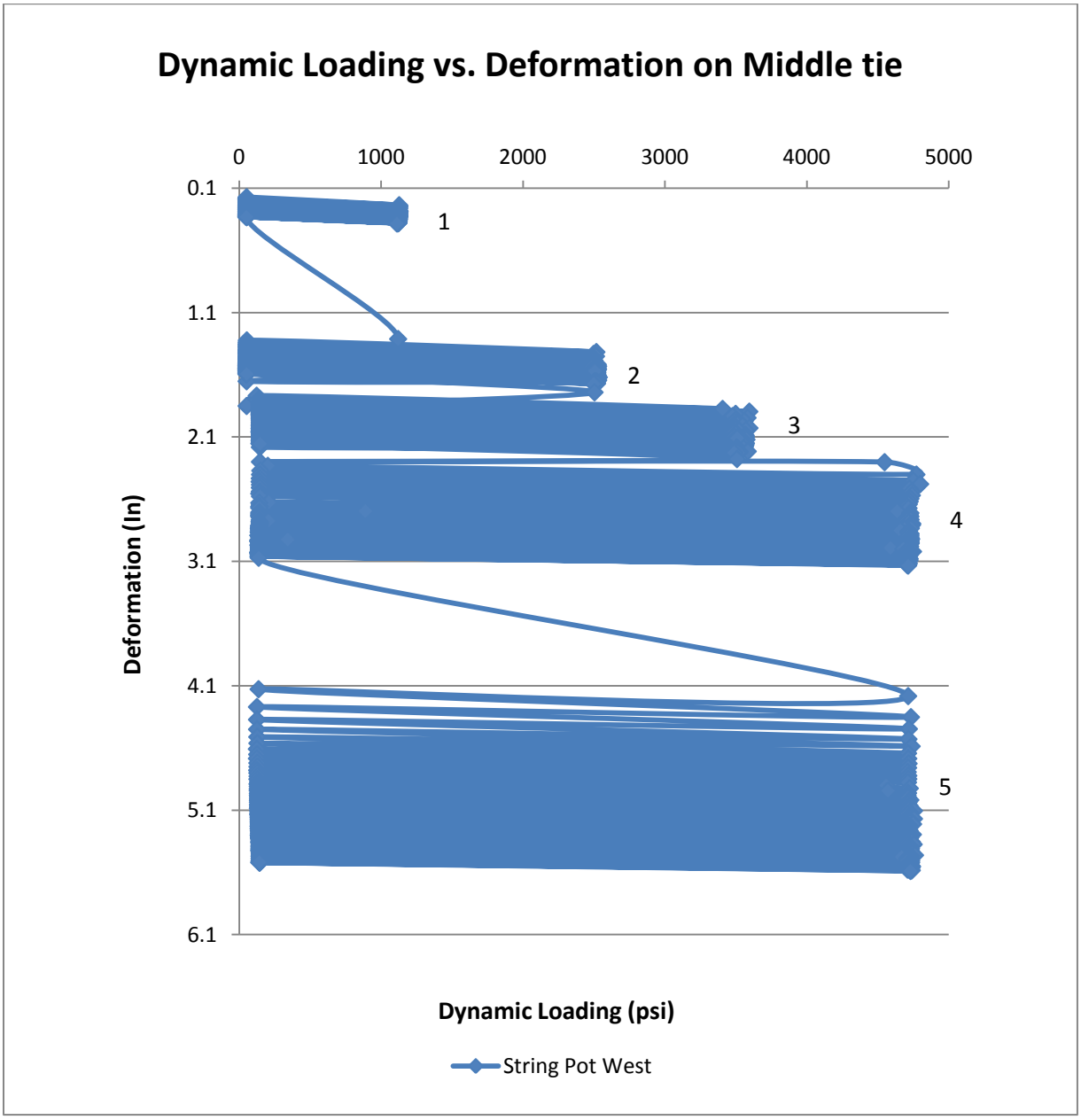

Figure 4.6.1 Dynamic loading vs. deformation. (reinforced test)

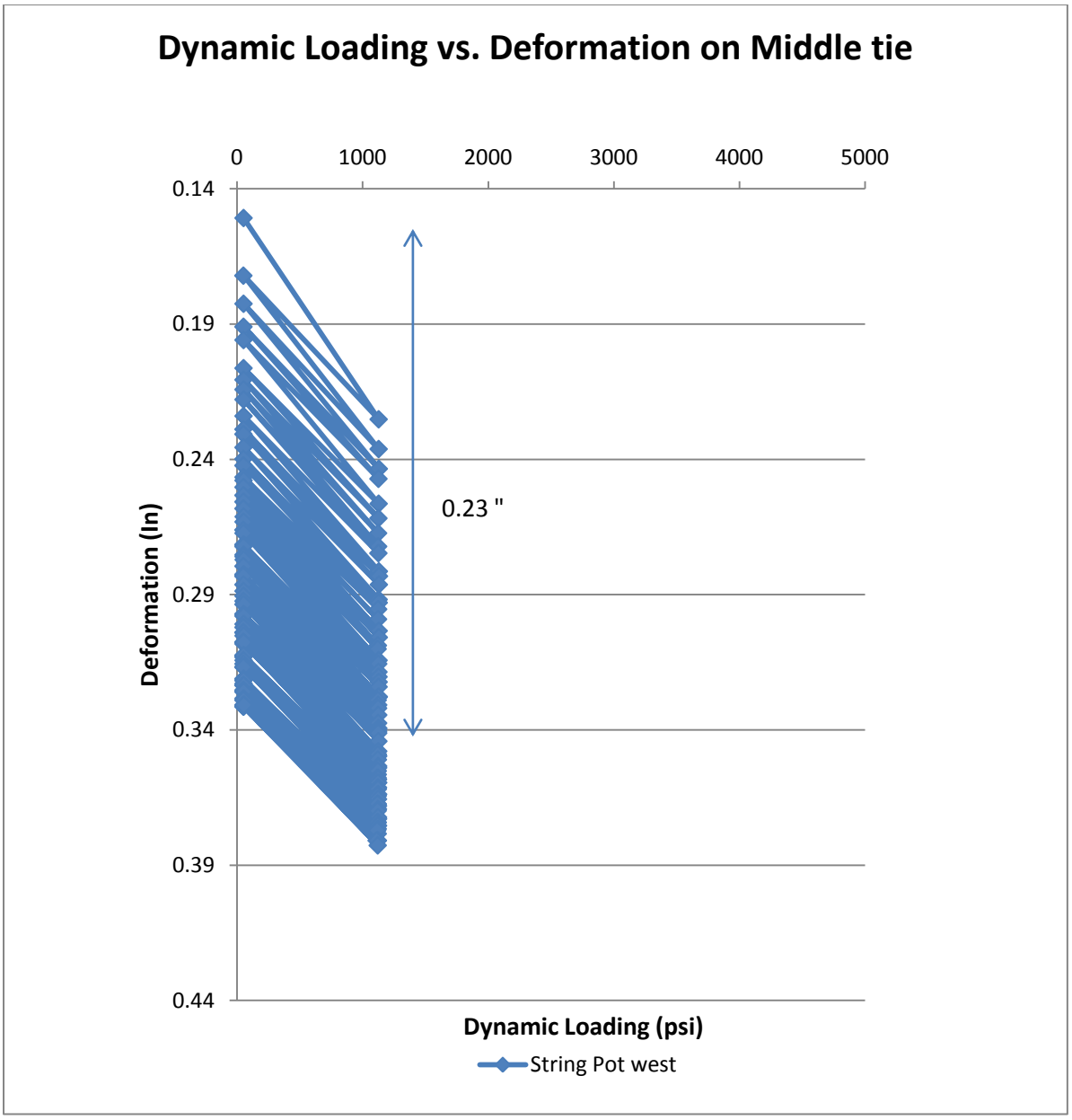

Figure 4.6.2 West string pot versus dynamic loading at 1100 psi

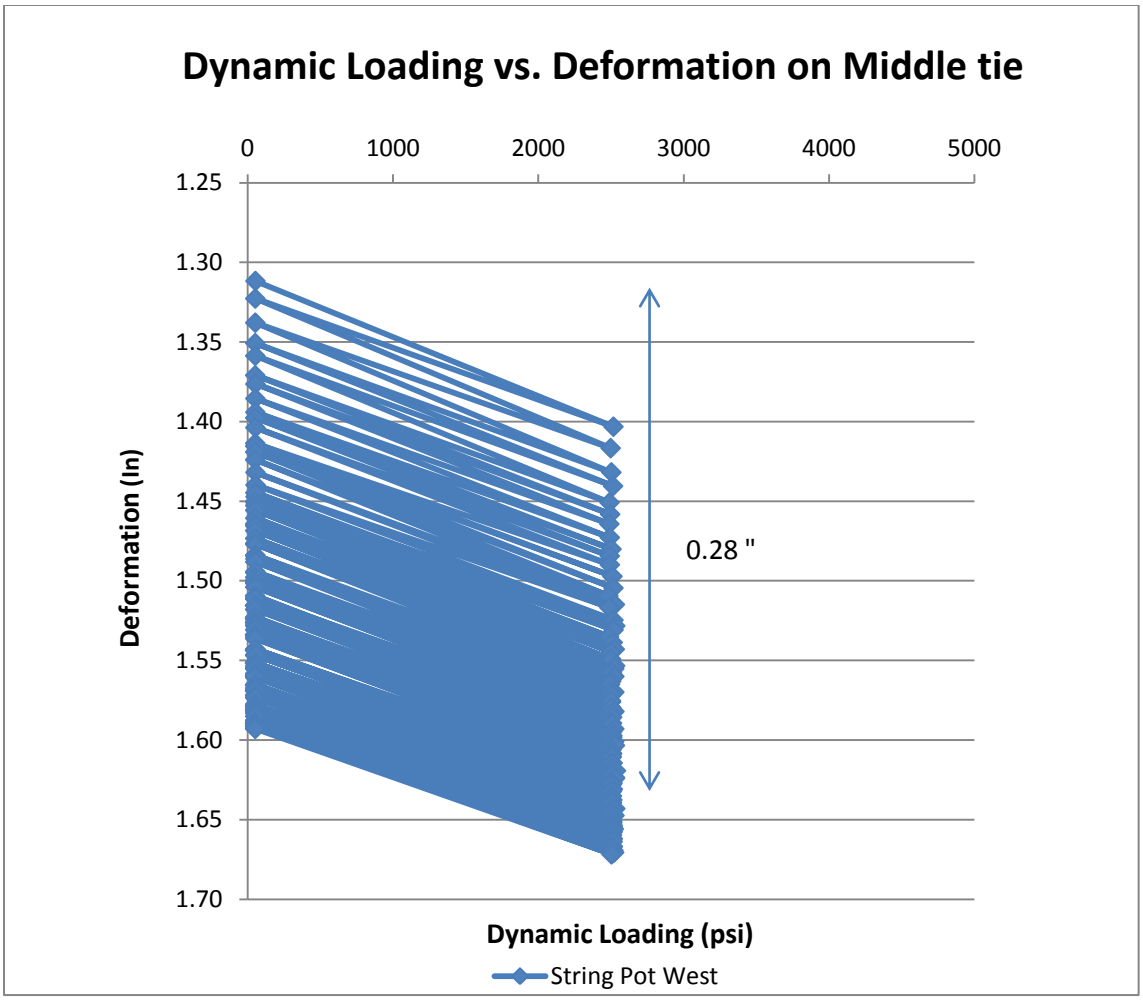

Figure 4.6.3 West string pot versus dynamic loading at 2500 psi

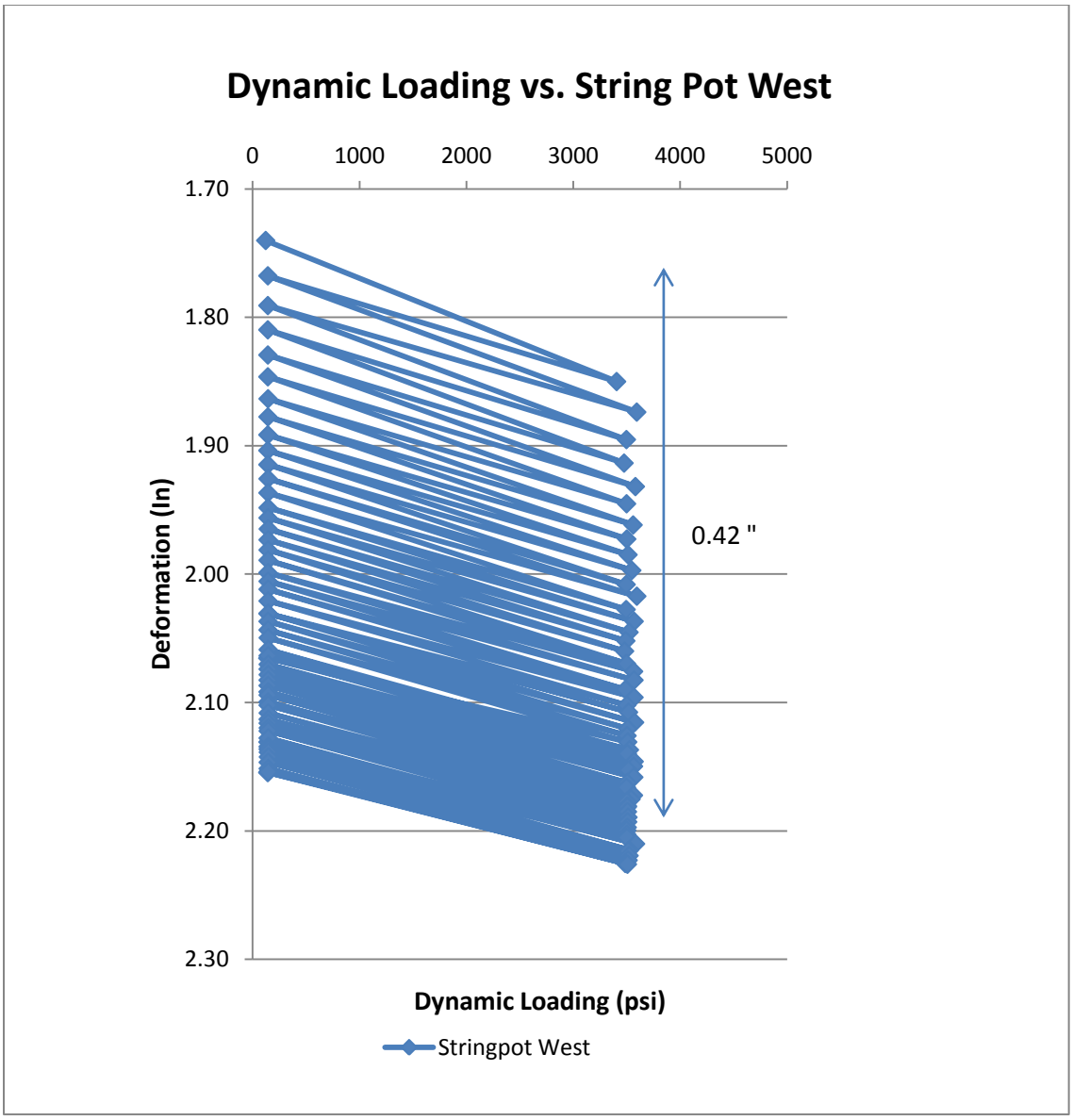

Figure 4.6.4 West string pot versus dynamic loading at 3500 psi

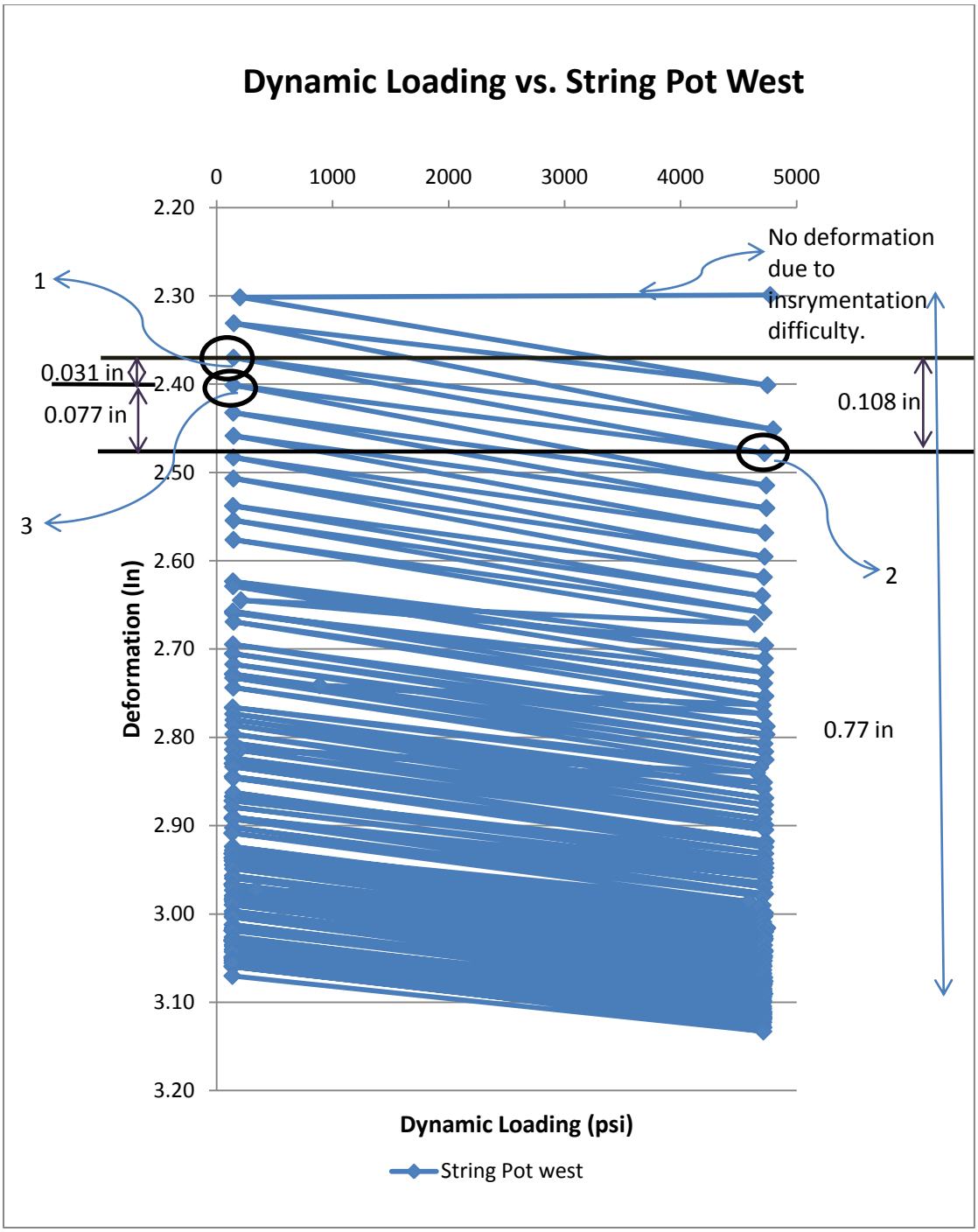

Figure 4.6.5 West string pot versus dynamic loading at 4500 psi (not soaked)

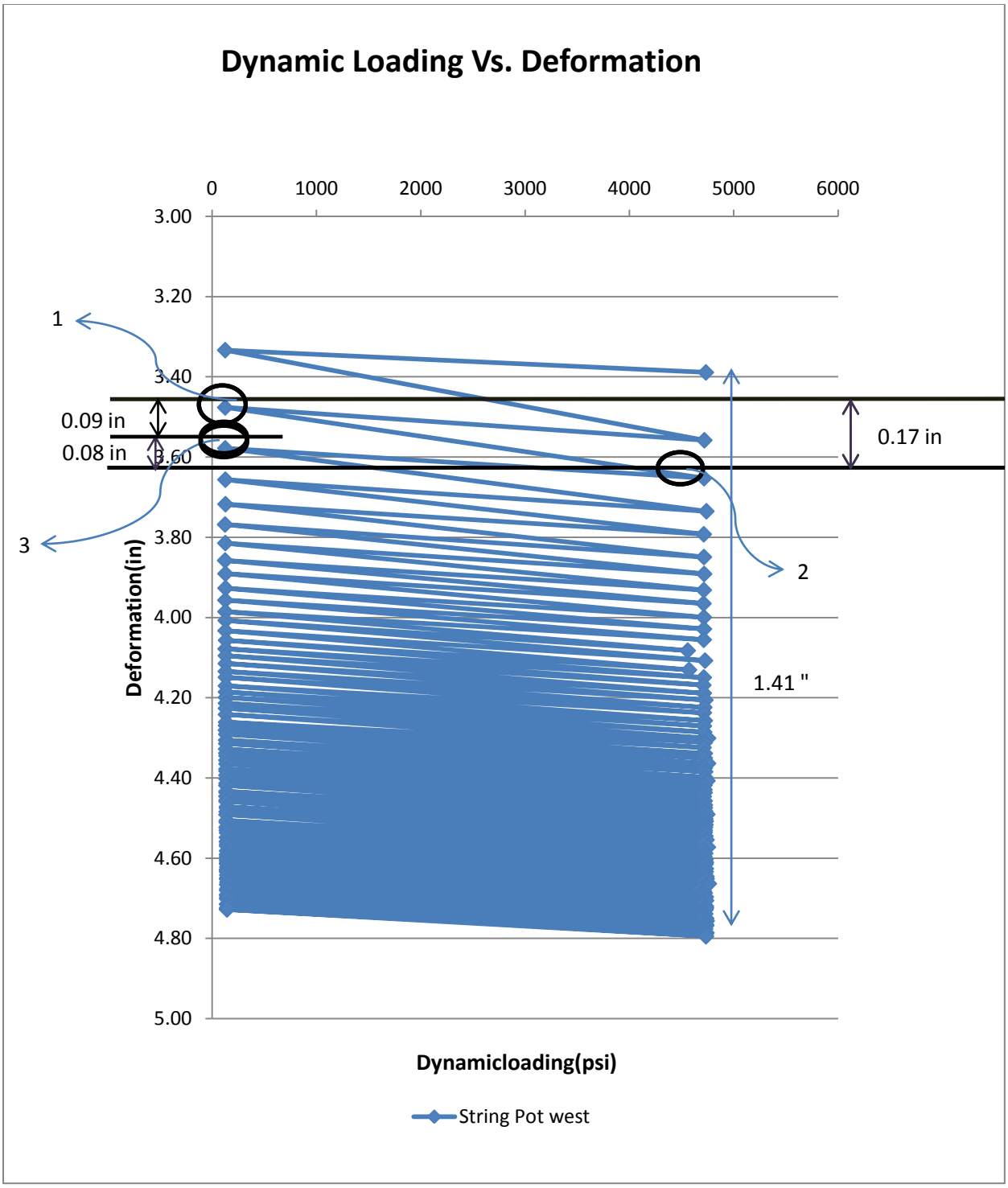

Figure 4.6.6 West string pot versus dynamic loading at 4500 psi (soaked)

4.7 Reinforced Test (Displacement Transducers)

Four displacement transducers were installed on the railroad track to measure the deformation near the ends of each rail on the track panel. Figure 4.7 shows the transducer locations. Some sliding of transducer ends during some load steps resulted in measurements that were not reliable and these results are not included in the analysis.

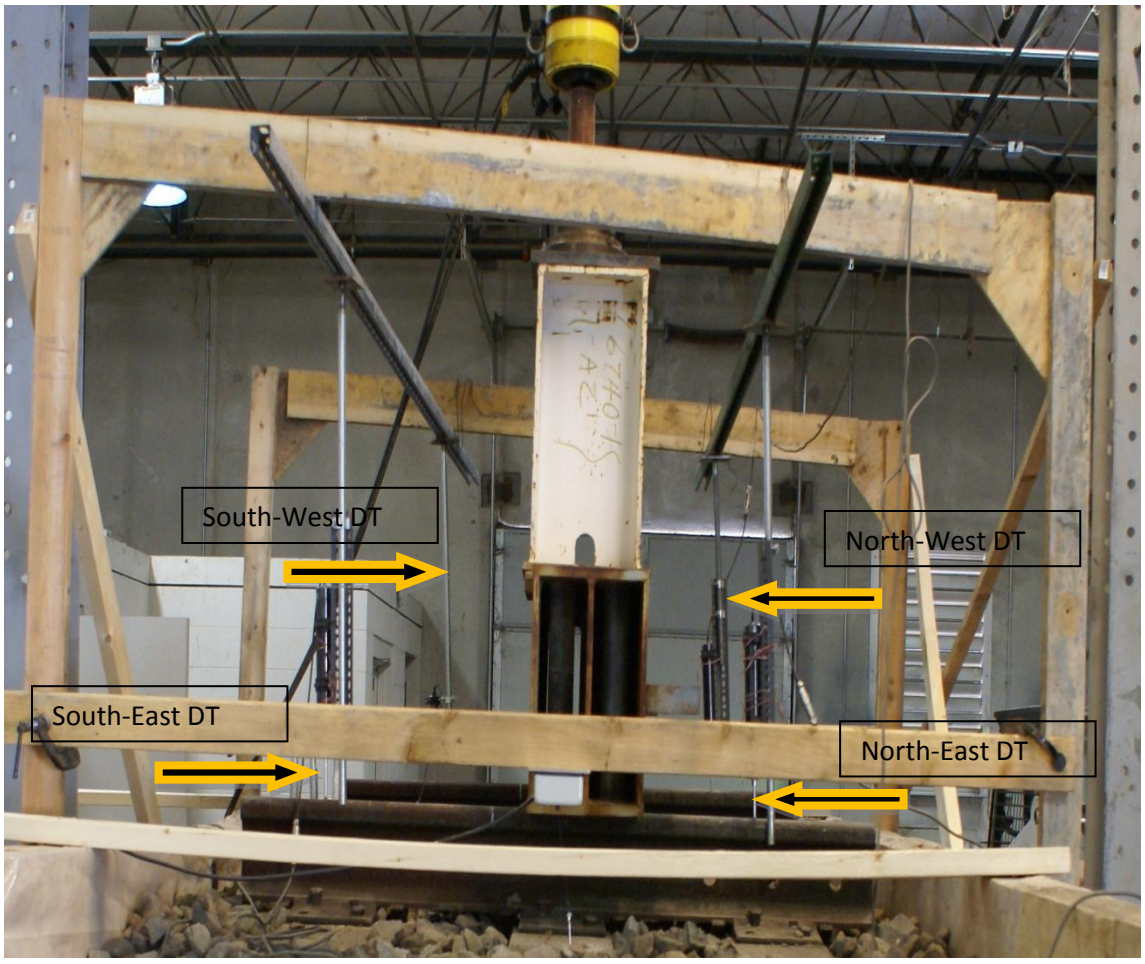

Figure 4.7 Displacement transducers

4.7.1 Displacement transducers (DT) at 1100 psi (South-East, 9psi bearing pressure)

Seventy-nine cycles were applied to the railroad section at 1100 psi. The total deformation measured by the south-east DT after seventy nine cycles was 0.55 in. Displacements of 0.36 and 0.33 were recorded at the north- west and south-west corners, respectively. The reading at the north-east corner was unreliable. No reliable readings were recorded at any of the later load steps. Figures 4.7.1 through 4.7.3 show DT readings versus dynamic loading.

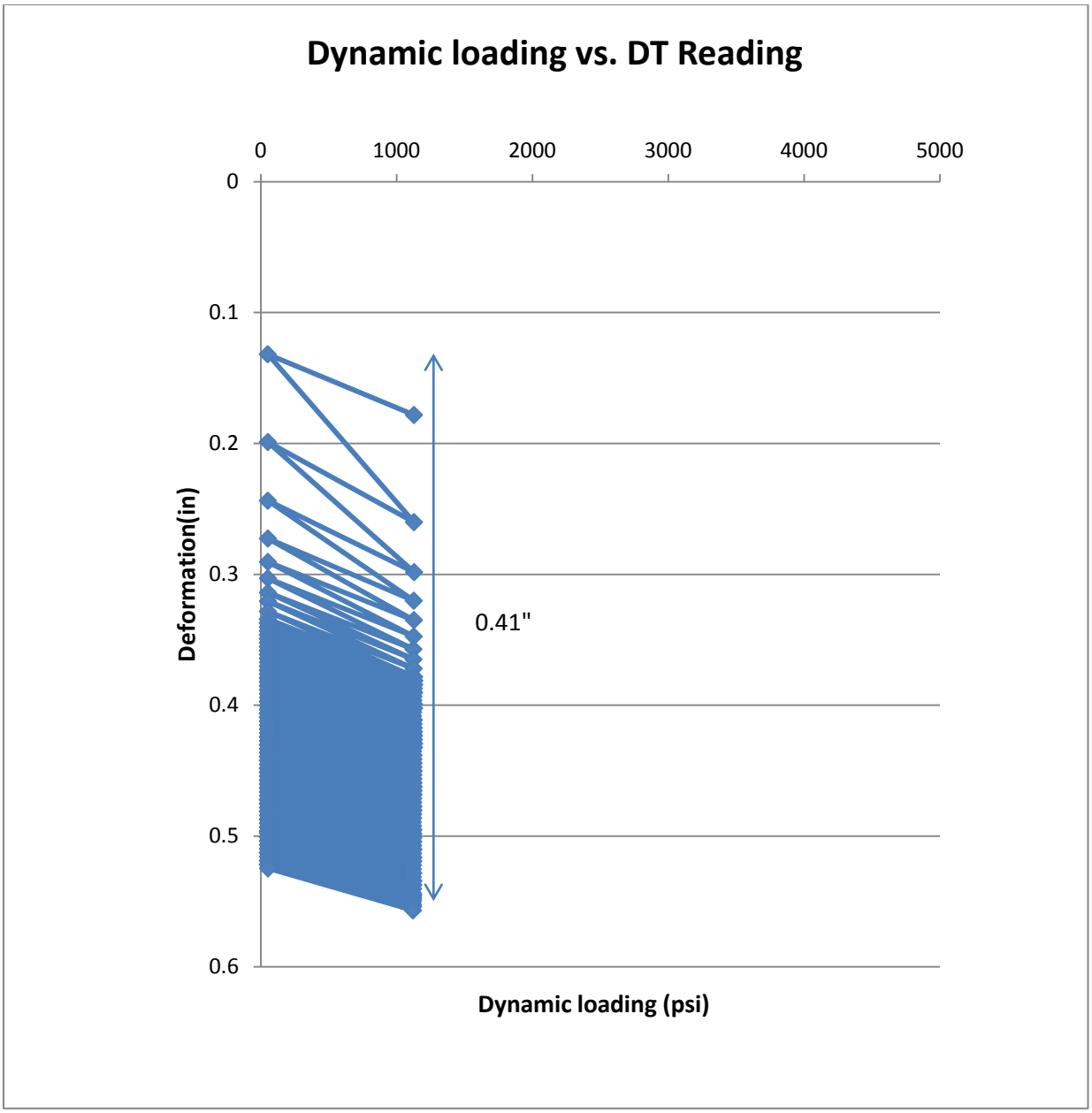

Figure 4.7.1 Displacement transducer readings at 1100 psi (south-east)

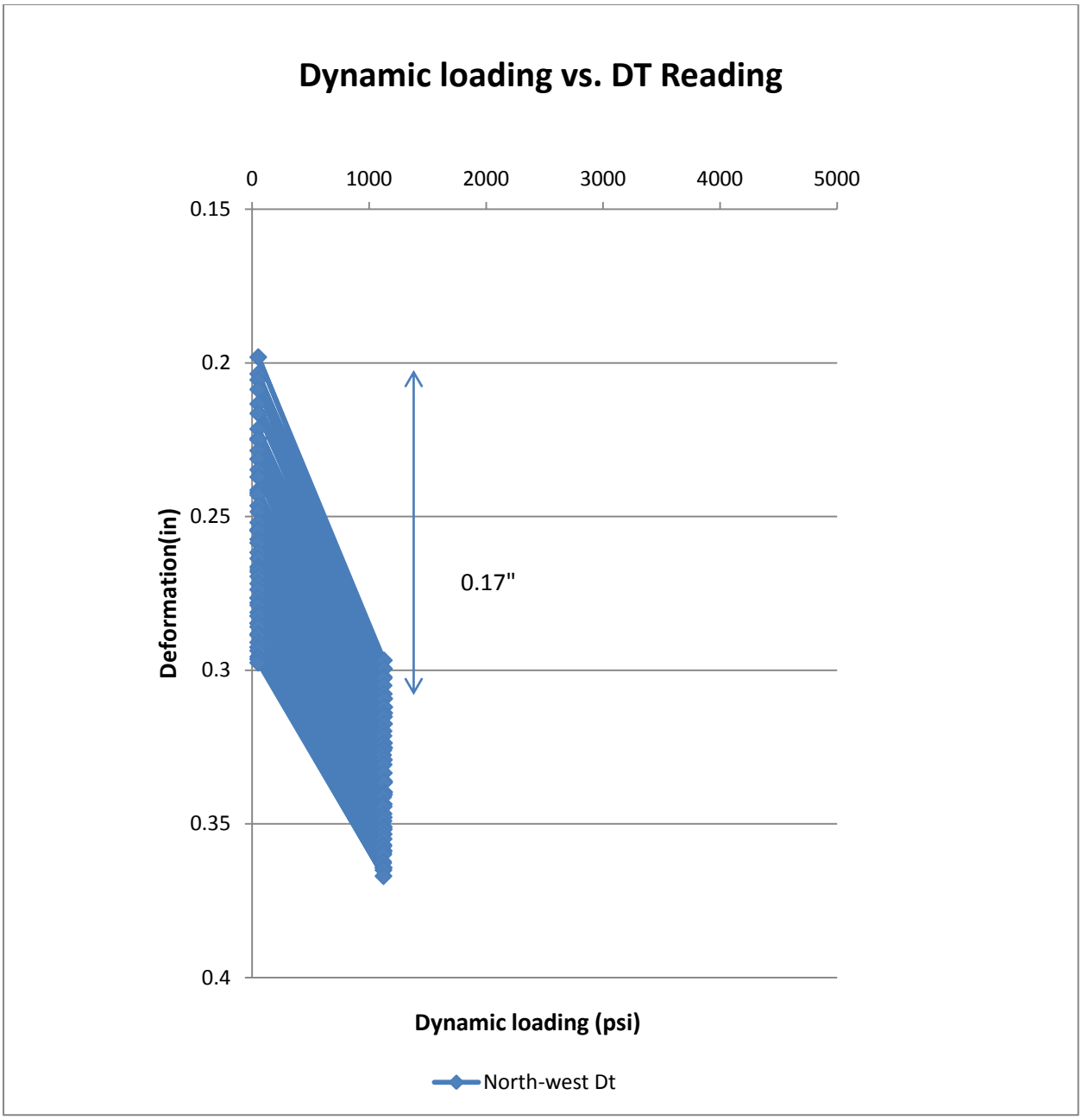

Figure 4.7.2 Displacement transducer readings at 1100 psi (north-west)

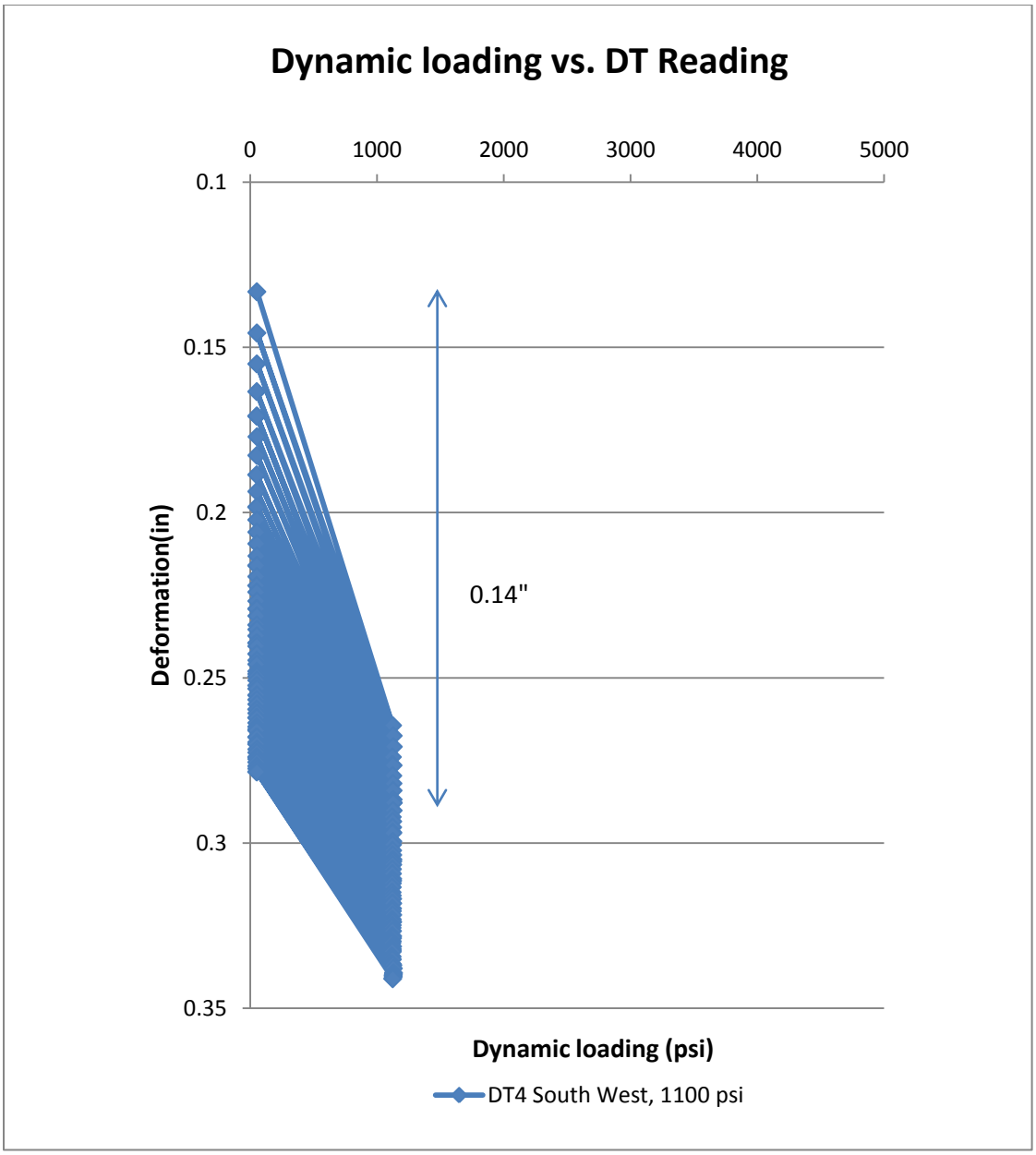

Figure 4.7.3 Displacement transducer readings at 1100 psi (south-west)

4.8.1 Pressure Cells Results for reinforced Test

Five Pressure Cells were installed as shown in Figure 4.8.1. Pressure Cells 1, 2 and 3 were installed at the interface of subgrade and ballast below the middle tie (1 and 3 were right below the rails road track). Pressure cells 4 and 5 were installed under the right tie.

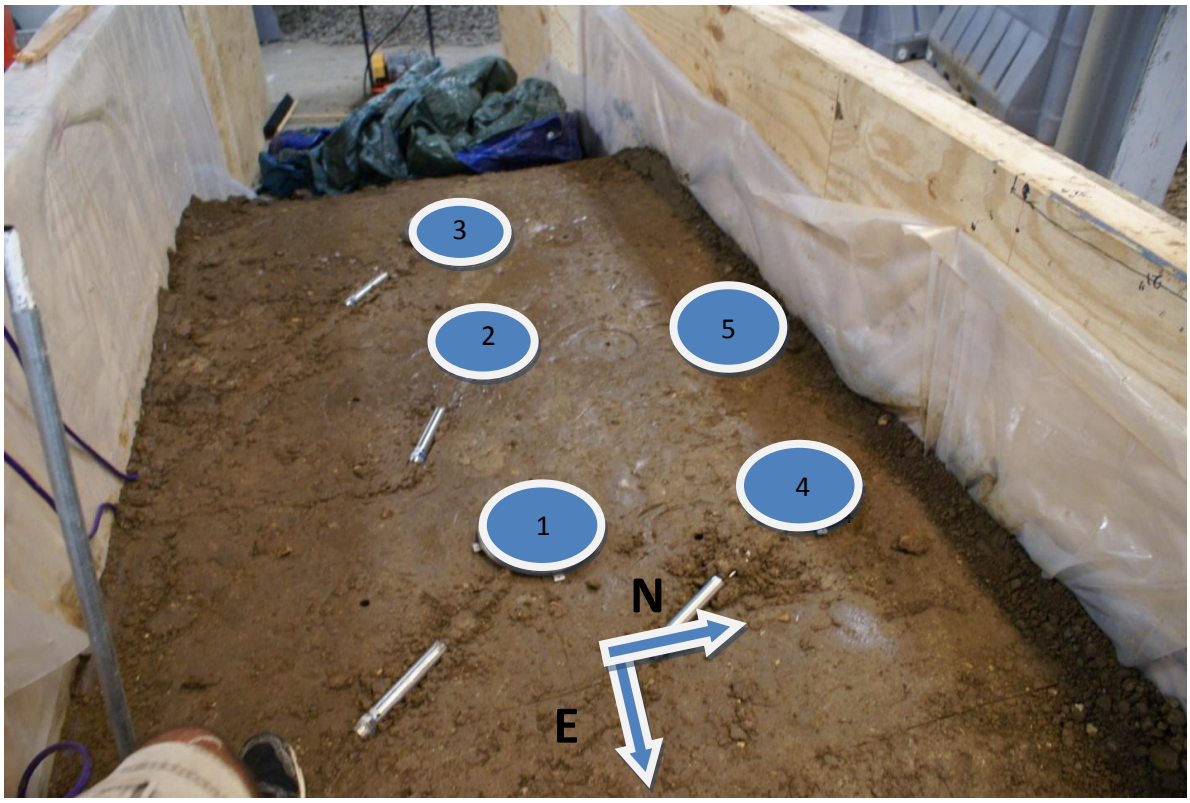

Figure 4.8.1 Pressure Cells

4.8.2 Pressure cells results at subgrade level

Figure 4.8.2 Table 4.8.2 and show the pressure cell data versus pressure transducer data for the reinforced case. Pressure cell 4 data was not recorded due to the failure of pressure cell 4. For this test unlike the unreinforced case, the subgrade did not fail at any location until it was soaked with 50 gallons of water. Pressure cell 2 experienced the highest pressure at approximately 21 psi. Figure 4.8.3 and Table 4.8.1 present the similar information vs. tie bearing pressure.

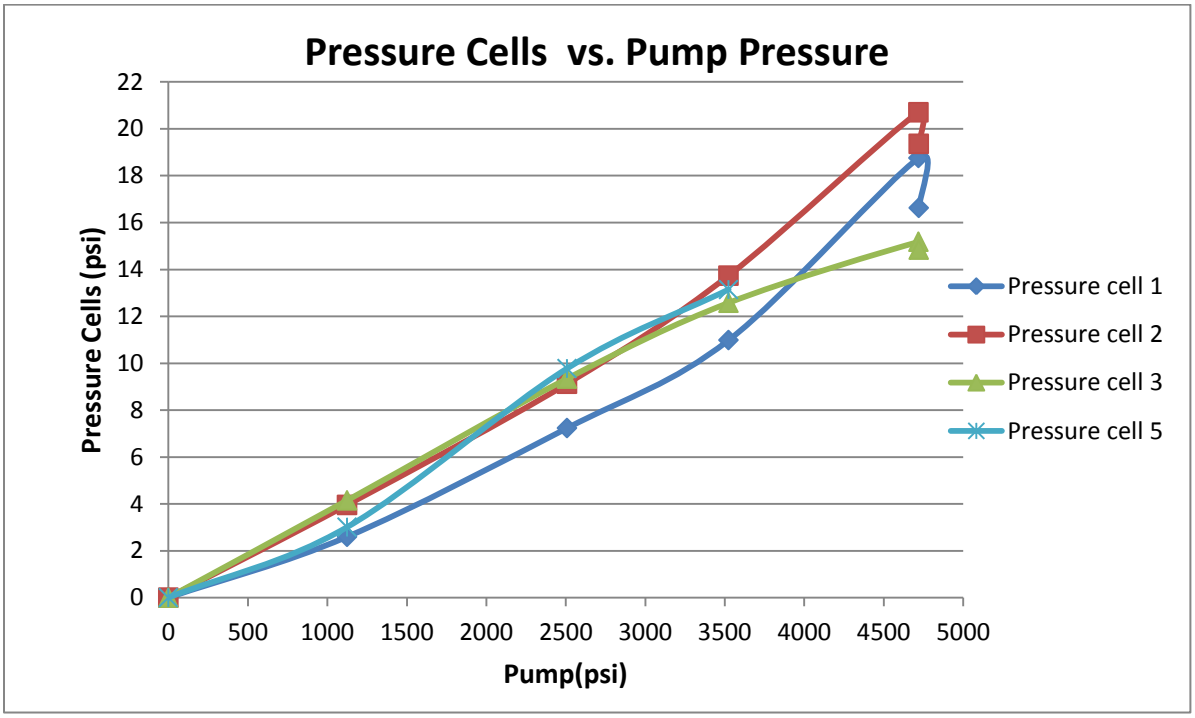

Figure 4.8.2 Pressure cells vs. pump pressure at subgrade level

Table 4.8.1 Pressure cells vs. pump at subgrade level

Load (lb)	Pressure Transducer (psi)	Pressure cell 1 (psi)	Pressure cell 2 (psi)	Pressure cell 3 (psi)	Pressure cell 4 (psi)	Pressure cell 5 (psi)
0	0	0	0	0	0	0
24356	1124	2.60	3.95	4.15	1.33	3.01
54340	2508	7.23	9.12	9.34	1.59	9.77
76351	3524	10.99	13.73	12.58	1.77	13.14
102245	4719	18.76	20.70	15.18	2.06	No Reading
102288	4721	16.63	19.36	14.85	1.98	No Reading

4.8.3 Pressure cells results under ties

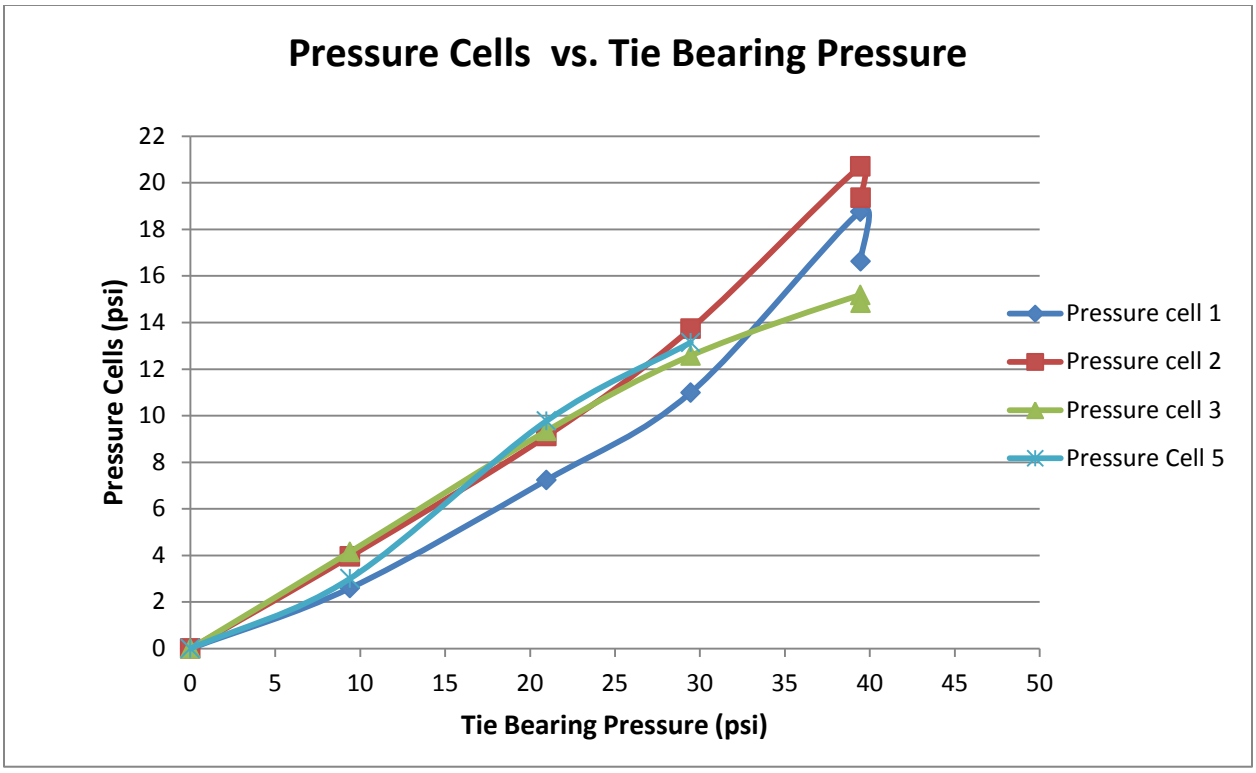

Figure 4.8.3 Pressure cells vs. tie bearing pressure

Table 4.8.2 Pressure cells vs. tie bearing pressure (reinforced)

Right below ties						
Load (lb)	**Tie Bearing Pressure (psi)**	**Pressure cell 1 (psi)**	**Pressure cell 2 (psi)**	**Pressure cell 3 (psi)**	**Pressure cell 4 (psi)**	**Pressure cell 5 (psi)**
0	**0**	**0**	**0**	**0**	**0**	**0**
24356	9	2.60	3.95	4.15	1.33	3.01
54340	21	7.23	9.12	9.34	1.59	9.77
76351	29	10.99	13.73	12.58	1.77	13.14
102245	39	18.76	20.70	15.18	2.06	0.00
102288	39	16.63	19.36	14.85	1.98	0.00

4.9 Unreinforced vs. Reinforced: Settlement Comparison

Table 4.9.1 shows the comparison between unreinforced and reinforced test for unit weight and number of cycles.

Table 4.9.1 Comparison of loading cycles and subgrade conditions

	Unreinforced	Reinforced
Prior to test Unit Weight (lb/ft^3)	91.5	93
Number of Cycles	447	447
Moisture Content Before Test	26	27
Moisture Content After Test	26.5	27.5
% Proctor	92%	93%

The results for the two tests are compared in this section. As shown in Figure 4.9.1, the reduction in settlement for the reinforced section is noticeable for both the west and east string pots. The improvement was minimal for the light early loading but became more significant as loading and settlements became larger.

Figure 4.9.1 (west string pot result comparison) shows a reduction in settlement of 0.64 inches of improvement in settlement.

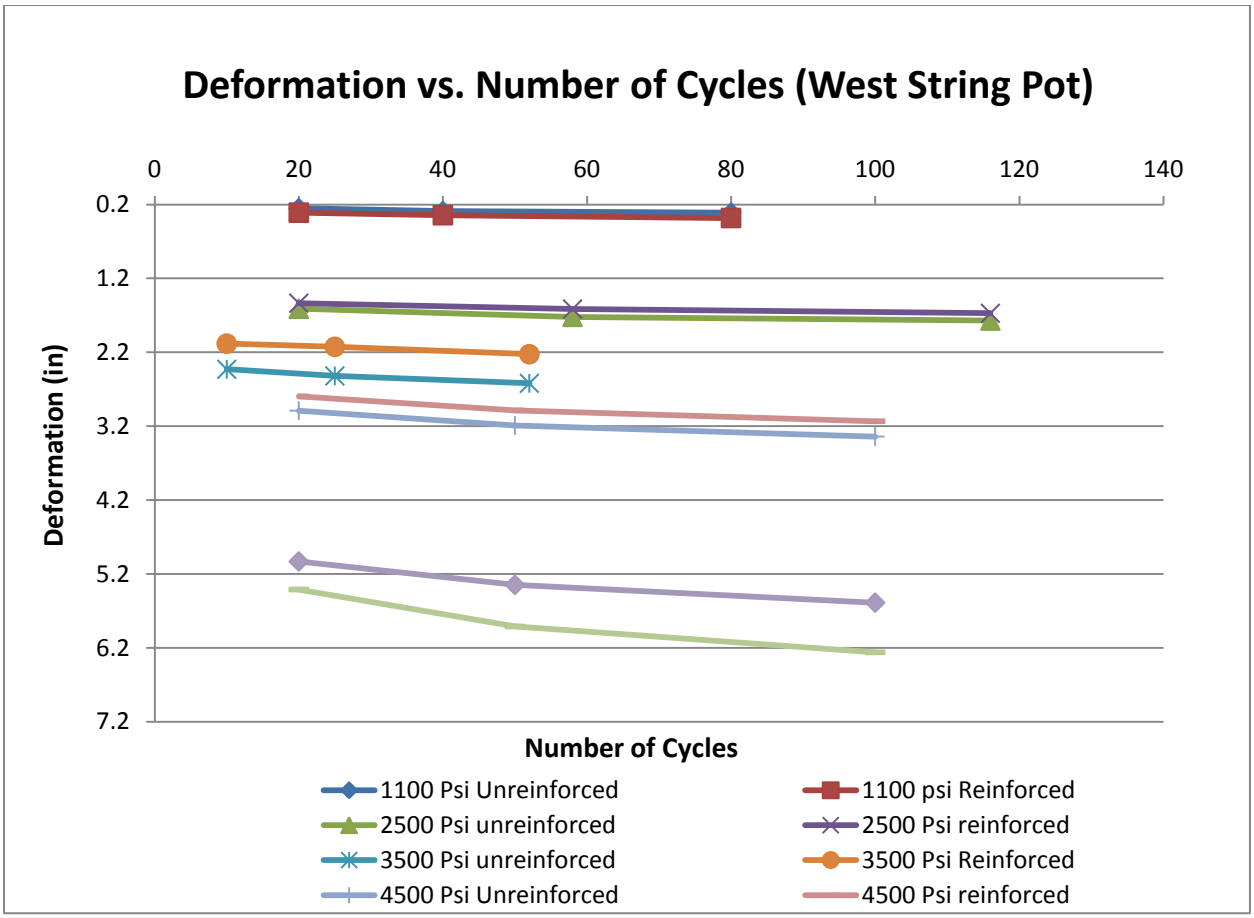

Figure 4.9.1 West string pot result comparison

Table 4.9.2 Comparison of settlement between the reinforced test and unreinforced test (west string pot)

Pressure (psi)	Deformation(in) West Stringpot		Number Of cycles	Actual Pressure applied Reinforced (psi)	Actual Pressure applied Unreinforced (psi)
	Unreinforced	Reinforced			
1100(Beginning)	0.25	0.31	20	1120	1070
1100(Middle)	0.29	0.34	40	1126	1080
1100(End)	0.31	0.38	80	1121	1070
2500(Beginning)	1.61	1.54	20	2487	2480
2500(Middle)	1.72	1.61	58	2512	2440
2500(End)	1.77	1.67	116	2505	2450
3500(Beginning)	2.43	2.08	10	3570	3580
3500(Middle)	2.52	2.13	25	3505	3680
3500(End)	2.62	2.23	52	3508	3670
4500(Beginning)	2.99	2.80	20	4741	4406
4500(Middle)	3.19	2.99	50	4590	4462
4500(End)	3.34	3.13	100	4714	4480
4500 Soaked(Beginning)	5.41	5.03	20	4715	4370
4501 Soaked(Middle)	5.91	5.35	50	4740	4470
4502 Soaked(End)	6.26	5.59	100	4735	4470

At the end of 1100 psi loading there is no substantial difference in settlement between the two sections. After the 2500 psi loading step an improvement of 0.09 in was observed for the reinforced case. The amount of improvement improved to 0.4 after the 3500 psi loading step, 0.2 in after the 4500 psi loading step (not soaked) and 0.6 in after loading of the soaked section.

Notice on Figure 4.9.1 how the trends for the reinforced and unreinforced case for 1100psi loading are nearly identical. As larger loads are applied the gap between the reinforced and unreinforced trends gets larger until the 3500 psi loading step. However, for the 4500 psi step the gap gets smaller. This is likely due to differences in the pressure applied for the unreinforced and reinforced cases. As shown in Table 4.9.3, the pressure applied to the reinforced section was slightly less than that for the unreinforced section at the 3500 psi load step, and the reverse was true for the 4500 psi load step. This explains the larger gap at the 3500 psi load step and the smaller gap at the 4500 psi load step. Figure 4.9.2 shows how loads difference contribute to the gap difference.

Table 4.9.3 Reinforced loading vs. unreinforced loading

Reinforced Loads(Lbs)	Unreinforced Loads(Lbs)	Load difference in percentage
24356	23194	5.0%
54340	53407	1.7%
76351	79116	-3.5%
102245	97500	4.9%
102288	104000	-1.6%

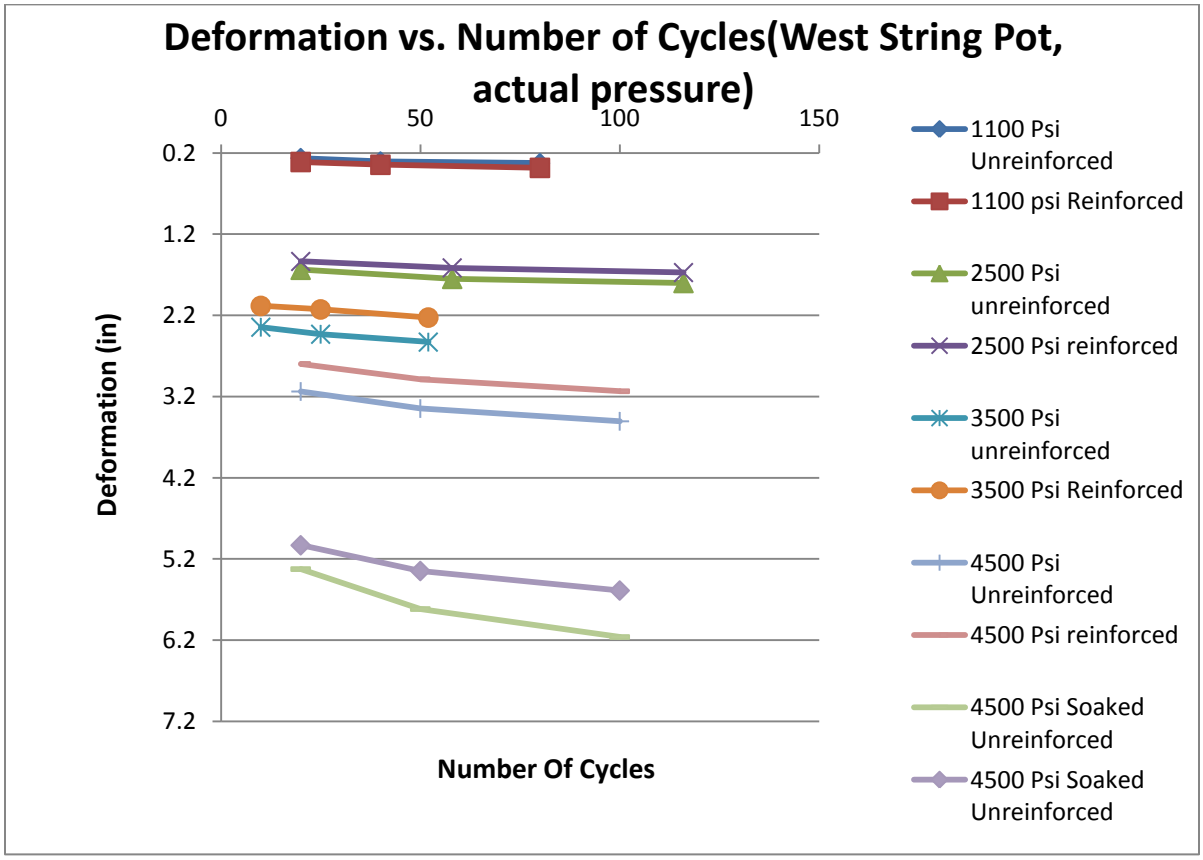

Figure 4.9.2 West string pot result comparison (after adjusting loads)

4.9.1 Reinforced vs. Unreinforced (East String Pot)

Figure 4.9.2 shows the deformation vs. number of cycles for the east string pot.

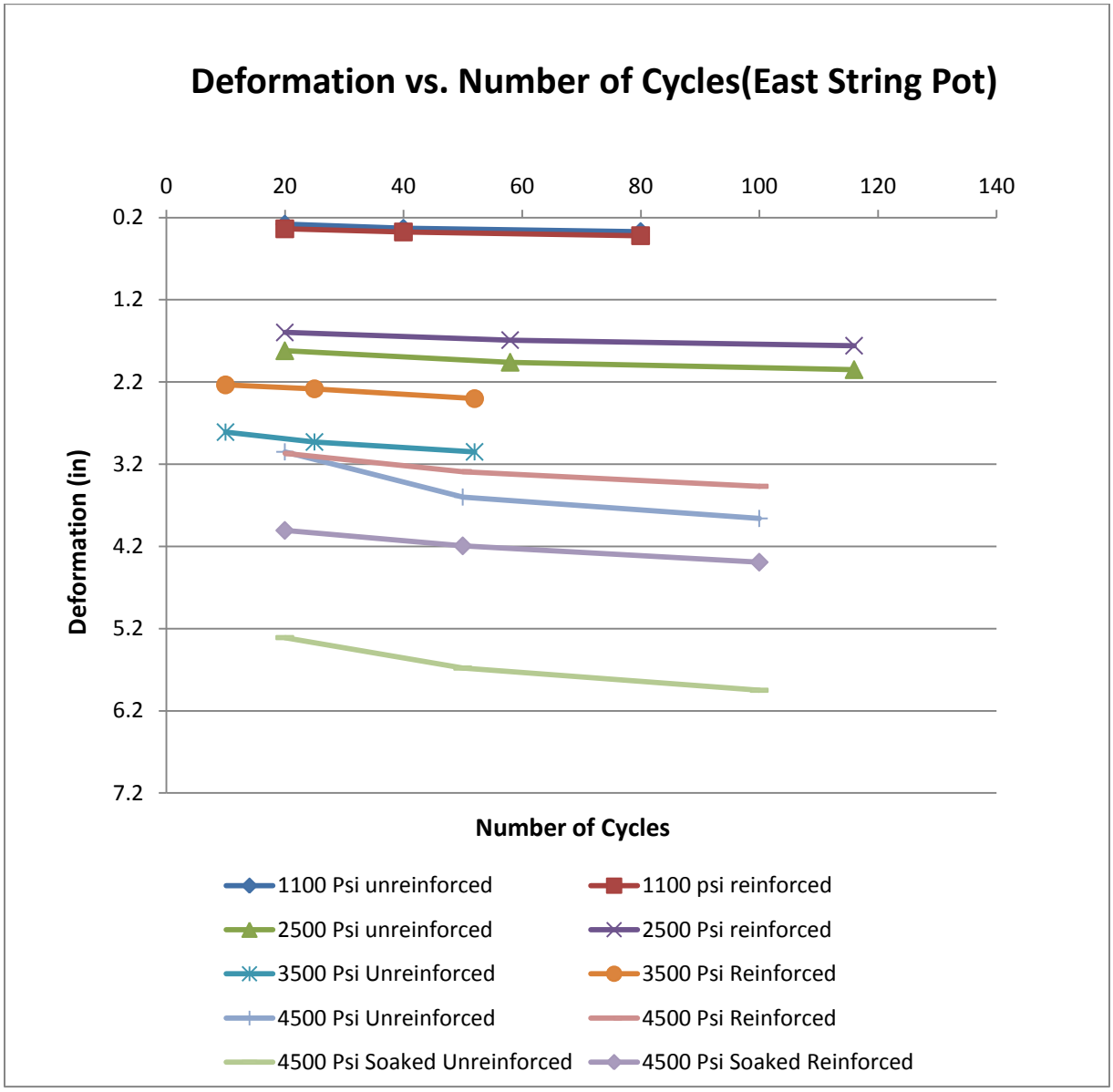

Figure 4.9.3 East string pot result comparison

Table 4.9.4 Comparison of settlement between reinforced test and unreinforced test (East string pot).

Pressure (psi)	Deformation(in) East Stringpot		Number Of cycles	Actual Pressure applied Reinforced (psi)	Actual Pressure applied Unreinforced (psi)
	Unreinforced	Reinforced			
1100(Beginning)	0.28	0.34	20	1120	1070
1100(Middle)	0.33	0.38	40	1126	1080
1100(End)	0.37	0.42	80	1121	1070
2500(Beginning)	1.82	1.60	20	2487	2480
2500(Middle)	1.96	1.69	58	2512	2440
2500(End)	2.05	1.76	116	2516	2450
3500(Beginning)	2.81	2.24	10	3570	3580
3500(Middle)	2.93	2.28	25	3505	3680
3500(End)	3.05	2.40	52	3508	3670
4500(Beginning)	3.6	3.07	20	4741	4406
4500(Middle)	3.86	3.29	50	4590	4462
4500(End)	4.05	3.47	100	4714	4480
4500 Soaked(Beginning)	5.31	4.01	20	4715	4370
4501 Soaked(Middle)	5.68	4.19	50	4740	4470
4502 Soaked(End)	5.95	4.39	100	4735	4470

As Table 4.9.4 shows, at the end of the 1100 psi loading no improvement was observed. After the 2500 psi loading a 0.3 in. improvement in settlement was observed. After the 3500 psi loading 0.64 in of settlement improvement was obtained, after 4500 psi loading (not soaked) about 0.58 in of settlement improvement has obtained and the end of soaked section loading about 1.55 in of settlement improvement has obtained. Notice on Figure 4.9.2 for the 1100psi how the reinforced and unreinforced curves are laid on top of each other. As the loads applied get bigger, the gap between the reinforced and unreinforced cases gets higher until the 3500 psi loading step. However in the case of the 4500 psi the loading step gaps get smaller. The reason for that is the pressure applied in the unreinforced and reinforced cases are not identical. Table 4.9.4 shows the percent difference in load applied in between both unreinforced and reinforced cases. . Figure 4.9.3 shows how loads difference contributes to the gap difference after load adjustment.

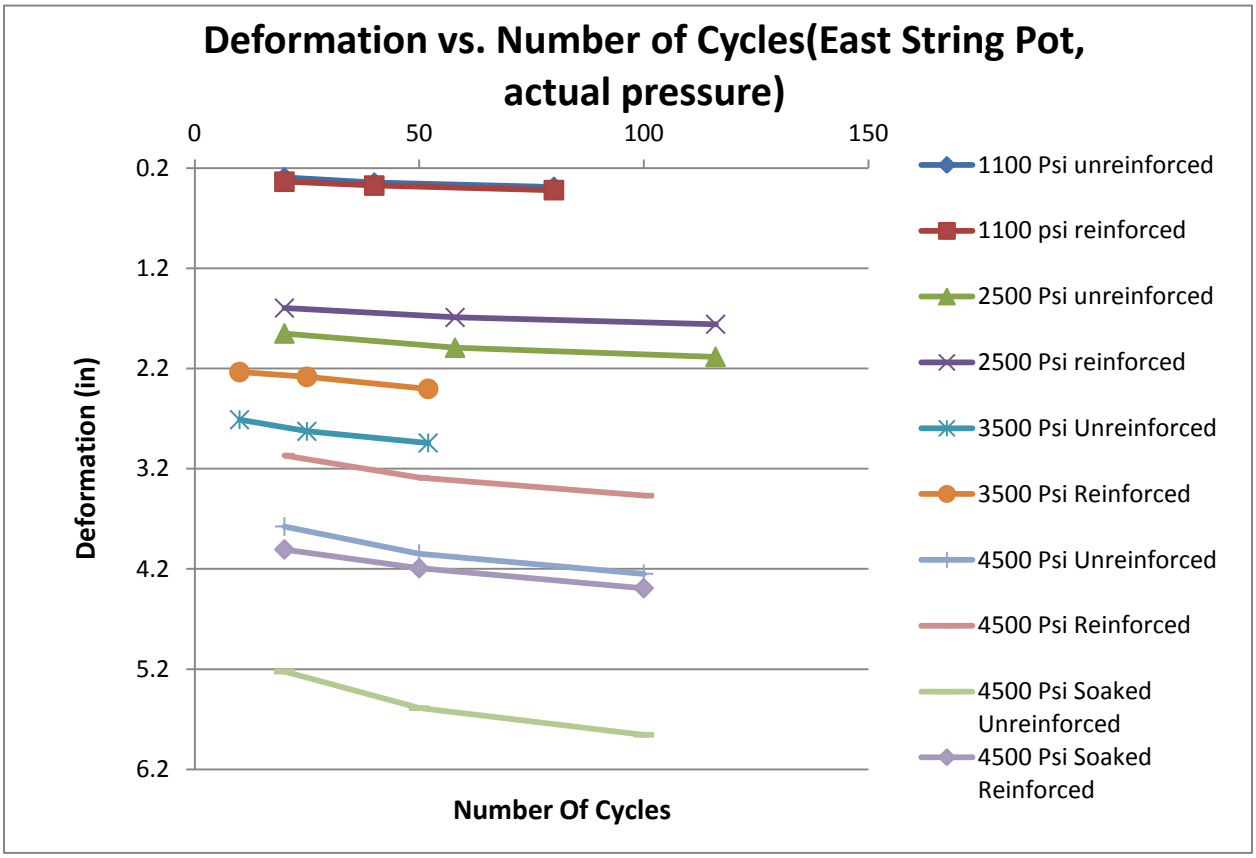

Figure 4.9.4 East string pot result comparison (after adjusting loads)

4.9.2 Number of cycles versus settlement (West string pot)

Figures 4.9.4 and 4.9.5 show the settlement with cycles for both tests observed by west and east string pots. These figures also show less settlement for the reinforced section.

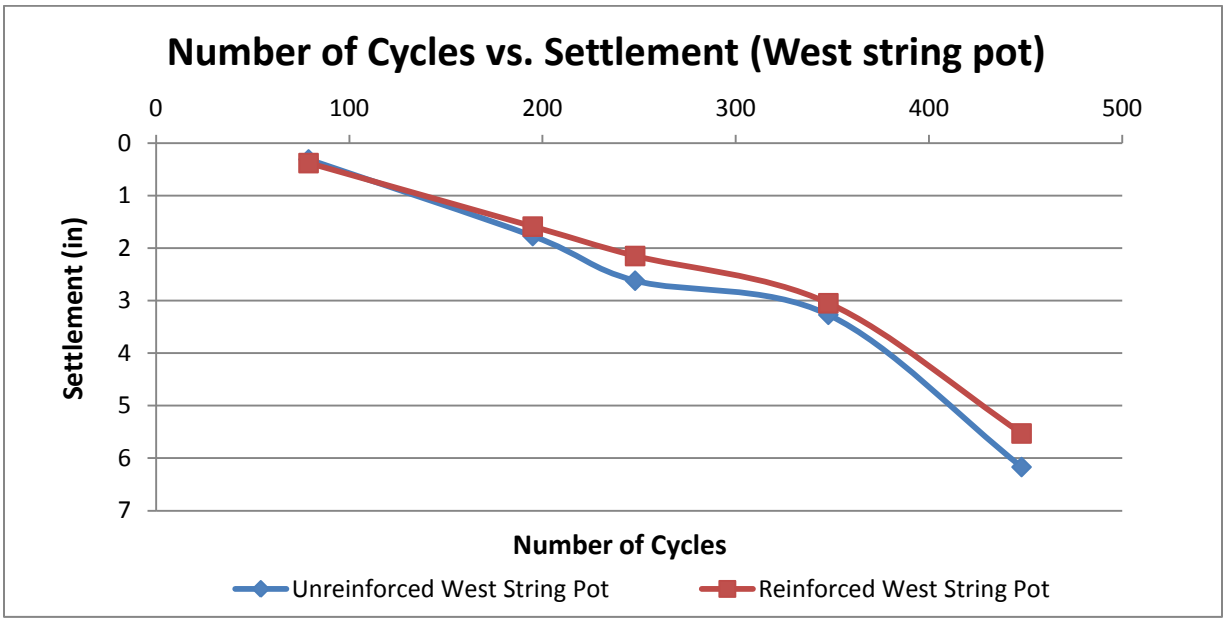

Figure 4.9.5 Number of cycles vs. settlement (west string pot)

4.9.3 Number of cycles versus settlement (East string pot)

Figure 4.9.6 shows the improvement in settlement obtained in reinforced case base on west string pot.

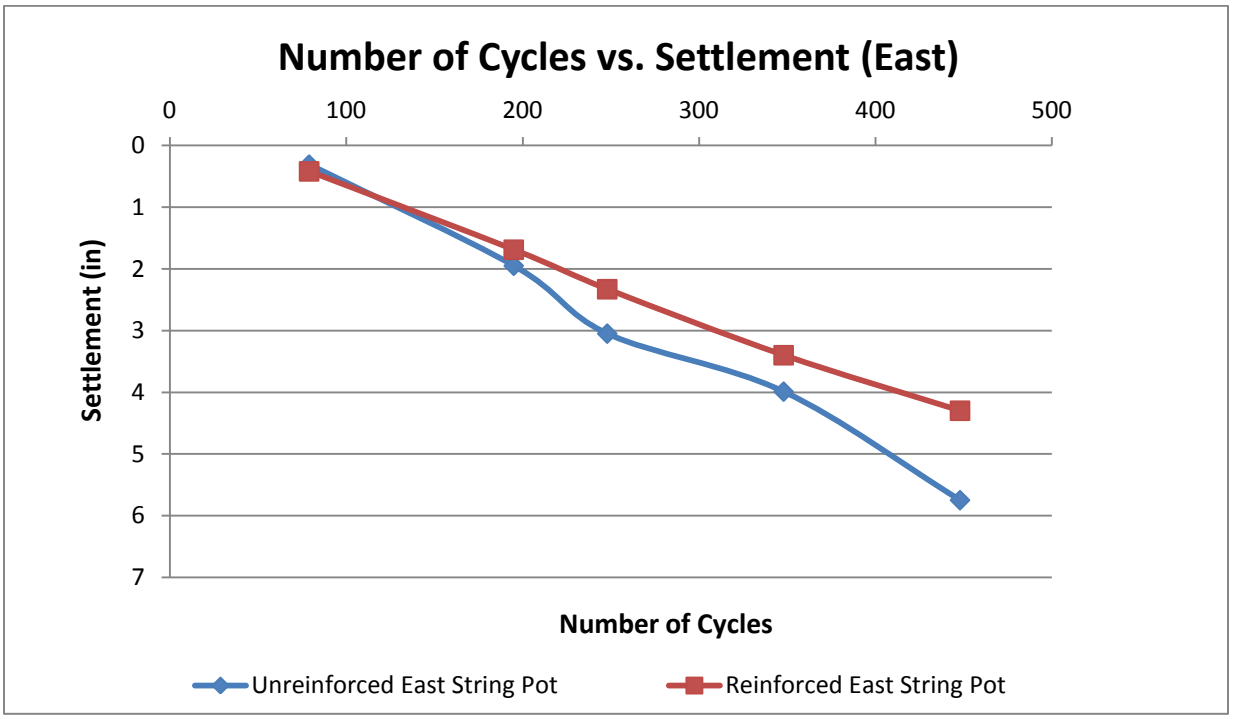

Figure 4.9.6 Number of cycles vs. settlement (east string pot)

4.9.4 Actual pressure vs. settlement

Figures 4.9.7 through 4.9.12 shows the actual tie bearing pressure versus settlement for the early cycles, middle cycles and later cycles.

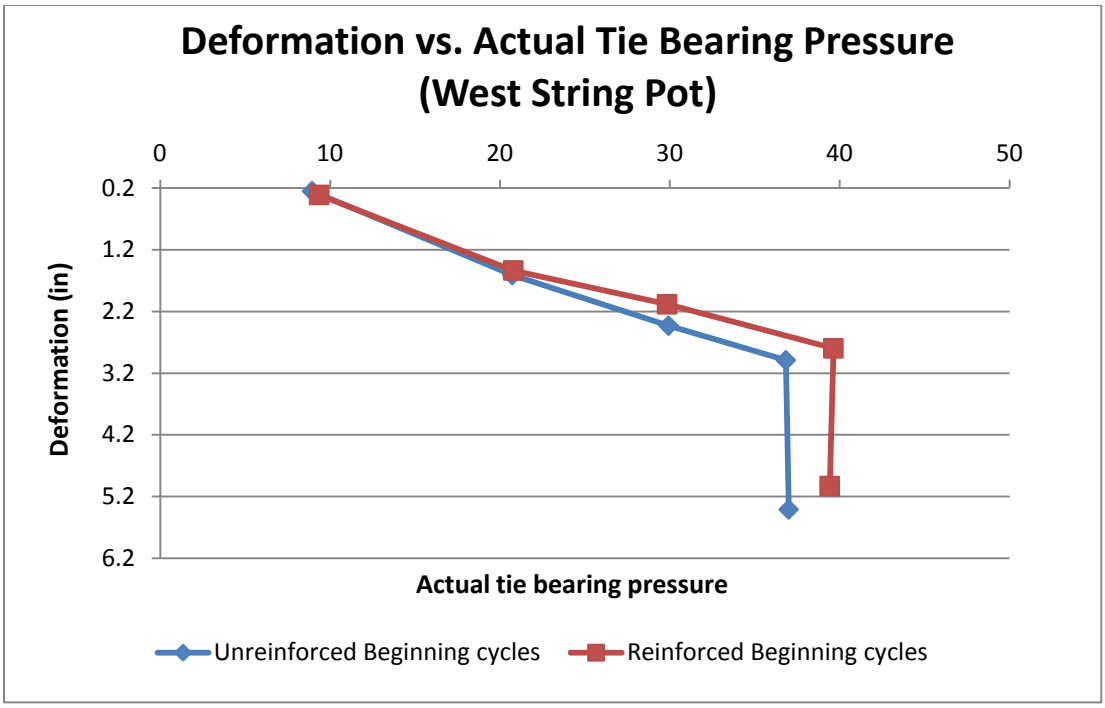

Figure 4.9.7 Deformation vs. actual tie bearing pressure at early cycles (west)

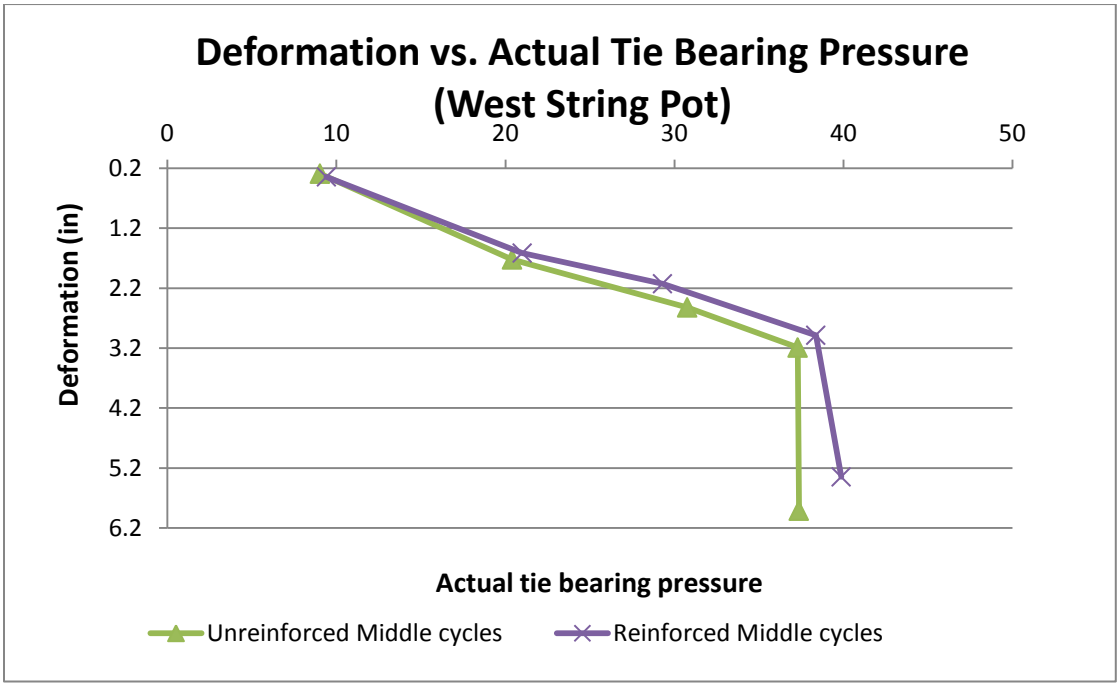

Figure 4.9.8 Deformation vs. actual tie bearing pressure at middle cycles (west)

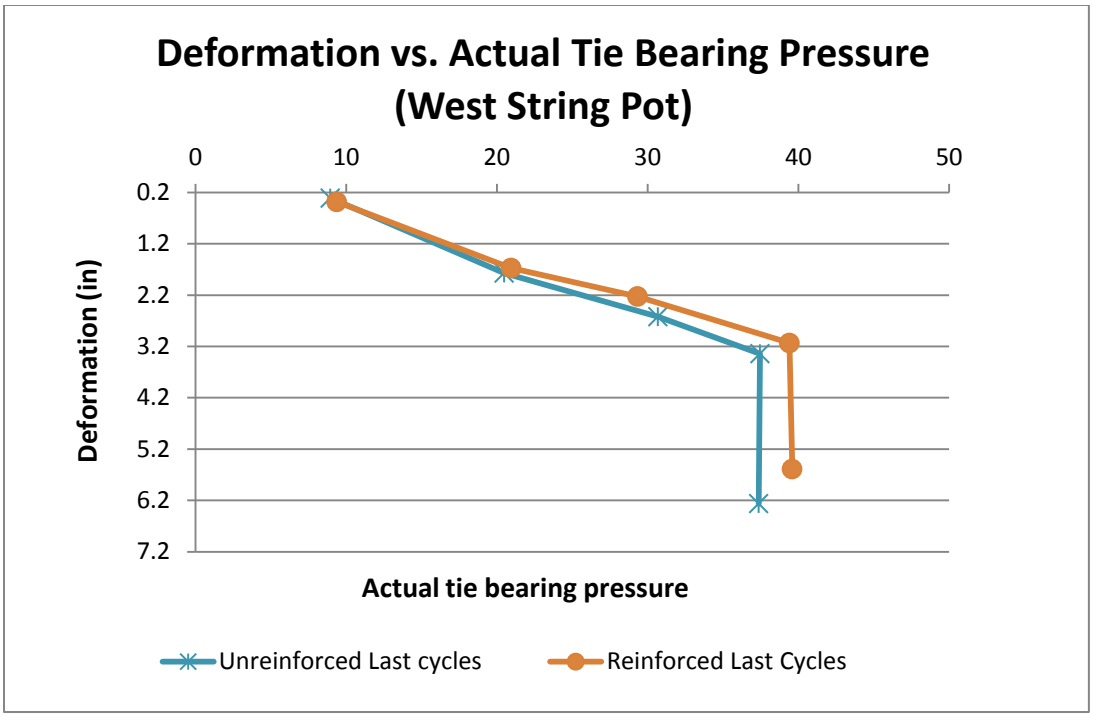

Figure 4.9.9 Deformation vs. actual tie bearing pressure at later cycles (west)

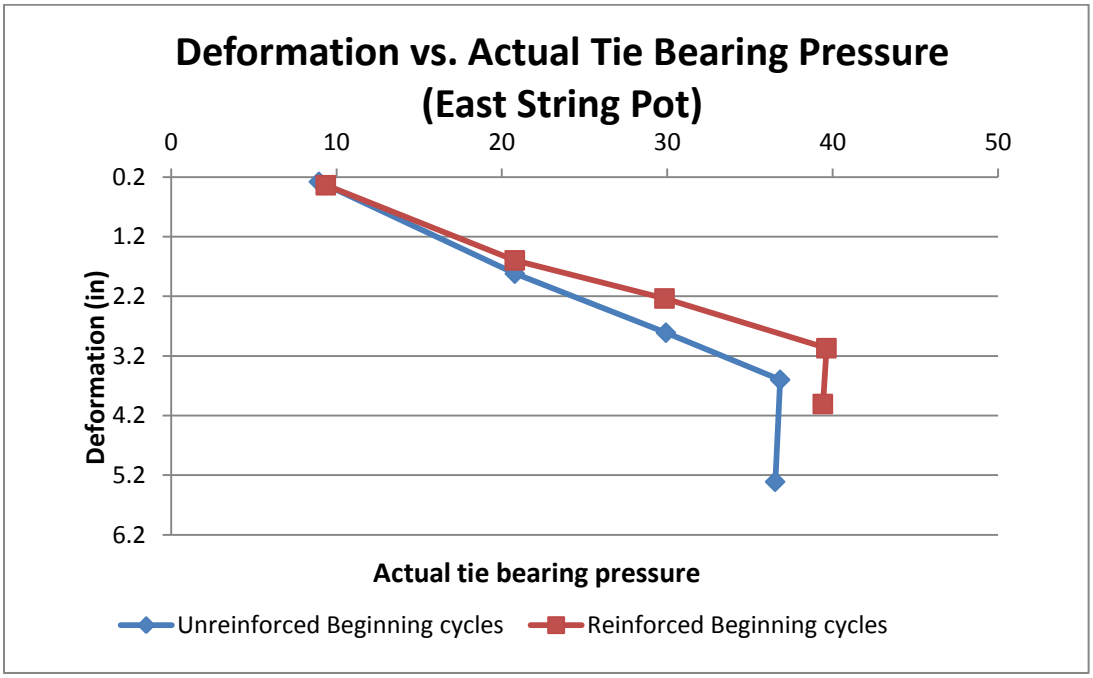

Figure 4.9.10 Deformation vs. actual tie bearing pressure at early cycles (east)

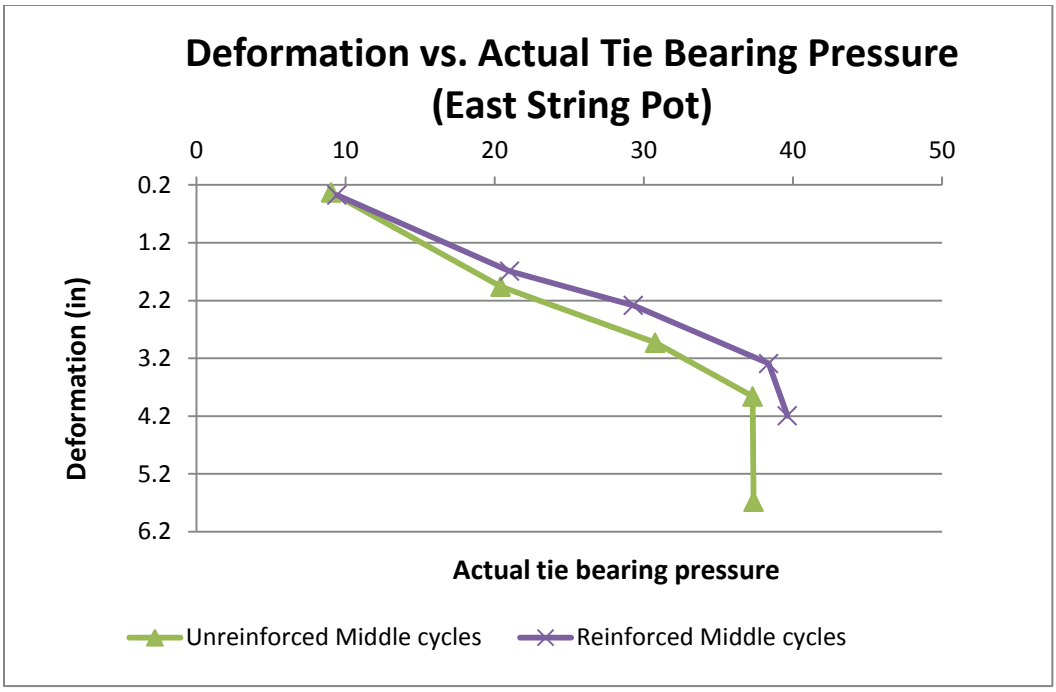

Figure 4.9.11 Deformation vs. actual tie bearing pressure at middle cycles (east)

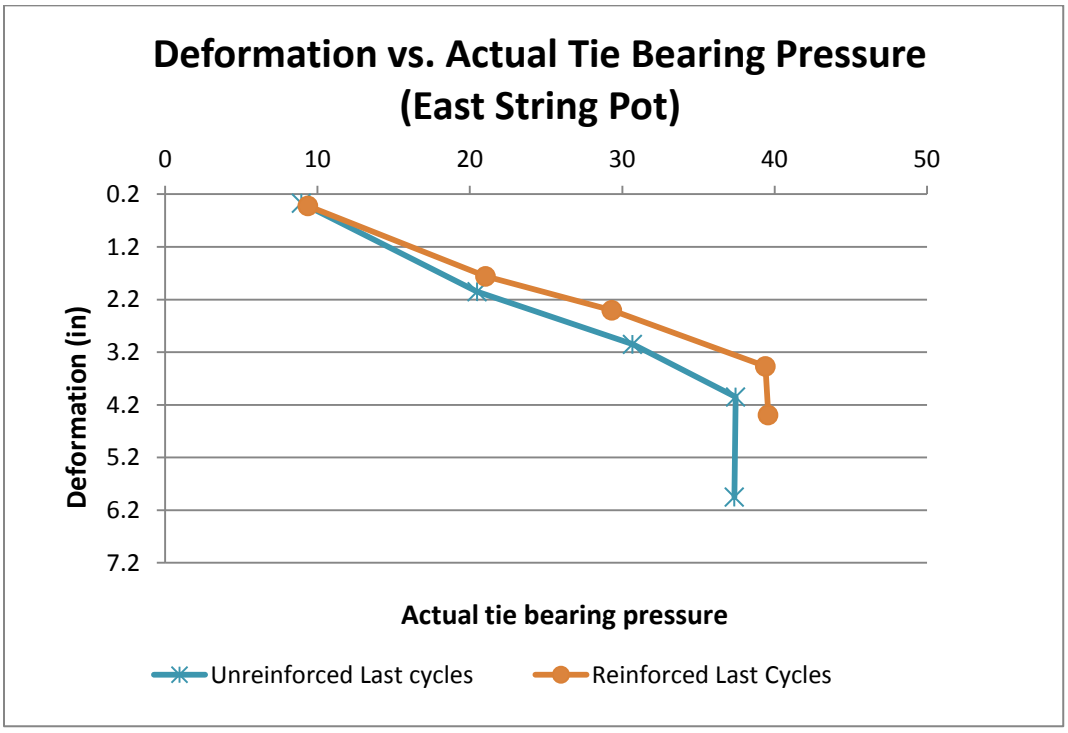

Figure 4.9.12 Deformation vs. actual tie bearing pressure at later cycles (east)

4.10 Additional testing such as LWD, CBR, Sieve Analysis and Tell-Tale readings

4.10.1 LWD

The light weight deflectometer (LWD) was used before and after testing of both the reinforced and unreinforced test sections to find the modulus of elasticity of the subgrade section at six locations as shown in Figure 4.10.1. The average modulus results for the six locations are shown in Table 4.10.1.

Table 4.10.1 LWD results

Subgrade	Plate Size (mm)	S_{avg}(mm)	s/v	E_{vd} MN/m^2
Before (unreinforced)	30	1.98	5.92	12.67
After (unreinforced)	30	1.78	6.53	12.98
Before (reinforced)	30	1.85	5.73	12.73
After (reinforced)	30	2.08	5.28	11.88

Note: In this table S_{avg} is the average settlement of the plate after 3 drops, s/v is Degree of Compactability, (if > 3.5, soil is further compactable and if <3.5, soil is not compactable)

The reinforced test has a lower E_{vd} after the test than unreinforced test. That is likely due to the higher moisture content (27%) before compaction in reinforced test than unreinforced test (26%).

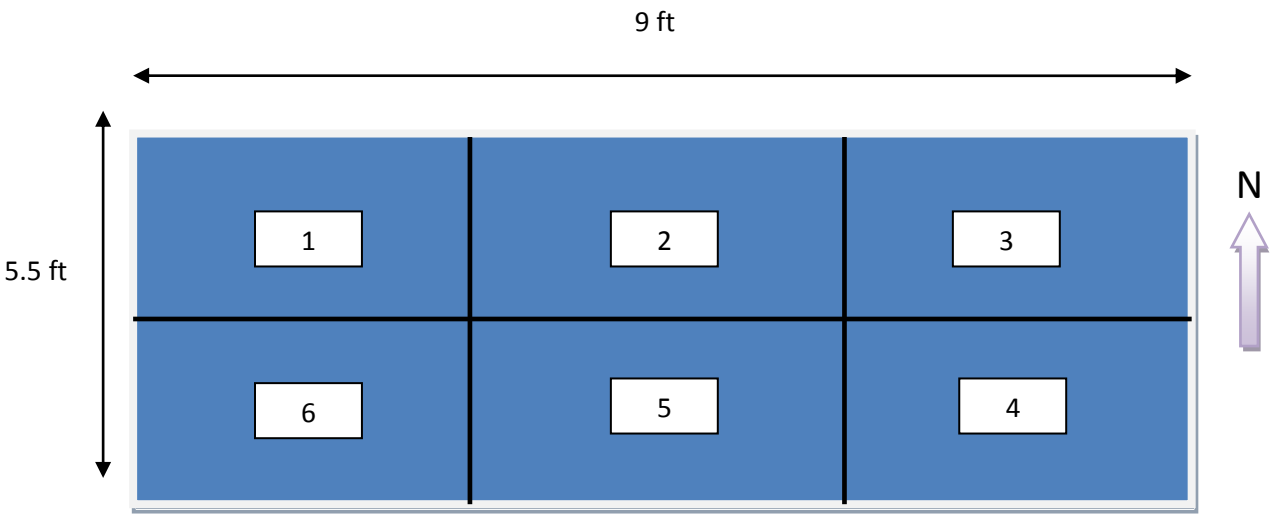

Figure 4.10.1 LWD reading locations

4.10.2 CBR

CBR values were estimated from dynamic cone penetrometer data from six locations before, and after the unreinforced and reinforced tests. Average results from six locations are shown in Figure 4.10.2. The average CBR value is approximately 2.0. It is slightly higher near the surface. Average CBR for the unreinforced test increased due to more compaction during the test. Also, the section was exposed for a longer period of time (7 days) in comparison to reinforced (3 days) test before removing the ballast.

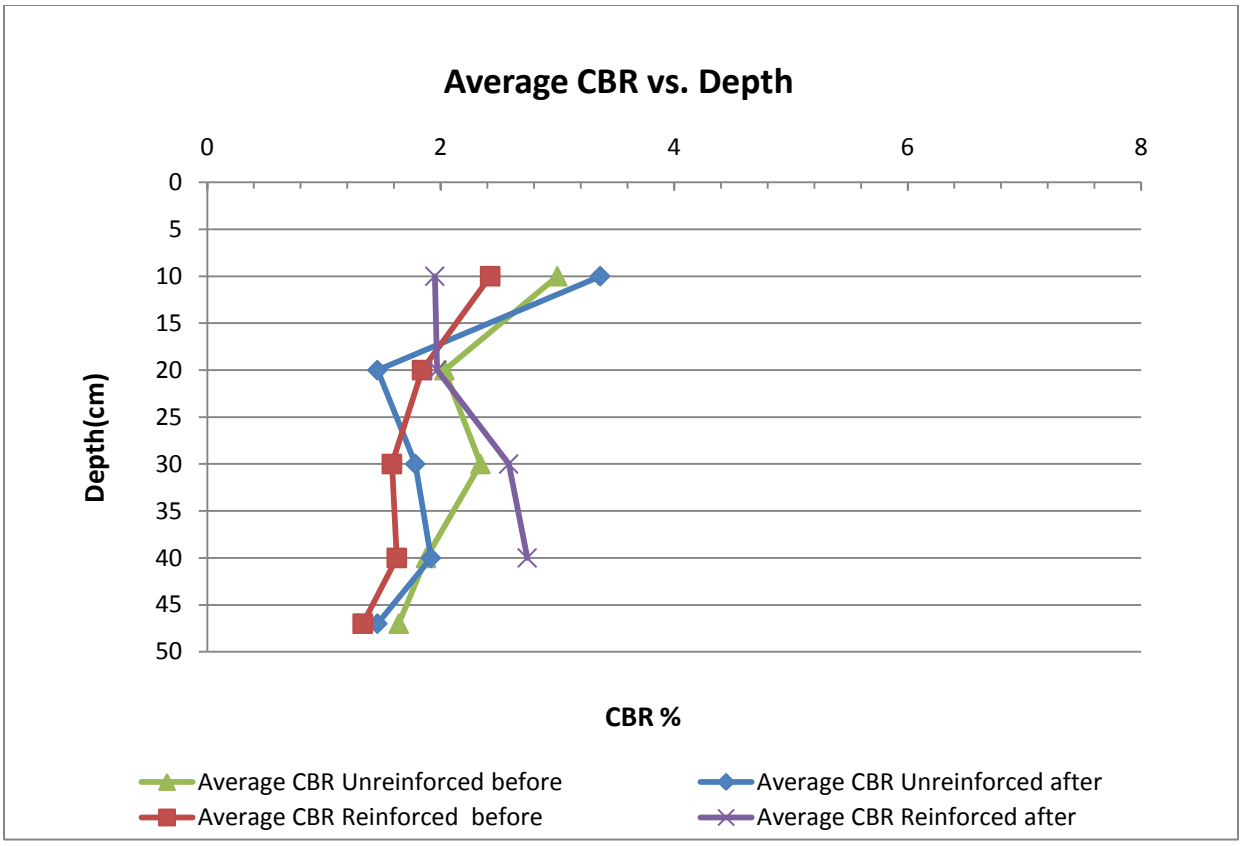

Figure 4.10.2 CBR vs. depth

4.10.3 Tell-Tales

Four tell-tales were located as shown in Figure 4.10.3. Two tell-tales were located at subgrade level (1 and 2) and two were located within the ballast (3 and 4). For both the unreinforced and reinforced cases these were located at 7" below the ties. Readings are reported for both the inner tube connected to the settlement plate and outer tube. Results are shown in Table 4.10.2. Readings were taken before and after each test.

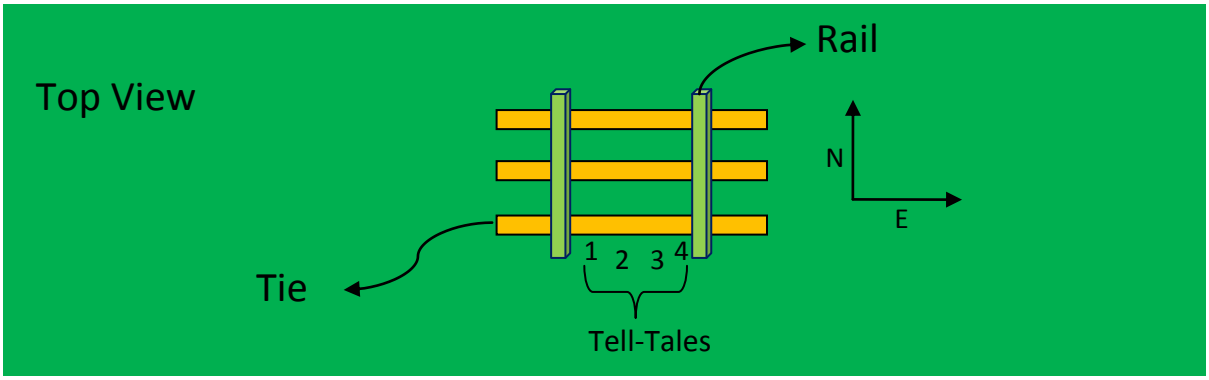

Figure 4.10.3 Tell-Tales locations (not to scale)

Table 4.10.2 Tell-Tale readings

Tell-Tales										
Unreinforced	**Subgrade**				**Ballast**				Avgrege	
	1in	1out	2in	2out	3in	3out	4in	4out	**Avg. In**	**Avg Out**
Before	7.5	6.30	8.5	6.9	17.5	16.25	17.5	13.9	**12.8**	**10.8**
After	4.5	3.25	5.5	3.25	13.5	12.5	13.25	10	**9.2**	**7.3**
Diffrence	3	3.05	3	3.65	4	3.75	4.25	3.9	**3.6**	**3.6**
Reinforced	**Subgrade**				**Ballast**				Avgrege	
	1in	1out	2in	2out	3in	3out	4in	4out	**Avg. In**	**Avg. Out**
Before	10	8.5	8.5	7.25	10	9	11.5	10.5	**10.0**	**8.8**
After	7.5	6.75	6.25	5.5	6	6	8	8	**6.9**	**6.6**
Diffrence	2.5	1.75	2.25	1.75	4	3	3.5	2.5	**3.1**	**2.3**

4.10.4 Generation of fouling material

During deconstruction of the unreinforced section, the presence of a significant amount of fines was observed in the lower portion of the ballast.

A series of ballast samples were taken after each test from different locations to determine if the presence of the geogrid reduced the breakage of ballast during reinforced test. Results are shown in Figure 4.10.4 and 4.10.5. As Figure 4.10.5 shows, the percentage of fines beneath the tie was substantially less for the reinforced test.

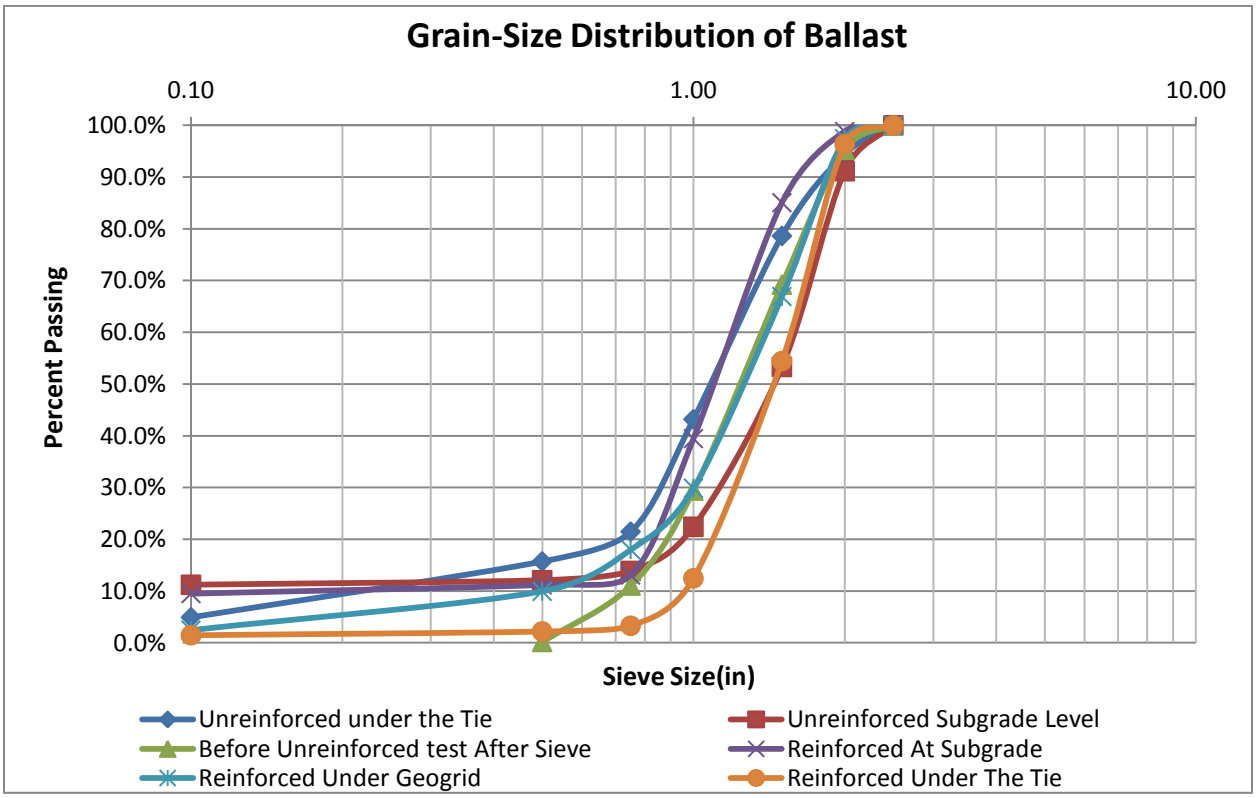

Figure 4.10.4 Grain size distribution of ballast

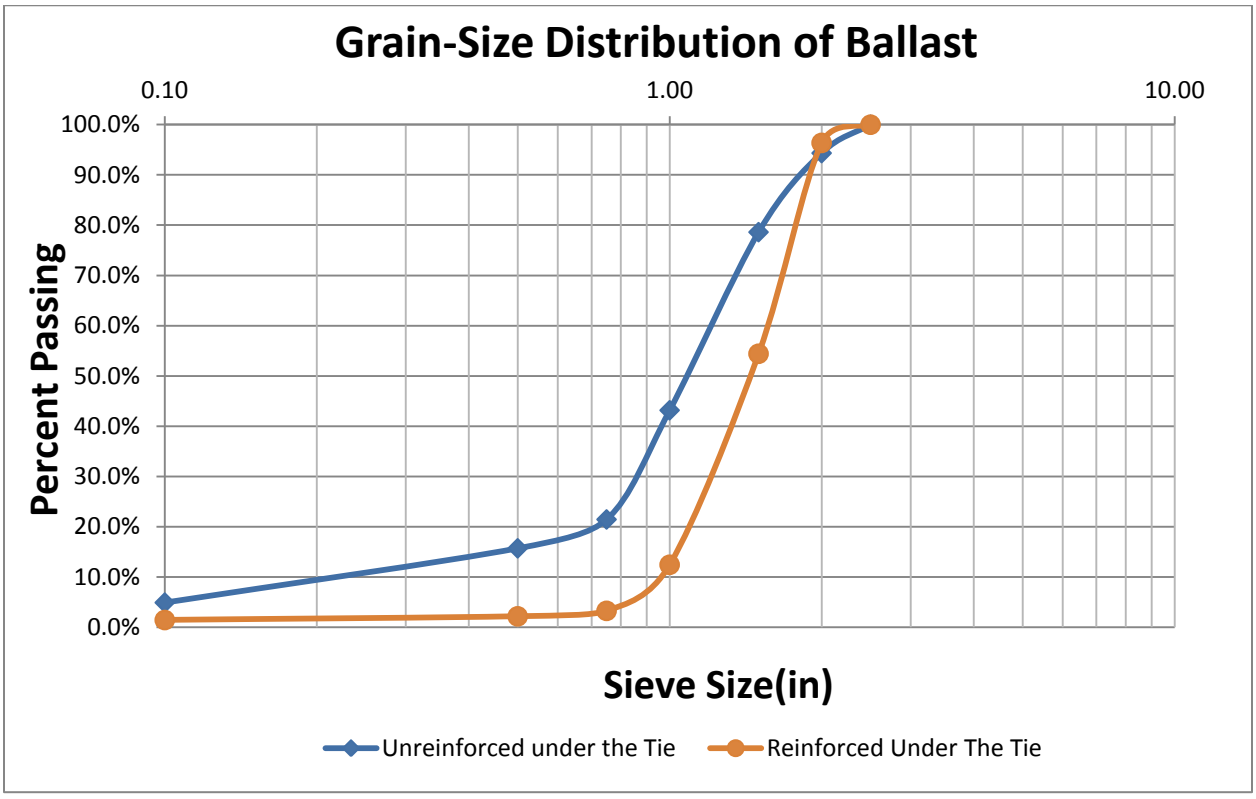

Figure 4.10.5 Grain size distribution of ballast under the tie

Figure 4.10.4 shows the amount of fines generated during testing of the reinforced section was less than what was generated during testing of the unreinforced section. This suggests the presence of the geogrid reduced fouling of the ballast. The improvement is particularly note worthy because the ballast was not re-sieved after the first test, therefore more fines were present in the second test at the beginning of the test. Table 4.10.3 shows improvement of ballast for percent passing the 0.5in sieve and percent passing less than 0.75in sieve.

Table 4.10.3 Compression of ballast after the test

Ballast Samples	Percent Passing 0.5 in	Percent Passing 0.75 in
Unreinforced Under Tie	4.9%	15.7%
Reinforced Under Tie	1.5%	2.2%
Unreinforced Subgrade Level	11.2%	12.1%
Reinforced Subgrade Level	9.5%	11.2%
Before Unreinforced Test	0%	11.1%
Reinforced at Geogrid Level	2.4%	9.9%

4.11 General observations

1. Unevenness of the subgrade after both tests was observed.
2. During excavation after the unreinforced test there were some damp ballast 8 inch below the tie.
3. During excavation after the reinforced test there were some damp ballast 9 inches below the tie.
4. Some ballast was penetrated the subgrade in both tests (approximately 1 inch).
5. The amount of fines generated close to the subgrade level was higher than under the ties.

Chapter Five

Conclusions and Recommendations

5.1 Conclusions

Full scale testing of railroad sections constructed with unreinforced recycled ballast and reinforced recycled ballast yielded the following observations:

- Settlement of the ballast in reinforced section was 1.05 inches less at the completion of testing under soaking.
- Fouling in the reinforced section was 30% less than for the unreinforced section.
- Less fine ballast was created during testing of the reinforced section
- The reinforced section supported more load prior to subgrade failure than the unreinforced section

Based on these observations it was concluded that ballast reinforcement provided benefits with regard to reduction of fines from the grinding and crushing of ballast and some reduction in the settlement.

5.2 Recommendations for Future Study

The experimental work in this study has shown a benefit from using geogrid to reinforce railroad ballast. However, there is a need for additional research. Some area where additional research would be beneficial include:

a) This study has considered only one type of geogrid (TX190LA). Other studies are recommended with different geogrids (different stiffnesses) to verify the improvements.

b) A more thorough investigation of ballast breakdown and the potential benefits of breakdown prevention is warranted.

c) Use of cyclic loading with a higher frequency to better simulate real world application is recommended.

d) It is recommended this work be extended to other subgrade soils and that testing continues for a longer duration.

e) It is recommended test sections with reinforcement be constructed on lines in service.

References:

1. Chrismer,S.M. (1987). "*Ballast and subgrade Maintenance: Working Group progress Report*"; Association of American Rail Roads report WP-129.
2. Emersleben, A., Meyer, N. (2005*) The use of geocells in road constructions over soft soil: vertical stress and falling weight deflectometer measurement.* Euro geo4 paper number 132.
3. Indraratna, B., Shahin, M.A., Rujikiatkamjiron, C., Christe, D. (2006). *Stabilization of Ballasted Rail Tracks and underlying soft formation soils with geosynthetic grids and drains.* University of Wollongong 2006.
4. Kea, J.K., Grabe, P.J., Maree J.S.(2007). *Geotechnical And field Measurements At Amandelbult* Test section Version 1.
5. Menglet,M.J.,Edil, T.B., and Benson,C.H.(2006). *Resilient modulus and plastic deformation of Soil Confined in a Geocell. Geosynthetic International.* Vol. 13, No 5, pp 195-205.
6. Rea,M and Mitchell,J.K. (1987). *Sand reinforcement using paper grid cells. Regular meeting- Rocky Mountain Coal Mining Institute.* pp 644-663.
7. Tutumluer, E., Dombrow, W., and Huang , H. (2008). *Laboratory Characterization of Coal dust Fouled Ballast Behavior*. Draft Manuscript Submitted for the AREMA 2008 Annual Conference & Exposition September 21-24, 2008, Salt Lake City, UT.
8. Webster,S.l. (1979a). *Investigation of Beach Sand Trafficability Enhancement Using Sand-Grid Confinement and Membrane Reinforcement Concepts*, Report GL-79-20 (1). U.S. Army Engineer Waterways Experiment Station, Vicksburg, MS.
9. Indraratna, B. , Rujikiatkamjorn, C. and Nimbalkar, S.(2011) *Use of Geosynthetics in Railways including Geocomposites and Vertical Drains.* Geo-Frontiers 2011.
10. Zarembski, Allan M. and John F. Cikota, Jr. "Estimating Maintenance Costs for mixed High-Speed Passenger and Freight Rail Corridors." TR News, 225, March-April 2008:29-31.

11. Kea, J.K. "*Improving Poor Track Formations Using Geosynthetics*." 2007. Web. 2011.

12. Grabe, Hannes. "*Geosynthetics for Improving Poor Track Formations*." 2010. Web. 2011.

13. *Indraratna, Buddhima. Use of Gesynthetics in Railways including Gecomposites and Vertical Drains. 2011. Web. 2011.*